This thesis is dedicated to my parents
for their love, endless support
and encouragement.

ABSTRACT

The objective of this research work was to study the degradation (corrosion and tribocorrosion) resulting from mechanical (wear) and electrochemistry (corrosion) interactions in Al/Al_3Ti and Al/Al_3Zr functionally graded materials (FGMs). The influence of the spatial distribution of the platelets on the corrosion and tribocorrosion behaviour was evaluated. The Al/Al_3Ti and Al/Al_3Zr FGMs were produced by centrifugal casting, originating samples in the form of rings that presented radial gradients of the reinforcements.

The corrosion resistance of Al/Al_3Ti and Al/Al_3Zr FGMs was studied using electrochemical techniques namely, open circuit potential (OCP), potenciodynamic polarization and electrochemical impedance spectroscopy (EIS). Additionally, the tribocorrosion behaviour was evaluated in a pin-on-plate configuration, under reciprocating sliding. During the tribocorrosion tests, the samples were immersed in a 0.6 M NaCl solution, and the corrosion current was measured while the samples were under potentiostatic control. Through the integration of the current density curve vs. time, the electric charge was determined, allowing the electrochemical contribution to the overall degradation process to be distinguished from that arising from the mechanical wear. The synergic action mechanisms of the system were further explained based on scanning electron microscopy (SEM) analysis. The experimental results showed that the tribocorrosion degradation of these materials is governed essentially by mechanical processes.

Finally, in an attempt of further investigation of possible applications for these materials, a tribological study, in unlubricated sliding conditions, of the Al-5 mass % Ti alloy plastically deformed by equal-channel angular pressing (ECAP) was carried-out. The tribological behaviour was studied in two directions, parallel and perpendicular to the deformation direction. In spite of the fact that the increase of passes in the ECAP

process results in an increase of the hardness of these materials, the wear resistance becomes lower.

RESUMO

O objectivo deste trabalho de investigação foi estudar a degradação (corrosão e tribocorrosão) resultante de interacções mecânicas (desgaste) e electroquímicas (corrosão) em Al/Al_3Ti e Al/Al_3Zr com gradiente funcional de propriedades (FGMs). A influência da distribuição espacial de partículas intermetálicas de reforço no comportamento à corrosão e à tribocorrosão foi avaliada. Os Al/Al_3Ti e Al/Al_3Zr FGMs foram produzidos por fundição centrífuga, tendo sido obtidas amostras com geometria anelar, as quais apresentavam gradientes radiais de partículas de reforço.

A resistência à corrosão de Al/Al_3Ti e Al/Al_3Zr FGMs foi estudada através de técnicas electroquímicas, nomeadamente, potencial em circuito aberto (OCP), polarização potenciodinâmica e espectroscopia de impedância electroquímica (EIS). Adicionalmente, o comportamento à tribocorrosão foi avaliado numa configuração de teste pino-placa, com movimento linear alternativo. Durante os testes de tribocorrosão, as amostras permaneceram imersas numa solução de NaCl 0.6 M e ao seu potencial de corrosão. Através da integração da curva de densidade de corrente vs. tempo, a carga eléctrica foi determinada, permitindo distinguir no processo global de degradação, a contribuição electroquímica da contribuição de desgaste mecânico. Os mecanismos da acção sinergética do sistema foram explicados através da análise de microscopia electrónica de varrimento (SEM). Os resultados experimentais mostraram que a degradação por tribocorrosão destes materiais é governada essencialmente por processos mecânicos.

Finalmente, numa tentativa de investigação adicional de possíveis aplicações para estes materiais, foi realizado um estudo tribológico, com ausência de lubrificante (a seco) da liga Al-5 mass % Ti deformada através da técnica de prensagem angular de secção transversal constante (ECAP). O comportamento tribológico foi estudado em duas direcções: paralelo e perpendicular à direcção de deformação. Apesar do aumento do número de passagens através do canal de secção transversal constante resultar num aumento de dureza, a resistência ao desgaste destes materiais diminui.

ACKNOWLEDGMENTS

The realization of this work was only possible due to the several people's collaboration, to which desire to express my gratefulness.

To Professors Luís Augusto Rocha and Edith Ariza, my supervisors, I am grateful for the trust deposited in my work and for the motivation demonstrated along this arduous course. Their support was without a doubt crucial in my dedication this investigation.

I would like to thank from a special way to Professor António Sousa Miranda, like Director of the Research Centre on Interfaces and Surfaces Performance, having been a privilege to belong this work-team, and Professor Ana Maria Pinto, like director of the Master Degree, for the unconditional support her.

To Professor José Ramos Gomes, I express my gratefulness for the discussion and interpretation of some results presented in this thesis.

The all my colleagues and researchers of CIICS, Ana Catarina Vieira, Ana Rosa Ribeiro, Paulo David Sequeira and Jorge Pereira, wants for the encouragement, advices and suggestions of the work, wants for the friendship that always demonstrated along these months of realisation of the work.

I would also to express my appreciation to my friends, Cristina and Jessica for the mode that me enthusiasm and encouragement.

Finally, I would like to thank to my parents, my brother and my nephews, their love gave me forces to make this work.

TABLE OF CONTENTS

CHAPTER 1

Introduction

Metal matrix composites (MMCs) have been considered as materials of broad technological and commercial significance during the past two decades. MMCs emerged as a distinct class of materials when improved performance for advanced military systems becomes necessary, this constituting a primary motivation for the development of these materials. Today, MMCs have important applications in the ground transportation (auto and rail), thermal management, aerospace, recreational and infrastructure industries because they offer an interesting balance of physical and mechanical properties. MMCs may possess high thermal and electrical conductivity, good resistance to aggressive environments, superior impact and erosion resistance and improved fatigue and fracture properties. In addition to this set of characteristics, MMCs usually possess higher strength and stiffness, excellent wear resistance and lower coefficient of thermal expansion, when compared with the matrix alloy. Additional functionalities can be designed into some MMCs through appropriate selection of constituents. Since the metal matrix and the ceramic reinforcement have vastly different physical, thermal, electrical and mechanical properties, MMCs properties can be varied over a very broad range that spans from those characteristic of metals to those of the ceramics. This confers a degree of tailor ability that is unusual in materials engineering. Thermal and electrical properties, for example, can be varied by appropriate adjustment of reinforcement volume fraction, morphology and distribution [1].

Through the centrifugal casting method conventional MMCs may be produced in the form of functionally graded materials (FGMs). The importance of these materials arises from the fact that functionally graded MMCs show a reinforcement concentration

higher at the surface than in the interior. Consequently, these materials will have higher surface hardness as well as improved resistance to crack growth towards the interior of the part. Essentially, FGMs are a relatively new class of composites exhibiting spatial gradient in composition, microstructures and properties along a certain direction [2-4].

Fabrication of intermetallic compounds (Al_3Ti or Al_3Zr) dispersed in an aluminium alloy – functionally graded materials – produced by centrifugal casting is a recent research area which aims at compensating the brittleness of intermetallic materials by dispersing them in a ductile metal matrix. Using this approach, it might be possible to use the expected superior characteristics of intermetallics such as high resistance, hardness and stability at elevated temperature, avoiding the disadvantages arising from their intrinsic brittleness. Thus, the advantageous properties can in practice be used in a structural material because the ductility of metal matrix can assure that the material as whole is not brittle [5-11]. In recent works, Sequeira et al. [12-14] in addition to the detailed study of the processing conditions of Al/A_3Ti and Al/Al_3Zr FGMs, investigated the evolution in the microstructure and mechanical properties of these materials.

Considering the Al-Ti and Al-Zr phase diagrams in Figures 1.1 and 1.2, the dotted blue lines in these figures show the compositions of the master alloy ingots used in this study. Since the melting point of Al_3Ti and Al_3Zr (1615 and 1860 K, respectively) are significantly higher than the processing temperature (1173 K), Al_3Ti and Al_3Zr particles remain solid in the liquid Al matrix during the centrifugal method [15]. Centrifugal force applied to mixture of molten metal and dispersed material, leads to the formation of a desired composition gradient. Here, the gradient is controlled mainly by the difference in density between the matrix (2.7 $g.cm^{-3}$) and the dispersed material (Al_3Ti = 3.4 and Al_3Zr = 4.1 $g.cm^{-3}$). This occurrence is similar to ceramic-dispersed FGMs [9].

The main objective of the work presented in this dissertation is to contribute for the knowledge of the corrosion and tribocorrosion behaviour of Al/Al_3Ti and Al/Al_3Zr FGMs, as a function of the reinforcement particles distribution. Additionally, the tribological behaviour of Al/Al_3Ti composite deformed by equal-channel angular pressing (ECAP), as a function of the number of passes (1 up to 6) was investigated.

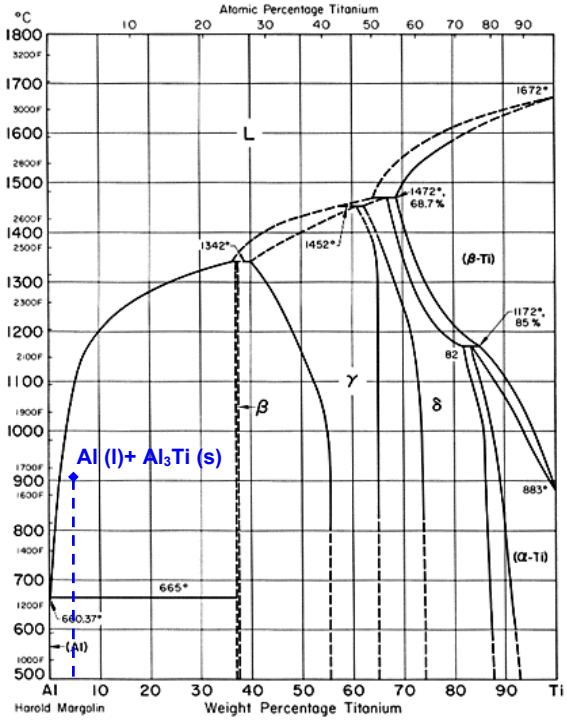

Figure 1.1 – Al-Ti phase diagram [16].

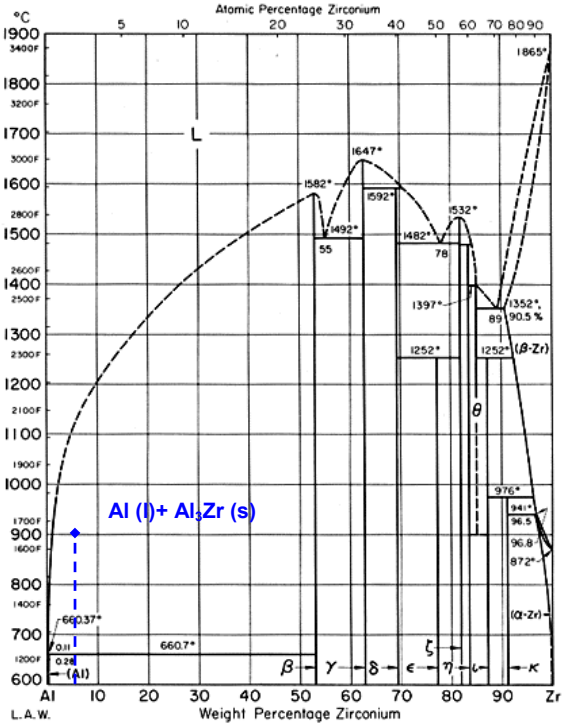

Figure 1.2 – Al-Zr phase diagram [16].

This dissertation is presented in nine chapters. In Figure 1.3, the structure of the dissertation is presented and correlated with the materials considered in the work.

An introduction and a global presentation of the work of the thesis are provided in Chapter 1.

In Chapter 2, a literature survey is presented, in which the relevant information found in the literature related with the topics addressed in this dissertation is revised. This includes aspects concerning the electrochemical characteristics and tribological behaviour of the particulate aluminium matrix composites as well as some basic concepts regarding the tribocorrosion phenomenon.

Chapter 3 describes the corrosion behaviour of Al/Al_3Ti and Al/Al_3Zr FGMs processed by a centrifugal casting with centrifugal forces of 30, 60 and 120 *G* (units of gravity). The studied region on the material was the outer region of the FGMs rings, in the perpendicular plane to rotation axis (OP1) that was immersed in 0.6 M NaCl solution (see Figure 1.3). Open circuit potential, potentiodynamic polarisation and electrochemical impedance spectroscopy (EIS) tests were carried out. The EIS spectra

were modelled and analysed with an equivalent circuit that reflected the evolution of corrosion behaviour during 1, 3, 6 and 10 days of immersion.

Chapter 4 regards the tribocorrosion behaviour of Al/Al_3Ti and Al/Al_3Zr FGMs samples in the same regions of the FGMs rings studied, in terms of corrosion in Chapter 3. The tribocorrosion tests were performed under reciprocating sliding.

Chapter 5 considers the tribocorrosion behaviour of Al/Al_3Zr FGMs in two regions (outer and inner) with different gradients of intermetallic compounds in the perpendicular plane to the rotation direction (OP2).

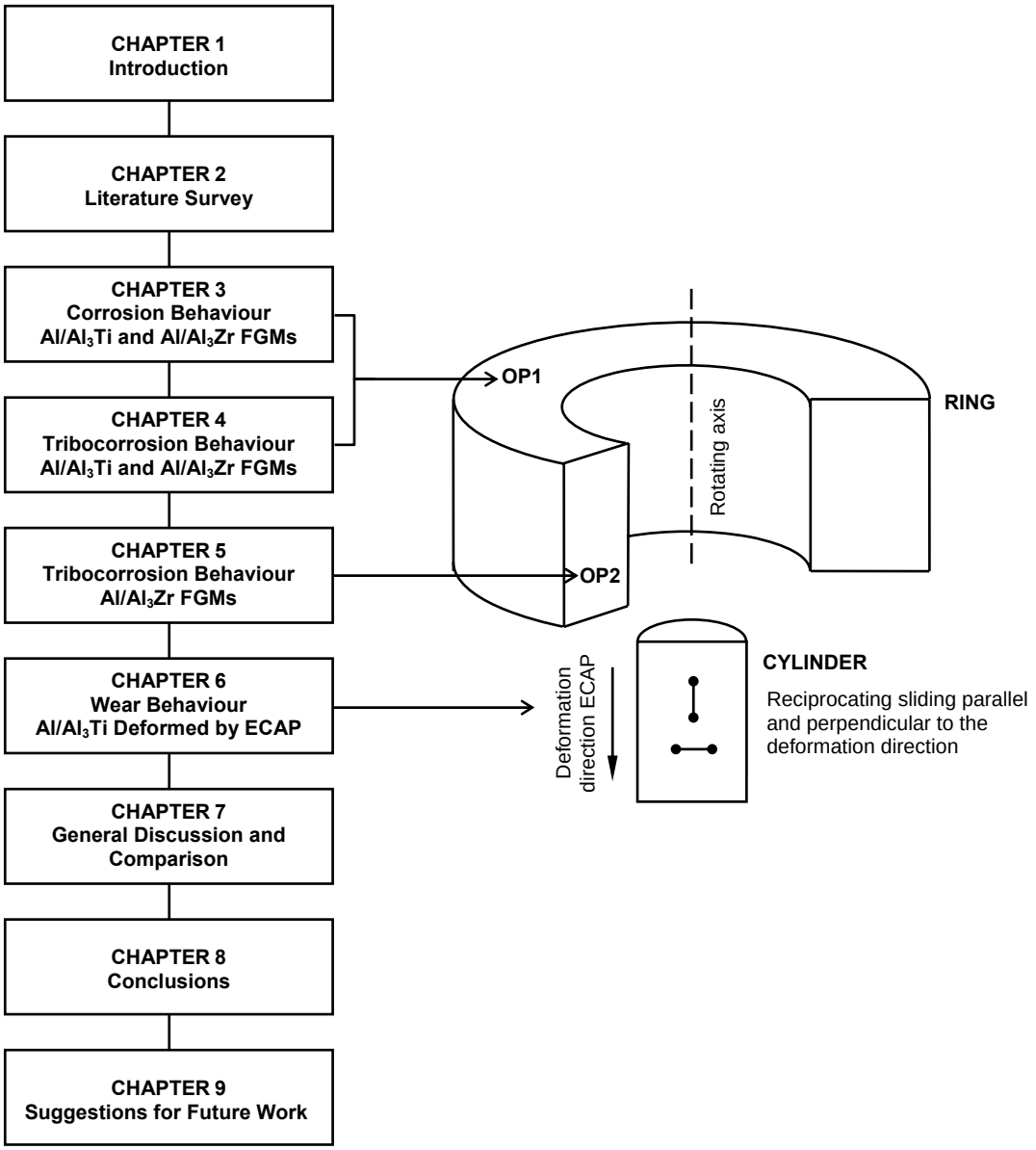

Figure 1.3 – Thesis structure.

Chapter 6 explains the wear behaviour of an Al/Al_3Ti composite plastically deformed by ECAP from 1 up to 6 passes. Wear resistance experiments were carried out in two directions, parallel and perpendicular to the deformation direction.

In Chapter 7, the experimental results obtained in Chapters 3 to 6 are compared and discussed.

Chapter 8 summarizes the main conclusions of the present work.

Finally, Chapter 9 provides some suggestions for future research.

Table 1.1 – List of publications

Scientific Articles
S.C. Ferreira, L.A. Rocha, E. Ariza, P.D. Sequeira, Y. Watanabe, *Corrosion Behaviour of Al/Al_3Ti and Al/Al_3Zr FGMs Produced by Centrifugal Casting*, to be submitted for publication in Composites Science and Technology.
P.D. Sequeira, S.C. Ferreira, Y. Watanabe, L.A. Rocha, E. Ariza, J.R. Gomes, *Microstructural Characterization and Tribocorrosion Behaviour of Al/Al_3Ti and Al/Al_3Zr FGMs*, to be submitted for publication in Tribology International.
P.D. Sequeira, S.C. Ferreira, Y. Watanabe, L.A. Rocha, E. Ariza, J.R. Gomes, *Microstructural Characterization and Wear Behaviour of Two-Phase Al-5 mass % Ti Alloy Deformed By Equal-Channel Angular Pressing*, to be submitted for publication in Scripta Materialia.
Communications
S.C. Ferreira, L.A. Rocha, E. Ariza, J.R. Gomes, P.D. Sequeira, Y. Watanabe, *Tribocorrosion Behaviour of Al/Al_3Ti and Al/Al_3Zr FGMs*, Proceedings of the EUROCORR 2005 – European Corrosion Congress, Lisbon, Portugal, 4-8 September, 2005.
S.C. Ferreira, E. Ariza, L.A. Rocha, P.D. Sequeira, Y. Watanabe, *Influence of the Reinforcing Particles Distribution on the Study of Tribocorrosion of Al/Al_3Zr FGMs Produced by Centrifugal Casting*, Proceedings of the LATINCORR 2006 – Congresso Latino-Americano de Corrosão, Fortaleza, Brasil, 21-26 Maio, 2006.

Chapters 3, 4 and 6 resulted in three scientific articles and Chapter 5 in a communication (see Table 1.1). These research works were developed in two institutions: Engineering Physics, Electronics and Mechanics Department, Graduate School of Engineering, Nagoya Institute of Technology, Japan, in which was realized, with the cooperation of P.D. Sequeira and Y. Watanabe, the processing of the Al/Al_3Ti and Al/Al_3Zr FGMs by centrifugal casting and the Al-5 mass % Ti alloy deformed by

ECAP; and the Research Centre on Interfaces and Surface Performance, Minho University, Portugal, in which was realized, by myself, S.C. Ferreira, with collaboration of L.A. Rocha, E. Ariza and J.R. Gomes, the study of corrosion and tribocorrosion behaviour of Al/Al_3Ti and Al/Al_3Zr FGMs and the tribological behaviour of the Al-5 mass % Ti alloy deformed by ECAP.

1.1 – References

[1] D. B. Miracle, Comp. Sci. Tech. 65 (2005) 2526.

[2] R. Rodríguez-Castro, R.C. Wetherhold, M.H. Kelestemur, Mater. Sci. Eng. A323 (2002) 445.

[3] R. Rodríguez-Castro, J. Mater. Sci. 37 (2002) 1813.

[4] A. Velhinho, P.D. Sequeira, R. Martins, G. Vignoles, F.B. Fernandes, J.D. Botas, L.A. Rocha, Nuclear Instr. Methods Phys Res. B 200 (2003) 295.

[5] Y. Watanabe, N. Yamanaka, Y. Fukui, Z. Metallkd. 88 (1997) 717.

[6] Y. Watanabe, N. Yamanaka, Y. Fukui, Metall. Mater. Trans. A 30A (1999) 3253.

[7] Y. Watanabe, Y. Fukui, Rec. Res. Devel. Metall. Mater. Sci. 4 (2000) 51.

[8] Y. Watanabe, Y. Fukui, Aluminum Trans. 2 (2000) 195.

[9] Y. Watanabe, H. Eryu, K. Matsuura, Acta Mater. 49 (2001) 775.

[10] Y. Watanabe, A. Kawamoto, K. Matsuda, Compo. Sci. Tech. 62 (2002) 881.

[11] Y. Watanabe, Y. Fukui, in Current Issues on Multidisciplinary Microscopy Research and Education, ed A. Méndez-Vilas and L. Labajos-Broncano, FORMATEX, Badajoz, (2004) 189.

[12] P.D. Sequeira, Y. Watanabe, L.A. Rocha, Mater. Sci. Forum, 492 (2005) 609.

[13] P.D. Sequeira, Y. Watanabe, L.A. Rocha, Sol. Stat Phen. 105 (2005) 425.

[14] P.D. Sequeira, Ph.D. Thesis, Nagoya Institute Technology, Nagoya, 2006.

[15] Y. Watanabe, T. Nakamura, Intermetallics 9 (2001) 33.

[16] http://www.infomet.com.br/diagramas_fases.php.

CHAPTER 2

Literature Review

In this chapter a brief literature survey, referring to the most important topics related with this dissertation is presented. This includes subjects such as the properties of intermetallic phases in aluminium alloys, the microstructural difference between MMCs and FGMs, the effect of the processing parameters by centrifugal casting on the gradient distribution of the dispersed particles in FGMs, the electrochemical characteristics of intermetallic phases in aluminium matrix composites, a succinct description of the EIS technique, the tribological behaviour of the particulate aluminium matrix composites and finally some concepts related with the tribocorrosion phenomenon. Some results obtained by other authors will be presented.

2.1 – Intermetallic Phases in Aluminium Alloys

Recently transition metal tri-aluminides have received increasing attention due to their low densities, good oxidation resistance, high melting point and good thermal stability. Such attractive characteristics make tri-aluminides Al_3X (Ti, V, Zr, Nb, Hf, Ta) potential candidates for high temperature structural materials. However, britleness at low temperatures has limited the application of these materials [1-5].

According to the Al-Ti and Al-Zr phase diagrams (see Figure 1.1 and 1.2), the intermetallics Al_3Ti and Al_3Zr are formed through peritectic reaction and congruent melting, respectively. Both compounds have similar atomic structures, $D0_{22}$ in Al_3Ti and $D0_{23}$ in Al_3Zr, with the same tetragonal (space group: I4/mmm) [3]. However, as it was said previously, there are problems to be overcome for the practical use of Al_3Ti and Al_3Zr as structural materials. The lack of ductility of tri-aluminides is attributed to

their low crystal symmetry of the tetragonal $D0_{22}$ or $D0_{23}$ structures [1-5]. That is, they do not have a sufficient number of equivalent slip systems to satisfy the von-Mises criterion for slip deformation in polycrystals. In Al_3X intermetallics, the tetragonal $D0_{22}$ or $D0_{23}$ structure is closely related to the cubic $L1_2$ structure (Pm3m) that has five independent slip systems [1]. Structural isotropy is expected to improve the deformability of the material because the isotropy increases the variants of active slip systems for dislocation motions. Thus, the stabilization of the $L1_2$ structure is of great interest for practical purposes as well as for the comprehensive understanding of stabilization. A number of studies have recently been devoted to determine the effect of the presence of third elements (Cr, Mn, Fe, Co, Ni, Cu, Zn, Ag and Pd) in the stabilisation of the $L1_2$ structure [4]. Since the $L1_2$ structure has more slip systems, the ductility of Al_3Ti and Al_3Zr is improved. However, neither the origin of this effect nor the influences of atom-species/quantities is fully understood yet. One alternative solution that improves this problem is to disperse intermetallic compound particles in a ductile phase material [6,7]. A proper gradient distribution of intermetallic compounds would result in better properties than a homogeneous distribution, based on the concept of functionally graded materials (FGMs) [8-14].

2.2 – Al-Based FGMs Manufactured by Centrifugal Method

In last years, gradients at the microstructure level, composition and/or properties in some specific directions are being introduced in advanced engineering components. In particular, an extensive work has been made in the area of aluminium based alloys-functionally graded materials produced by centrifugal casting and reinforced with particles [15-26].

Figure 2.1 illustrates the functional and compositional differences between conventional and FGM composites. Particle-dispersed composites shown in Figure 2.1 a) are regarded as macroscopically homogeneous and microscopically inhomogeneous and thus the characteristics of the composite are assumed homogeneous on a macroscopic scale. The properties of this material do not change significantly within the samples. Figure 2.1 b) induces non-uniform distributions of reinforcement in composite,

creating multiple functions within the material. That is, the composition and/or microstructure vary gradually from one surface to the other. In the absence of a macroscopic interface in FGMs, their properties should change continuously [10,11,23,26].

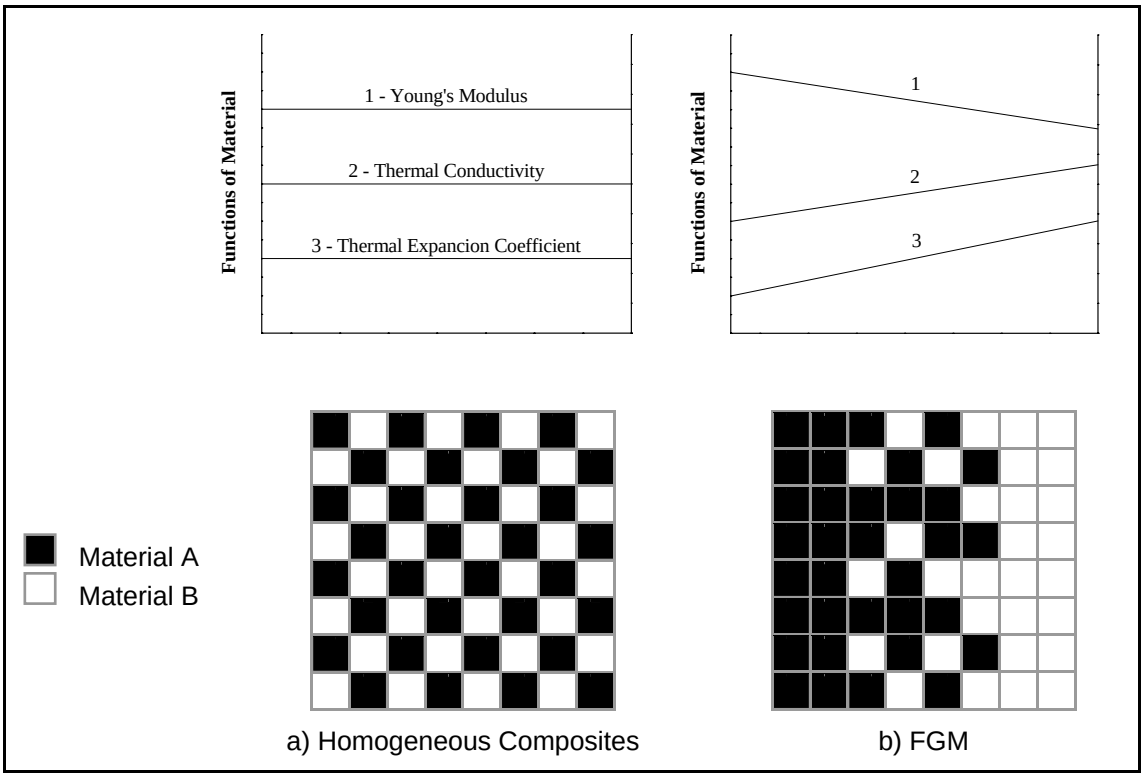

Figure 2.1 – The functional and compositional differences between conventional composites and FGM. (Adapted from [11]).

In Al/intermetallic compound FGMs, the particles are used to provide mechanical resistance, hardness, heat resistance, while, the aluminium matrix are used to offer the ductility, thermal conductivity and mechanical strength.

An advanced composite in the form of a functionally graded material (FGM) holds continuous changes of the microstructure, composition and/or properties in some specific directions. The variation of properties can be adjusted by controlling the microstructure and/or composition and is an important factor to describe the functions of FGMs.

One of the promising FGM fabrication methods is the centrifugal method. Fukui and colleagues [8-17,19,20,25-27] have studied and optimized both the FGM fabrication method, as well as possible systems of Al alloys that can form a FGM by centrifugal method.

The centrifugal method is applicable to mass production of both small and large FGMs components at a low cost. In this method, a centrifugal force is applied to a homogeneous molten composite, dispersed with ceramic or intermetallic compounds particles driving the formation of the desired gradation. Several parameters determine the microstructure and the distribution of particles inside the casting. These parameters are the size and initial concentration of particles, the centrifugal force, and the cooling rate, which is controlled by: temperature of the mould, pouring temperature, cooling delay, cooling of the mould, cooling of the casting, and heat transfer between the mould and the melt [22].

The centrifugal casting is a pressure casting method in which the force of gravity, when pouring molten metal into the mould, is increased by rotating or spinning the mould assembly [8-27]. The main advantages of centrifugal casting are good mould filling combined with good microstructural control, which usually give excellent mechanical properties [10,11].

The centrifugal casting techniques have already been tested with aluminium alloy melts containing ceramics particles, Al/SiC [21-23], Al/Shirasu [10,11,19], Al/AlB_2 [24] and intermetallic compounds Al/Al_3Ti [8,9,12,13,26], Al/Al_3Zr [13,26], Al/Al_3Ni [28], Al/(Al_3Ti+Al_3Ni) [29] and Al/Al_2Cu [30] to obtain non-homogeneous materials.

Al/intermetallic compounds FGMs fabricated by centrifugal casting have been extensively studied because they overcome the interface problem found in artificial composites such as Al/SiC or Al/Al_2O_3 for example, and have a lot of advantages such as clean interfaces between reinforced phase and matrix, excellent properties, simple fabrication technology, easiness to control technology parameters, small investment and adaptability to large-scale industry production [31].

2.3 – Al/Intermetallic Compound FGMs

The fabrication of the Al/intermetallic compounds FGMs by the centrifugal method can be classified into two categories based on the relation between the processing temperature and the *liquidus* temperature of master alloy [10,11,20,26-28,30]. One is the centrifugal solid-particle method where the processing temperature is lower than the *liquidus* temperature of the master alloy and the dispersed solid phase in the master alloy remains in a liquid matrix. The mechanism to form a graded composition is the same as the case of metal/ceramic FGMs by the centrifugal method. The other is the centrifugal *in-situ* method where the processing temperature is higher than the *liquidus* temperature of the master alloy. Al/Al_3Ti and Al/Al_3Zr FGM are typical examples of systems fabricated by the centrifugal solid-particle method. The *liquidus* temperature of Al-Ti and Al-Zr master alloys are higher than the processing temperature. Al/Al_3Ni and Al/Al_2Cu FGMs are examples of the application of the centrifugal *in-situ* method. The *liquidus* temperatures of both Al-Ni and Al-Cu master alloys are lower than the processing temperature. It should be referred that a system such as the Al/(Al_3Ti+Al_3Ni) is named a hybrid FGM because the fabrication is done at the same time with the centrifugal solid-particle and *in-situ* methods [27,29]. It uses Al-Ti and Al-Ni master alloys simultaneously and the processing temperature is lower than the *liquidus* temperature of the Al-Ti master alloy but higher than that of the Al-Ni master alloy.

In this work the processing method of the systems Al/Al_3Ti and Al/Al_3Zr FGMs, will be described, where Al_3Ti and Al_3Zr have a higher melting point than the processing temperature. The initial master alloys for the fabrication of the Al/Al_3Ti and Al/Al_3Zr FGMs were commercial Al alloys with 5 mass % Ti and 5 mass % Zr, which contains Al_3Ti and Al_3Zr in Al matrix, respectively. Since the melting temperature of these intermetallics platelets are relatively high (i.e., 1615 K for Al_3Ti [11], and 1860 K for Al_3Zr [31]), the alloys were heated to a temperature (1173 K) where the platelets remained solid in the liquid Al matrix and a centrifugal force was applied during the casting process. Three levels of centrifugal force were applied, which are characterized by *G* numbers of 30, 60 and 120. Here, the *G* number is the ratio of the centrifugal force to gravity and is given by the following equation [10,11,17,20,25]:

$$G = 2D_0N^2 \qquad (2.1)$$

where D_0 is the diameter of the cast ring (m) and N is the velocity of the mould rotation (s^{-1}).

It is well known that the particle size distribution, as well as, the volume fraction of particles in particle-reinforced, or dispersion-strengthened, composite material plays an important role in controlling its properties [20]. Therefore, a detailed knowledge of particle distributions is required to predict the corrosion, wear and tribocorrosion behaviour of the FGMs.

It is also known that the motion of a particle in a viscous liquid under centrifugal force is explained theoretically by the Stokes law [11,20,25]. Because the velocity of a particle is proportional to the square of the particle diameter, the migration distance is greater in the case of larger particles. In the FGMs fabricated by the centrifugal solid-particle method, therefore, the particle size and the volume fraction are also expected to be distributed along the radial direction. Results show that large particles migrate faster than small particles i.e. the gradient of particle size arises [20]. The gradients, depending on the characteristics of the particles, can be controlled by the difference of migration rate among particles contained in the melt [17]. Consequently, the density of the ring will increase toward the outer periphery of the ring when the densities of particles are higher than that of the melt matrix [25]. Another important feature is that a large number of platelets are arranged with their platelet planes nearly normal to the radial direction, i.e., the centrifugal force direction. There is a tendency for the platelets to align their platelet planes perpendicular to the centrifugal force direction. It was also found that as the G number becomes larger, the orientation of the platelets becomes stronger. The orientation of the platelets was from the angular velocity gradient of the melt along the radial direction produced by the difference in the viscosity [10,11].

Since various processing parameters significantly influence the gradient distribution of dispersed particles during FGM fabrication, it becomes difficult to control the distribution of particles. The composition gradation was studied by computer simulation by Watanabe et al. [11,17]. The process of the composition gradient formation under a centrifugal force was simulated by considering the movement of each spherical particle, which is suspended in the viscous liquid. The effect of processing parameters on the gradient distribution of dispersed particles is show in Table 2.1.

Table 2.1 – Effect of processing parameters on the gradient distribution of the dispersed particles [11].

Processing Parameter	Gradient distribution	
	Gentle	Steep
G number	Small	Large
Volume fraction of particle	Large	Small
Particle size	Small	Large
Difference in density between the melt and particle	Small	Large
Viscosity of the melt	Large	Small
Applied period	Short	Long
Ring thickness	Thick	Thin

Figure 2.2 shows a schematic representation of the apparatus that was used for the manufacture of Al/Al_3Ti and Al/Al_3Zr FGMs by the centrifugal method. The ingots are melted inside the furnace under an argon gas atmosphere and the plug is pulled out to cast the molten metal directly into the rotation mould through the inlet. The rotating mould is preheated before the casting process. After casting, the mould-heating furnace is removed and the mould is cooled in air until complete solidification occurred. The manufactured rings have an outer diameter of 90 mm, 25 mm in height and a length of 20-25 mm.

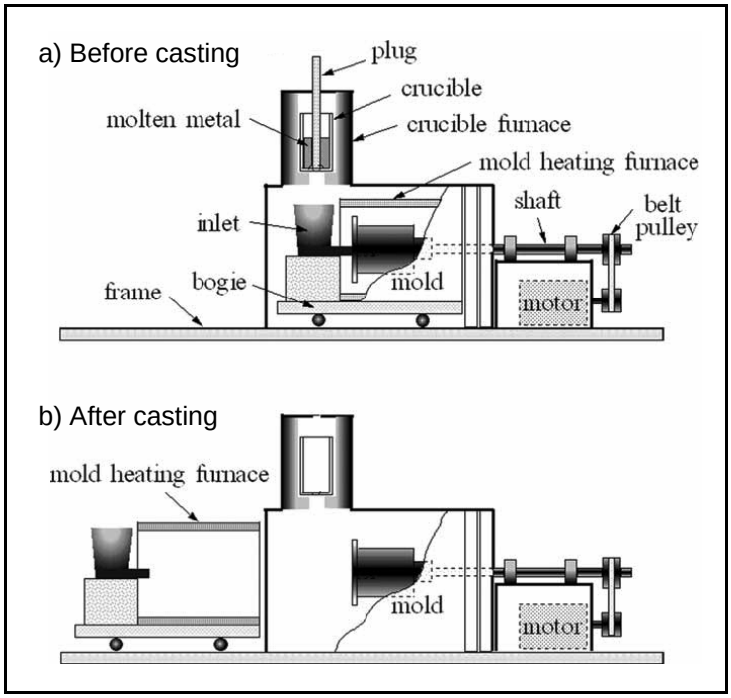

Figure 2.2 – Schematic representation of the centrifugal casting system [26].

2.4 – Electrochemical Characteristics of Intermetallic Phases and Al-MMC

Research on the mechanical and corrosion properties of aluminium matrix composites is still at the development stage, but the outlook is very promising. In recent years the aerospace, military and automotive industries have been promoting the technological development of composite materials to achieve good mechanical strength/density and stiffness/density ratios [13,14,23,26,33].

One of the main obstacles to the use of composite materials is the influence of the presence of the reinforcement on the corrosion resistance. This is particularly important in Al alloy based composites, where a protective oxide film imparts corrosion resistance. The addition of a reinforcing phase could lead to further discontinuities in the film, increasing the number of sites where corrosion can be initiated and rendering the composite liable to severe attack [33]. In the case of pure metals, pitting resistance is dependant on the electrochemical stability of the passive film. However in the case of Al alloy based composites, pitting is influenced by the distribution of particles. Commonly such particles will exhibit electrochemical characteristics that differ from the behaviour of the matrix, rendering the alloy susceptible to localized forms of corrosion [33-36].

Pitting attack is reported to be the major form of corrosion in Al/SiC MMCs. Studies on aluminium matrix composites have shown that a larger amount of pits are formed on composites than on unreinforced alloys. Investigations to date have focused on the effect of reinforcement and intermetallic cathodic phases on the pitting behaviour [33-36]. Preferential attack occurs at the reinforcement/matrix interface. Furthermore, pores, matrix second phases and interfacial reaction products can all influence corrosion behaviour in a significant way [33].

In Al alloy based composites, the pit morphologies are circumferential and appear as a ring of attack around a more or less intact particle or particle colony. The attack appears to be mainly in the matrix phase. This type of morphology has been ascribed to localized galvanic attack of the more active matrix by the nobler particle [33-36].

Birbilis and Buchheit [34] characterized the electrochemical behaviour of intermetallics found in 7XXX series alloys, many of which are applicable to several other alloys and which are present in systems under study in this dissertation: Al_3Ti and Al_3Zr. The electrochemical characterization of the intermetallics was carried out using a microcell method, which was filled with 0.01, 0.1 and 0.6 M NaCl solution at pH 6 (see Table 2.2). The results took to the following classification: Al_3Ti are noble particles with high electrochemical activity, $E_{Al3Ti}>E_{alloy}$, with the ability to sustain large cathodic current. Such intermetallics are possibly associated to peripheral pitting; Al_3Zr are noble particles with low electrochemical activity. Although $E_{Al3Zr}>E_{alloy}$, these particles do not produce large cathodic currents and may be too small to adversely affect corrosion kinetics. Pitting is not often associated with these intermetallics.

Table 2.2 – Corrosion potential immersed in 0.01, 0.1 and 0.6 M NaCl solutions.

Stoichiometry	Corrosion potential (mV_{SCE})		
	0.01 M	0.1 M	0.6 M
Al (99.9999)	- 679	- 823	- 849
7X75 Matrix*	- 699	- 799	- 812
Al_3Zr	- 752	- 776	- 801
Al_3Ti	- 620	- 603	- 799

*The phase denoted as 7X75 matrix is the particle-free matrix-phase ofAA7474.

Pardo et al. [33] studied the influence of the volume fraction of SiC reinforcement in aluminium matrix composites (A360/SiC/10p, A360/SiC/20p, A380/SiC/10p, A380/SiC/20p) immersed in 3.5 mass % NaCl solution by potentiodynamic polarization. The experimental results showed that in both cases the corrosion of the composites intensifies as the concentration of SiC particles increases. During the first 5 days of immersion, chloride ions cause nucleation and gromassh of pits. The nucleation pits begin preferentially at the matrix/SiC_p and matrix/ intermetallic compounds interfaces. After approximately 5 days of immersion, there is very significant hydration induced growth of an $Al_2O_3 \cdot 3H_2O$ porous layer. The formation of this layer leads to a decrease in the corrosion rate and to an increase of the degree of protection in the materials.

The desirable mechanical properties of Al/Al_3Ti and Al/Al_3Zr FGMs are developed as a result of heterogeneous microstructures of Al-Ti and Al-Zr commercial aluminium alloys by the centrifugal method [26]. This work intends to study the effect of the particle intermetallics, Al_3Ti and Al_3Zr on the corrosion resistance of Al/Al_3Ti and Al/Al_3Zr FGMs, respectively, by electrochemical techniques.

2.5 – EIS Fundamentals and Equivalent Circuits

A perturbation sinusoidal voltage $E = E_0 \sin(\omega t)$ is applied at frequency ω to the electrode system under test in electrochemical impedance spectroscopy (EIS) measurement. The response is analysed in terms of the resultant current $I = I \sin(\omega t + \alpha)$, where α represents a characteristic phase angle shift. The corresponding complex impedance spectrum $Z(\omega)$, obtained by varying the signal frequency ω, is expressed in terms of the displacement of the vector $Z(\omega)$. In the plane of Cartesian co-ordinates, an impedance is expressed by its real (Z_R) and imaginary (Z_I) parts, i.e., $Z(\omega) = Z_R + jZ_I$. The modulus $|Z|$ and phase angle α of $Z(\omega)$ can be obtained from $|Z| = \sqrt{Z_R^2 + Z_I^2}$ and $\alpha = \arctan(Z_R / Z_I)$, respectively. Over a frequency bandwidth of interest, the impedance spectrum can be presented in various ways; typically in the well-known plot of Nyquist (Z_I as the Y-axis and Z_R as the X-axis vs ω) or Bode plots ($|Z|$ and α vs ω) [37-40].

The impedance spectrum reflects dialectic behaviour, oxidation-reduction reactions and mass migration across the electrochemical interface, which is determined by the electrical and chemical properties of the corrosive medium, and the electrode materials. Modelling of EIS spectra, which forms an essential part of EIS studies, uses an equivalent circuit to describe the electrochemical interface, such that the theoretical impedance of a proposed circuit can be derived as a multivariable function. By adjusting the variables one can achieve the fit of the theoretical spectrum to the experimental one within the frequency domain. Then, the information regarding the electrochemical corrosion can be extracted through the appropriate interpretation of the variables [37,38,40]. Followed it is described two types of behaviours, non-active metals and active metals.

The non-active metals may have high enough chemical stability in molten-salt systems. This fact may mean that these metals do not have enough activation to react

easily with molten salts [39]. The equivalent circuit for this impedance response is simple and can be described by Figure 2.3 a), where R_Ω represents the molten-salt resistance, C_{pf} the capacitance of the passive film, and R_{pf} the resistance of the passive film [37,38].

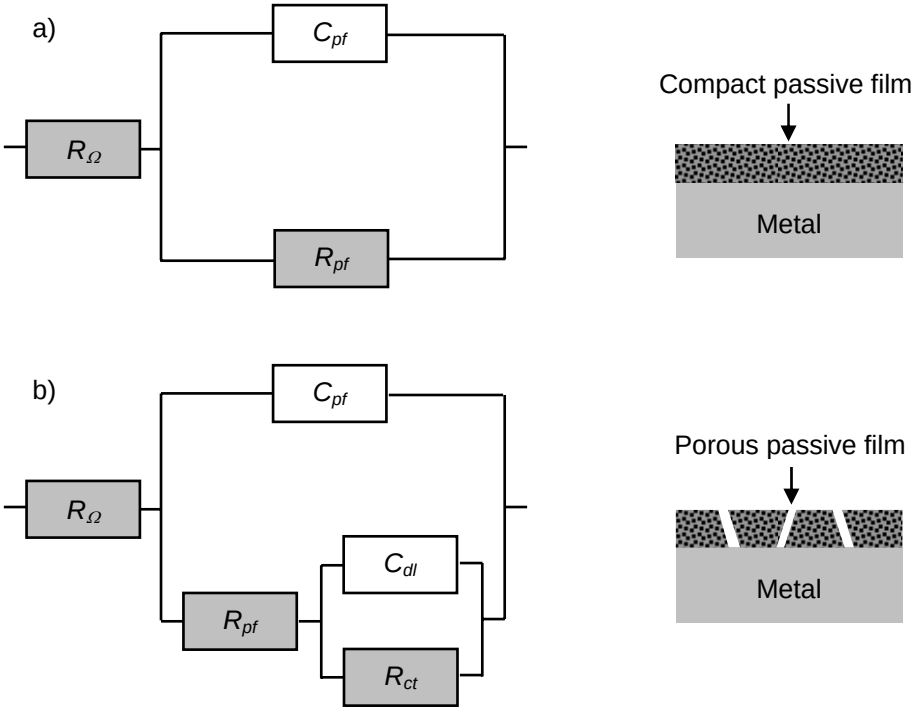

Figure 2.3 – Equivalent circuits: a) Compact oxide film; b) Porous passive layer.

In the case of active metals suffering from localized corrosion, the system will be different. Molten-salt corrosion often exhibits localized fast attack besides uniform attack. Under these conditions, the so-called localized fast attack just means the local fast growth of scale, not internal oxidation. The localized corrosion zone may be covered with a non-productive scale or directly exposed to the molten salts, while the rest (slow corrosion zone) is covered with a more protective scale. Obviously, the reaction along the slow corrosion site and that along the fast corrosion site occur co-ordinately. Both processes are physically parallel. At the slow corrosion zone, the charge transfer resistance at the scale/melts interface may be neglected compared with the transportation resistance of ions in the scale [39]. Thus, this kind of localized corrosion can be represented by the equivalent circuit of Figure 2.3 b), where R_Ω is the ohmic resistance of the electrolyte, R_{pf} the resistance of the passive film, C_{pf} the

capacitance of the passive film, C_{dl} double-layer capacitance, R_{ct} charge-transfer resistance [37,38].

The theory of this powerful analysis technique is detailed in Refs. 37 and 38.

2.6 – Tribogical Behaviour of the Particulate Reinforced Al-Based MMCs

MMCs, in particular the aluminium Al-based MMCs, have been widely researched for various applications, such aerospace and automotive components. This wider interest is because of the fact that these composites have better higher strength, hardness, strength to weight ratio, wear resistance and in some cases have higher strength at relatively elevated temperatures over conventional monolithic base Al alloys [41-45]. Ceramics fibres, whiskers, and particle reinforced aluminium alloys are now considered as candidate tribomaterials [42,44]. The strength of discontinuously reinforced MMCs is not as high as that of continuously reinforced composites, but the properties and cost of discontinuous MMCs make them useful as wear-resistance materials [41]. For example, Motorola's Iridium satellites structural parts are made of ceramic reinforced particle aluminium matrix composites (PMMC). Other examples include ventral fins guide vanes in Pratt & Whitney 4000 series turbine engines, GM Corvettes and pickups drive shafts, electric vehicle brake rotors, racing bicycle parts and golf clubs [43]. Most of PMMCs use reinforcement that range in diameter from 3 to 80 μm [43]. PMMCs can be produced through a number of routes including melt processing and powder metallurgy. Melt processing has some important advantages, e.g. better matrix–particle bonding, easier control of matrix structure, simplicity and low cost of processing compared with powder metallurgy [46].

There have been a large number of studies of the friction and wear properties of these materials. However, discrepancies among the results have been reported. These discrepancies may come from the large number of variables which can affect wear mechanisms and wear rates. These include, as principal tribological parameters that control the friction and wear performance of discontinuously reinforced aluminium composites, two categories [47]: mechanical and physical factors (extrinsic to the material undergoing surface interaction), e.g. the effect of normal load on the tribo-

contact, the sliding velocity, the sliding distance (transient and steady state period), the reinforcement orientation for non-equiaxed particulates, the environment and temperature, the surface finish and the counterpart; and material factors (intrinsic to the material undergoing surface interaction), e.g. the reinforcement type, the reinforcement size and size distribution, the reinforcement shape, the matrix microstructure, and finally the reinforcement volume fraction. As a result, a general statement can not be made concerning the wear rate of a composite in relation to the matrix. In some cases, the composite has a wear rate lower than that of the matrix alloy [41-46] and in others the composite has a higher wear rate than the matrix alloy [48].

Till date, the wear investigation on composites has been limited essentially to Al-composites reinforced with SiC [45,46,48,50] or Al_2O_3 [41,43,44,49] and the experiments were reportedly carried out mostly using pin-on-disc [41,43-46,48-50] and ball-on-plate tribometers [42] and under unidirectional sliding mode. The presence of these hard reinforcing particles reduced wear rates; however, sometimes they increased wear rates because of poor matrix bonding [45]. Since particulate reinforced aluminium matrix composites (AlMCp) are currently being considered as promising tribological materials it is of interest to study wear behaviour of Al-Al_3Ti and Al/Al_3Zr FGMs. Compared to ceramic reinforcements, employing intermetallics as wear resistant reinforcements has advantages. In addition to their high level of hardness, elastic modulus, melting temperature and thermal stability, the thermal expansion coefficients of intermetallics such as Al_3Ti and Al_3Zr are much closer to those of Al matrix because they are formed through peritectic reaction and congruent melting. This smaller difference in thermal expansion coefficients will lower the residual stress at reinforcement/ matrix interfaces when the composite is exposed to thermal cycles, hence assuring a lower degree of failure originated at the interface. These functionally graded composite materials contain reinforcement particles whose volume fraction varies continuously from the inner to the outer sections of the part thereby providing a controlled non-uniform microstructure with continuously changing properties [26]. This optimised combination of surface and bulk mechanical properties may be a promising solution for better wear resistance considering the aforementioned aspects of containing MMCs. Although, the real effect of the reinforced particle content on the improvement of wear behaviour is not yet clear [51].

Z.H. Melgarejo et al. [52] reported the wear response Al-FGM reinforced with AlB_2 particles produced by centrifugal casting process. The cylindrical samples obtained are show in Figure 2.4 (16 mm in diameter and 20 mm in length). The wear tests were conducted on the external and internal zones of the samples using ball-on-disk configurations using a AISI 410 martensitic stainless steel ball as counterbody. Results indicate that the hardness values, wear test results, and wear track analysis were consistent with the microstructural gradient (these FGMs have two distinct zones, a zone rich in particles and a particle – free zone). In effect, the higher volume density of reinforcing boride particles in the outer regions of the centrifugally cast samples translates into a higher hardness and higher overall wear resistance on those regions. On the other hand, the internal regions were fairly depleted of boride reinforcement particles and, thus, were subject to higher wear rates.

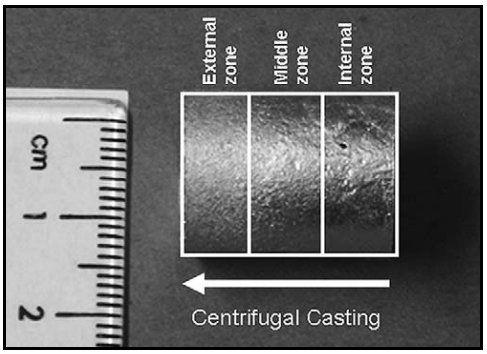

Figure 2.4 – Cylindrical sample obtained by centrifugal cast and mapped longitudinal zone [52].

J. R. Gomes et al. [53-55] have several papers where the tribological behaviour of Al-Si/SiC_p MMCs vs. FGMs against nodular cast iron is compared using the pin-on-disc configuration. Results indicated superior wear resistance of the FGM composites when compared to homogeneous MMCs.

Y. Watanabe et al [9] examined the wear properties on an Al/Al_3Ti FGM manufactured by centrifugal casting. In particular, the influence of the oriented Al_3Ti platelets in the matrix on the tribological behaviour was analysed. A block-on-ring type wear apparatus was used for the wear tests and a S45C steel disc as counterface. Results are shown in Figure 2.5. As it can be observed, Al/Al_3Ti FGM present superior wear resistance when compared with a pure Al specimen manufactured by the same process.

There was a notable difference in the wear volume among the three tested platelets orientations. Specimen B had a lowest wear resistance among the three orientations, while specimens A and C had similar and relatively better level of resistance than sample B. In the case of the specimen tested along the Al_3Ti platelets thickness direction, the Al_3Ti platelets could break easily.

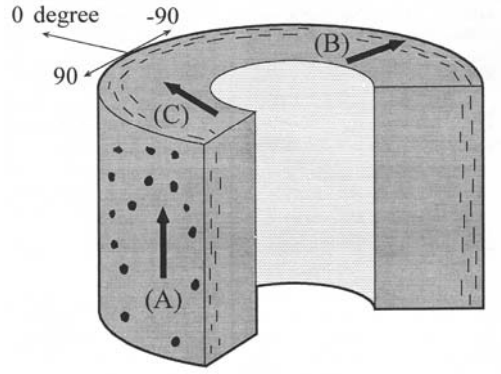

a) Schematic representation of the arrangement of Al_3Ti particles and wear test direction in an Al/Al_3Ti FGM ring. In it, (A) is the wear plane nearly coincides with Al_3Ti platelets planes; (B) and (C) are wear planes coincide with their two edge planes, namely, along the thickness direction and longitudinal direction of the Al_3Ti planes respectively.

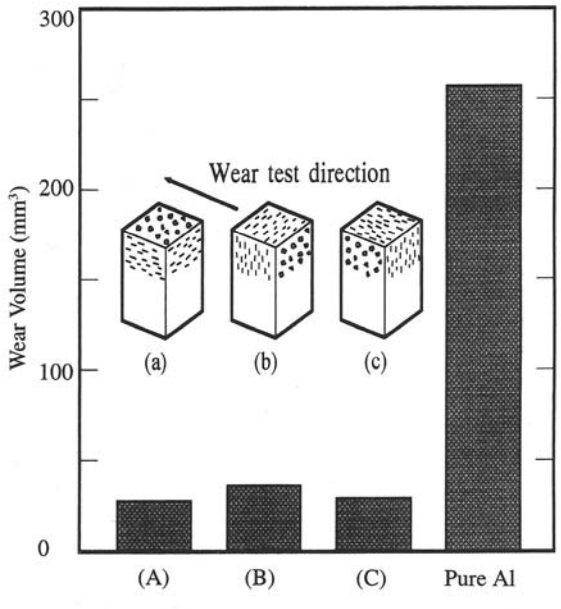

b) Histogram the effect of Al_3Ti reinforced particles on wear rates of the Al matrix FGM.

Figure 2.5 – Ring and wear behaviour of Al/Al_3Ti FGM manufactured by a centrifugal method [9].

However, still few studies have been devoted to the behaviour of these classes of materials under conditions where the material suffers degradation by chemical-electrochemical-mechanical processes. In fact, the investigation of the synergistic effects of wear and corrosion (tribocorrosion) in particulate-reinforced aluminium matrix composites is limited in published works. [56-57]. The interactions between both kinds of phenomena is, however, of the utmost importance for engineering applications.

2.7 – Tribocorrosion Process

Tribocorrosion results from the interaction of mechanical (wear) and chemical (corrosion), which contribute to material removal from sliding surfaces exposed to corrosive environments, such as aqueous lubricants. Two main mechanisms contribute to the material removal from a metal under tribocorrosion conditions: wear accelerated corrosion and mechanical removal from the sliding contact. Wear accelerated corrosion arises from the fact that an asperity sliding on a metal surface produces a track of clean metal which is usually more sensitive to corrosion than the same surface under no sliding conditions. The second mechanism involves the mechanical removal of metal particles by asperities digging below the surface [58-61].

In tribocorrosion phenomena is important to distinguish metal loss due to chemical or electrochemical oxidation from metal removed due to mechanical wear. In an electrochemical experiment the amount of anodically oxidized metal is determined from the measured current using Faraday's law [59]:

$$V_{chem} = \frac{Q \cdot M}{n \cdot F \cdot \rho} \qquad (2.2)$$

where V_{chem} is the volume of metal transformed by anodic oxidation, $Q = \int I\,dt$ is the electric charge generated during the process, which is obtained by integrating the measured current I over the time of the experiment, M is the atomic mass of the metal, n is the charge number for the oxidation reaction (apparent valence), F is the Faraday constant and ρ is the density of the metal.

To apply Eq. (2.2), two conditions must be fulfilled. Firstly, the measured current must be equal to the anodic partial current for metal oxidation, which means that cathodic partial currents due to the reaction of oxidizing agents must be negligible. While this condition is usually fulfilled for anodic polarization well into the passive potential region it may not apply when a highly reactive metal such as titanium is scratched in strongly acid media. Secondly, the charge number n for the oxidation reaction must be known [58].

The total wear volume V_t can be determined by measuring the volume of the wear scar after an experiment or by measuring the rate of descent of the pin during sliding. The latter method provides the instantaneous rate of wear but is applicable only

if no significant amounts of solid reaction products such as third body particles accumulate in the contact during the experiment. From the total wear volume V_t and the chemical wear volume V_{chem} determined from the electric charge, the mechanical wear volume, V_{mech}, which is the volume of metal removed mechanically is obtained by subtraction [59]:

$$V_{mech} = V_t - V_{chem} \qquad (2.3)$$

It should be mentioned that this equation is valid independent of whether anodic oxidation leads to formation of dissolved metal ions or of solid reaction products such as oxide films. Unfortunately, there is no simple way to determine V_{mech} directly.

The tribocorrosion behaviour of sliding contacts under electrochemical control depends on many factors (Figure 2.6). Thus, the performance of electrochemically controlled tribocorrosion systems is conditioned by four types of parameters, namely [58-61]:

1) The mechanical solicitations which are related to equipment design and operation;

2) The electrochemical conditions prevailing at the rubbing metal surfaces;

3) The solution properties at the contact region;

4) The materials involved in the contact and the surface properties of the sample and the antagonist.

These parameters usually do not act independently, but their effects on the tribocorrosion behaviour are mutually dependent.

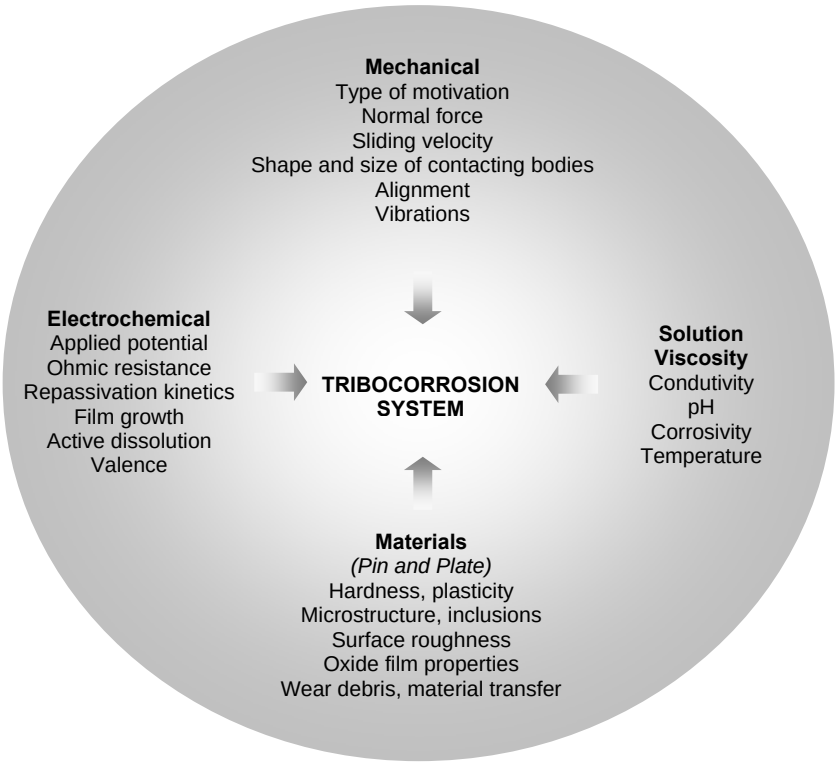

Figure 2.6 – Schematic representation of parameters which affect the tribocorrosion behaviour [59].

2.8 – References

[1] K.I. Moon, S.C. Kim, K.S. Lee, Intermetallics 10 (2002) 185.

[2] Z. Jinxu, H. Gengxiang, W. Jiansheng, J. Mater. Sci. Letters 19 (2000) 1685.

[3] M.V. Karpets, Y.V. Milman, O.M. Barabash, N.P. Korzhova, O.N. Senkov, D.B. Miracle, T.N. Legkaya, I.V. Voskoboynik, Intermetallics 11 (2003) 241.

[4] M. Takeda, T. Kikuchi, S. Makihara, J. Mater.Sci. Letters 18 (1999) 631.

[5] Y.V. Milman, D.B. Miracle, S.I. Chugunova, I.V. Voskoboinik, N.P. Korzhova, T.N. Legkaya, Y.N. Podrezov, Intermetallics 9 (2001) 839.

[6] S.H. Wang, P.W. Kao, Acta Mater. 46 (1998) 2675.

[7] S.H. Wang, P.W. Kao, Scripta Mater. 40 (1999) 289.

[8] Y. Watanabe, N. Yamanaka, Y. Fukui, Z. Metallkd. 88 (1997) 717.

[9] Y. Watanabe, N. Yamanaka, Y. Fukui, Metall. Mater. Trans. A 30A (1999) 3253.

[10] Y. Watanabe, Y. Fukui, Rec. Res. Devel. Metall. Mater. Sci. 4 (2000) 51.

[11] Y. Watanabe, Y. Fukui, Aluminum Trans. 2 (2000) 195.

[12] Y. Watanabe, H. Eryu, K. Matsuura, Acta Mater. 49 (2001) 775.

[13] P.D. Sequeira, Y. Watanabe, L.A. Rocha, Mater. Sci. Forum, 492 (2005) 609.

[14] P.D. Sequeira, Y. Watanabe, L.A. Rocha, Sol. Stat Phen. 105 (2005) 425.

[15] Y. Fukui, JSME Int. J. Series III 34 (1991) 144.

[16] Y. Fukui, H. Kinoshita, K. Nakanishi, JSME Int. J. Series I 35 (1992) 95.

[17] Y. Watanabe, N. Yamanaka, Y. Fukui, Composites Part A 29A (1998) 595.

[18] J.W. Gao, C.Y. Wang, Mater. Sci. Eng. A292 (2000) 207.

[19] Y. Watanabe, N. Yamanaka, Y. Oya-Seimiya, Y. Fukui, Z. Metallkd. 92 (2001) 53.

[20] Y. Watanabe, A. Kawamoto, K. Matsuda, Compo. Sci. Tech. 62 (2002) 881.

[21] R. Rodríguez-Castro, R.C. Wetherhold, M.H. Kelestemur, Mater. Sci.Eng. A323 (2002) 445.

[22] R. Rodríguez-Castro, J. Mater. Sci. 37 (2002) 1813.

[23] A.J.C. Velhinho, Ph.D. Tesis, Universidade Nova de Lisboa, Lisboa, 2003.

[24] N.B. Duque, Z.H. Melgarejo, O. M. Suárez, Mater. Characterization 55 (2005) 167.

[25] T. Ogawa, Y. Watanabe, H. Sato, I.-S. Kim, Y. Fukui, Composites Part A (2005) in press.

[26] P.D. Sequeira, Ph.D. Tesis, Nagoya Institute Technology, Nagoya, 2006.

[27] Y. Watanabe, Y. Fukui, in Current Issues on Multidisciplinary Microscopy Research and Education, ed A. Méndez-Vilas and L.Labajos-Broncano, FORMATEX, Badajoz, (2004) 189.

[28] Y. Watanabe, R. Sato, K. Matsuda, Y. Fukui, Sci. Eng. Compos. Mater. 11 (2004) 185.

[29] Y. Watanabe, Y. Fukui, Intermetallics 9 (2001) 33.

[30] Y. Watanabe, S. Oike, Acta Mater. 53(200)1631.

[31] Q. Wang, Y. Wei, W. Chen, Y. Zhu, C. Ma, W. Ding, Mater. Letters 57 (2003) 3851.

[32] W. Miao, K. Tao, B. Li, B.X. Liu, J. Phys. D: Appl. Phys. 33 (2000) 2300.

[33] A. Pardo, M.C. Merino, S. Merino, F. Viejo, M. Carboneras, R. Arrabal, Corros. Sci. 47 (2005) 1750.

[34] N. Birbilis, R. G. Buchheit, J. Electrochem. Soc. 152 (2005) B140.

[35] A. Aballe, M. Bethencourt, F.J. Botana, M.J. Cano, M. Marcos, Corros. Sci. 45 (2003) 161.

[36] A. Barbucci, G. Bruzzone, M. Delucchi, M. Panizza, G. Cerisola, Intermetallics 8 (2000) 305.

[37] R.G. Kelly, J.R. Scully, D.W. Shoesmith, R.G. Buchheit, Electrochemical Techniques in Corrosion Science and Engineering, Marcel Dekker Inc., New York (2003).

[38] W.S. Tait, An Introduction to Electrochemical Corrosion Testing for Practicing Engineers and Scientists. PairODocs Publications, Racine, WI (1994).

[39] C.L. Zeng, W. Wang, W.T. Wu, Corros. Sci. 43 (2001) 787.

[40] C. Liu, Q. Bi, A. Leyland, A. Matthews, Corros. Sci. 45 (2003) 1243.

[41] O. Yilmaz, S. Buytoz, Compos. Sci. Technol. 61 (2001) 2381.

[42] D. Roy, B. Basu, A.B. Mallick, Intermetallics 13 (2005) 733.

[43] A.M. Al-Qutub, I.M. Allam, T.W. Qureshi, J. Mater. Process. Technol. 172 (2006) 327.

[44] M. Kök, Composites: Parte A 37 (2006) 457.

[45] M. Muratoglu, M. Aksoy, J. Mater. Process. Technol. (2006) in press.

[46] Y. Sahin, Mater. Des. (2006) in press.

[47] A.P. Sannino, H.J. Rack, Wear 189 (1995) 1.

[48] R. Dasgupta, J. Compos. Mater.39 (2005) 1561.

[49] H. Sevik, S.C. Kurnaz, Mater. Des. 27 (2006) 676.

[50] P.N. Bindumadhavan, T.K. Chia, M. Chandrasekaran, H. K.Wah, L. N. Lam, O. Prabhakar, Mater. Sci. Eng. A315 (2001) 217.

[51] J.R. Gomes, A. Ramalho, M.C. Gaspar, S.F. Carvalho, Wear 259 (2005) 545.

[52] Z.H. Melgarejo, O. M. Suárez, K. Sridharan, Scripta Mater (2006) in press.

[53] J.R. Gomes, A.S. Miranda, D.F. Soares, A.E. Dias, L.A. Rocha, S.J. Crnkovic, R.F. Silva, Ceramics Trans. 114 (2000) 579.

[54] J.R. Gomes, A.S. Miranda, L.A. Rocha, S.J. Crnkovic, V. Silva, R.F. Silva, Int. J. Appl. Mech. Eng. 7 (2002) 791.

[55] J.R. Gomes, L.A. Rocha, S.J. Crnkovic, R.F. Silva, A.S. Miranda, Mater. Sci. Forum 423 (2003) 91.

[56] A. Velhinho, J.D. Botas, E. Ariza, J.R. Gomes, L.A. Rocha, Mater. Sci. Forum 455-456 (2004) 871.

[57] C.-K. Fang, C.C. Huang, T.H. Chuang: Met. Mater. Trans. A 30A (1999) 643.

[58] G. Zambelli, L. Vincent, Matériaux et Contact, Une Approche Tribologique, Press Polytechniques et Universitaires Romandes, Lausanne, (1998).

[59] D. Landolt, S. Mischler, M. Stemp, Electrochim. Acta 46 (2001) 3913.

[60] P. Jemmely, S. Mischler, D. Landolt, Wear 237 (2000) 63.

[61] P. Ponthiaux, F. Wenger, D. Drees, J.P. Celis, Wear 256 (2004) 459

CHAPTER 3

Corrosion Behaviour of Al/Al_3Ti and Al/Al_3Zr FGMs Produced by Centrifugal Casting

S.C. Ferreira[a], L.A. Rocha[a,b], E. Ariza[a], P.D. Sequeira[a,c], Y. Watanabe[c]

[a]Research Centre on Interfaces and Surface Performance, University of Minho, Campus de Azurém, 4800-058 Guimarães, Portugal

[b]Department of Mechanical Engineering, University of Minho, Campus de Azurém, 4800-058 Guimarães, Portugal

[c]Department of Engineering Physics, Electronics and Mechanics, Graduate School of Engineering, Nagoya Institute of Technology, Gokiso-Chu, Showa-Ku, 466-8555 Nagoya, Japan

Abstract

Aluminium alloys are used in several technological applications. Aluminium itself has weak mechanical properties; hence it is alloyed with other elements to improve its characteristics. The growth of intermetallics in the Al matrix allows a modification of the electrochemical properties of the alloy. In this paper the influence on corrosion behaviour of intermetallics (Al_3Ti or Al_3Zr platelets) formed *in-situ* in two binary alloys (Al-5 mass % Ti and Al-5 mass % Zr) produced by centrifugal casting based in functionally graded materials (FGMs) is evaluated. The corrosion resistance of Al/Al_3Ti and Al/Al_3Zr FGMs in the outermost regions of the ring samples was investigated and discussed with aid of electrochemical measurements (potentiodynamic polarization and electrochemical impedance spectroscopy, EIS). After polarization test, the morphological features of the surfaces were analysed by SEM to identify the

prevailing corrosion mechanisms on the surfaces. EIS measurements were performed at increased immersion times (1, 3, 6 and 10 days). All tests were performed at ambient temperature in a 0.6 M NaCl solution.

Keywords: Corrosion, Electrochemical Impedance Spectroscopy (EIS), Al/Intermetallics Compounds, Functionaly Graded Materials (FGMs)

3.1 – Introduction

The corrosion behaviour of aluminium alloys has been the subject of a large number of publications, since the naturally formed oxide film can give excellent protection against corrosion, in addition to the advantages resulting from aluminium's low density [1]. Many commercial aluminium alloys are developed with a wide range of mechanical properties stimulated by careful alloying additions and heat-treatments [2]. According to the Al-Ti and Al-Zr phase diagrams, the intermetallics Al_3Ti and Al_3Zr are formed through peritectic reaction and congruent melting, respectively [3]. Both compounds have similar atomic structures i.e. $D0_{22}$ in Al_3Ti and $D0_{23}$ in Al_3Zr with the same tetragonal space group of I4/mmm and show high melting temperature, low density, good oxidation resistance and good thermal stability [4].

The corrosion resistance of the aluminium alloys is usually dependent on the metal heterogeneities and/or to the medium or exposure conditions. Heterogeneities in the microstructure can cause formation of cathodic and anodic zones that promote different forms of localized corrosion [5]. The production of local galvanic cells promotes the dissolution of the less noble areas [6]. In the case of the aluminium alloys, the heterogeneities are frequently intermetallic compounds distributed throughout the metallic matrix that can be either anodic or cathodic relatively to the matrix. In the case of the Al_3Ti and Al_3Zr intermetallic compounds, they show a more cathodic potential in comparison with the pure Al. Consequently, depending on the experimental parameters, they are able of provoking localized corrosion in the metallic matrix surrounding the precipitates ($Al_{[99,9999]}$ = -849 mV_{SCE} ; Al_3Ti = -799 mV_{SCE} and Al_3Zr = -801 mV_{SCE} in 0.6 M NaCl solution) [2]. Additionally, the presence of intermetallics in the aluminium

matrix can difficult the growth or promote failures of the protective oxide layer formed in air or in aqueous solutions on alloys that are likely to be passivated [2,5].

Functionally graded metal matrix composites (FGMMCs) are considered as engineered materials systems to achieve optimum performance in the intended application. FGMMCs are produced using techniques that introduce spatial differential distribution of the reinforcing along the component. As end result a gradient of mechanical properties from the surface up to the bulk of the components is obtained. The fabrication of the Al/intermetallic compounds FGMs by the centrifugal method is similar to the fabrication of Al/ceramic FGMs [7-16]. This method, proposed by Fukui et al. [7], is named solid-particle method and is based on the application of a centrifugal force to homogeneous molten composites, dispersed with ceramics or intermetallic particles, leading to the formation of the desired gradation. The composition gradient is then achieved primarily by the difference in the centrifugal force produced by the difference in density between the molten metal and particles. The processing conditions by centrifugal solid-particle as well as the mechanical properties of Al/intermetallic compound FGMs, namely of the Al/Al_3Ti and Al/Al_3Zr systems, have been investigated [15].

In this paper, corrosion behaviour of the Al/Al_3Ti and Al/Al_3Zr FGMs in a 0.6 M NaCl has been studied in the outer region of the FGMs rings manufactured by centrifugal casting. For such, open-circuit potential, potentiodynamic polarisation and electrochemical impedance spectroscopy (EIS) tests were carried out. The EIS spectra were modelled and analysed with an equivalent circuit that reflected the evolution of corrosion behaviour during 1, 3, 6 and 10 days of immersion.

3.2 – Experimental Methods

The Al/Al_3Ti and Al/Al_3Zr FGMs were produced by the centrifugal method, from Al-5 mass % Ti and Al-5 mass % Zr commercial alloys, respectively, as described by Sequeira et al. [15]. Since the relative atomic masses of Al, Ti and Zr are 26.98, 47.88 and 91.22, respectively, the theoretical volume fraction of Al_3Ti in the master alloy was calculated to be approximately 11 vol % and that of Al_3Zr as approximately 7 vol %.

In the centrifugal method the alloy is heated up to a temperature located between its *solidus* and *liquidus* temperatures, were most of the intermetallic platelets remain solid in a liquid Al-based matrix. It is then poured into a rotating mould in order to obtain ring-shaped samples which have an outer diameter of 90 mm, 25 mm in height and a length of 20-25 mm. The temperature of the melting furnace was 1173 K and the applied centrifugal casting forces were 30, 60 and 120 *G* (units of gravity).

The samples were cut (see Figure 3.1.) and grinded using SiC abrasive sandpapers of 180, 400, 600, 800 and 1200 mesh. The polishing was made with diamond abrasive suspensions of 9, 3 and 1 μm. After polishing, samples were ultrasonically cleaned in ethanol for 15 minutes and then in distilled water for 10 minutes and finally dried.

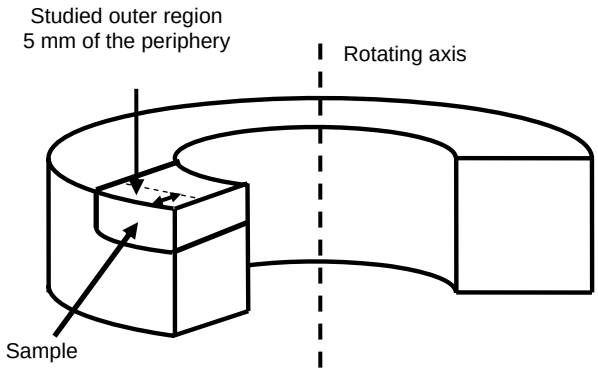

Figure 3.1 – Schematic drawing of the FGM ring and positioning of the cut sample.

The roughness of the specimens was evaluated in a Perthometer S5P roughness meter. Table 3.1 shows the superficial roughness of the samples, calculated as the average of three measurements. The high standard deviation values observed in the Al/Al_3Ti FGMs produced at centrifugal acceleration of 30 *G* and 60 *G* were attributed to the presence of open porosity at the surface of the samples.

The corrosion behaviour was evaluated by potentiodynamic polarization and electrochemical impedance spectroscopy (EIS) tests. All electrochemical tests were performed at ambient temperature in a 0.6 M NaCl solution. The electrochemical cell consisted in a standard three electrode arrangement. The counter electrode was a

platinum sheet with an area of 1 cm^2 and a saturated calomel electrode (SCE) was used as reference. The area of the working electrode was set in 0.385 cm^2. A PGP201 Potentiostat/Galvanostat (Radiometer Denmark), controlled by the VoltaMaster-1 software, was used to carry out the polarization measurements, while a Voltalab PGZ100 Potentiostat (Radiometer Analytical), controlled by the VoltaMaster-4 software, was used for the EIS measurements. Prior to polarization tests, the open-circuit potential (OCP) was monitored during 3600 s, after which the samples were polarized, in the anodic direction, from -1400 to 200 mV at a scan rate of 2 mVs^{-1}. After the polarization test the samples were examined using a scanning electron microscope (SEM). The EIS measurements were performed in the frequency range from 100 kHz to 5 mHz, with an AC sine wave amplitude of 10 mV applied to the electrode at its corrosion potential. EIS measurements were performed at increased immersion times (1, 3 and 6 and 10 days). For EIS data simulation, the ZView2 software was used.

Table 3.1 – Superficial roughness of the samples.

FGMs		$R_a \pm \sigma$ (µm)
Al/Al_3Ti	**30 *G***	0,62 ± 0,53
	60 *G*	0,76 ± 0,66
	120 *G*	0,39 ± 0,03
Al/Al_3Zr	**30 *G***	0,22± 0,06
	60 *G*	0,49 ± 0,16
	120 *G*	0,30 ± 0,23

3.3 – Results and Discussion

3.3.1 – Open-Circuit Potential and Potentiodynamic Polarisation Tests

After being immersed in the 0.6 M NaCl solution, the corrosion potential (E_{corr}) of the samples was monitored during 60 min. The obtained curves are presented in Figure 3.2. As it can be observed all samples reveal an increase in the corrosion potential with the time, indicating the growth of a passive film. The Al/Al_3Ti FGMs samples show similar behaviour (Figure 3.2 a), in terms of thermodynamic stability,

regardless the processing conditions (E_{corr} between -850 and -800 mV). Conversely, the Al/Al_3Zr FGM samples present a more dispersed behaviour. The sample of 30 *G* reveals a E_{corr} (-825 mV) clearly higher than the 60 *G* and 120 *G* samples (E_{corr} ~ -950 mV). The more active corrosion potential exhibited by these last samples reflects its less thermodynamic stability and therefore its higher corrosion tendency.

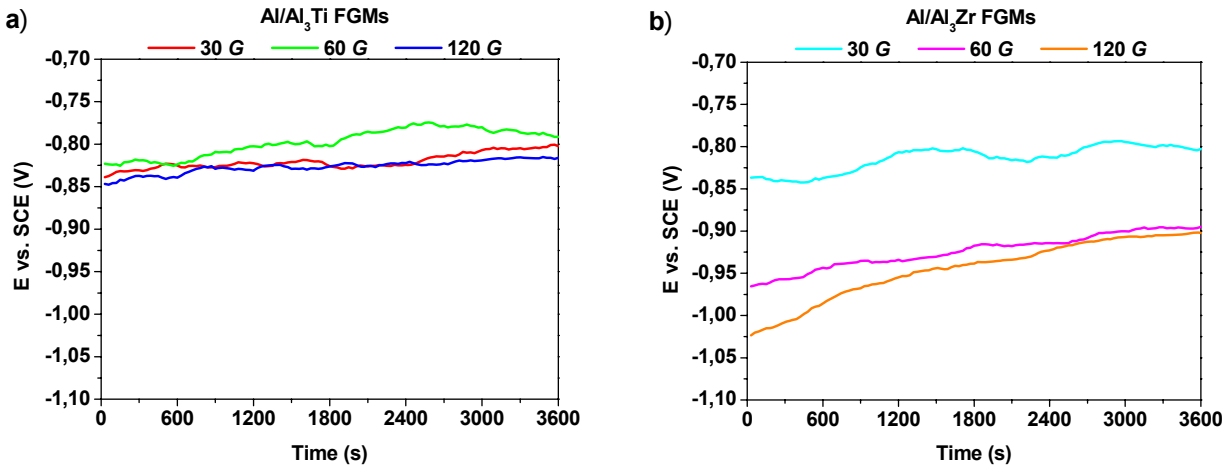

Figure 3.2 – Evolution of corrosion potential with time: a) Al/Al_3Ti FGMs; b) Al/Al_3Zr FGMs.

Figure 3.3 presents the anodic polarisation curves obtained for all samples. As it can be observed in Figure 3.3 a), the corrosion behaviour of Al/Al_3Ti samples is very similar. However, in the case of the Al/Al_3Zr FGMs (Figure 3.3 b), the samples obtained with 60 *G* and 120 *G*, in accordance to the open circuit potential results, reveal the worst corrosion behaviour.

In none of the samples a passive plateau was not detected, indicating active dissolution of the materials. Also, as it can be observed in this figure, the determination of the corrosion current density (i_{corr}) for all samples presents some difficulties because of the signal noise and instability of the samples immersed in the electrolyte.

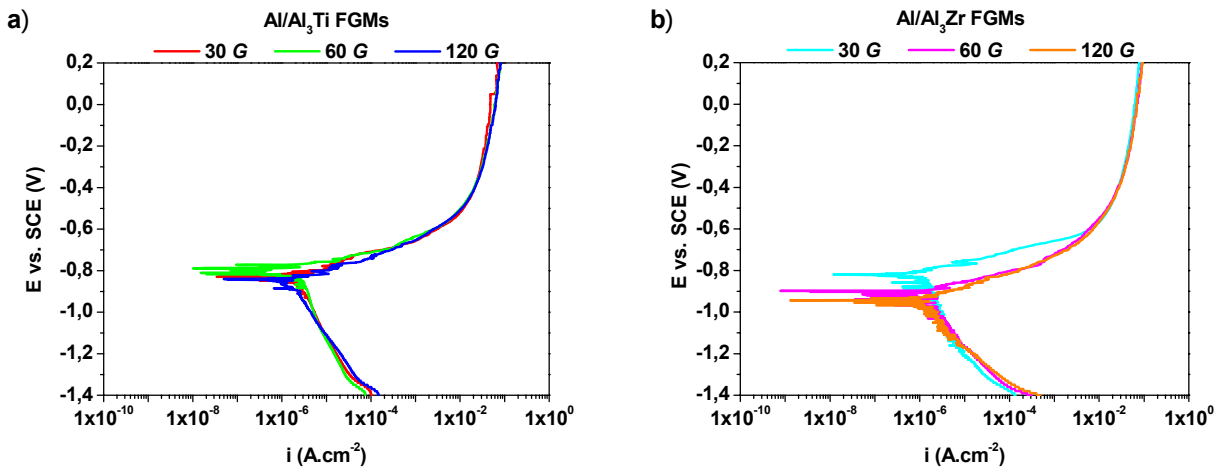

Figure 3.3 – Anodic polarisation curves obtained on FGMs samples: a) Al/Al$_3$Ti FGMs; b) Al/Al$_3$Zr FGMs.

Figure 3.4 shows the surface morphology of the Al/Al$_3$Ti FGMs 120 *G* sample before and after the polarization test. As it can be observed (Fig. 3.4 a) and b), before polarisation the sample presented some porosity, typical of a material processed by casting technologies, that might have contributed to facilitate the penetration of the electrolyte in the material inducing corrosion. Also, the presence of this porosity introduces non-measurable errors on the calculation of the effective area of contact between the material and the solution. After the polarisation tests (Fig. 3.4 c) and d) the sample reveals a large degradation, especially in the adjacent regions to the reinforced particles. As it can be seen the Al$_3$Ti platelets are not attacked (see Figure 3.4 c) and d). Similar behaviour was obtained for the other Al/Al$_3$Ti FGMs samples.

In the case of Al/Al$_3$Zr FGMs samples, representative micrographs obtained by SEM analyses are presented in Figure 3.5. As it can be seen, the concentration of small platelets in Al/Al$_3$Zr FGMs sample appears to be higher than that found in Al/Al$_3$Ti sample (see Figure 3.4). While, Al/Al$_3$Ti 120 *G* sample present platelets with similar thickness, but with some variation on the longitudinal dimension, in the case of Al/Al$_3$Zr 120 *G* , some thick and long platelets are observed together with those possessing smaller dimensions. As observed in Figure 3.5 c) and d), all Al/Al$_3$Zr FGMs samples suffered a high degradation in the adjacent regions to the platelets, with a morphology similar to that observed in the Al/Al$_3$Ti samples, after the polarisation test.

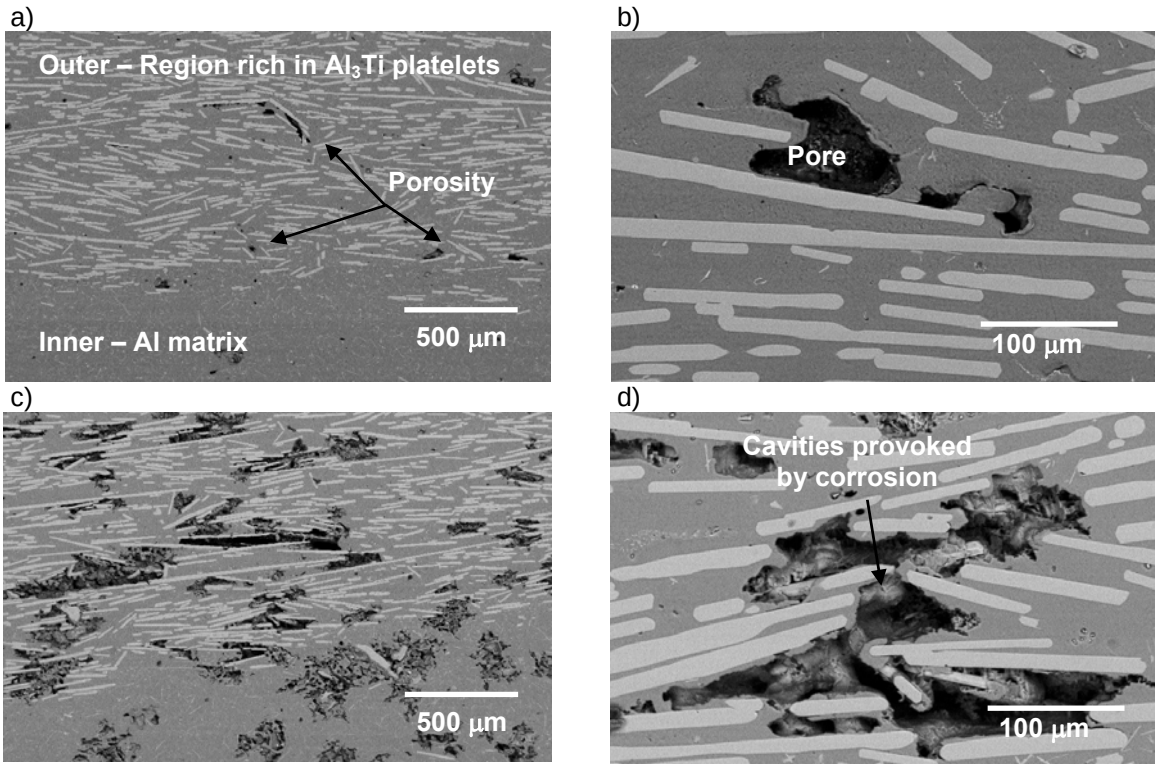

Figure 3.4 – SEM micrographs obtained on Al/Al_3Ti FGMs 120 *G*: Before polarization test: a) and b). After polarisation tests: c) and d).

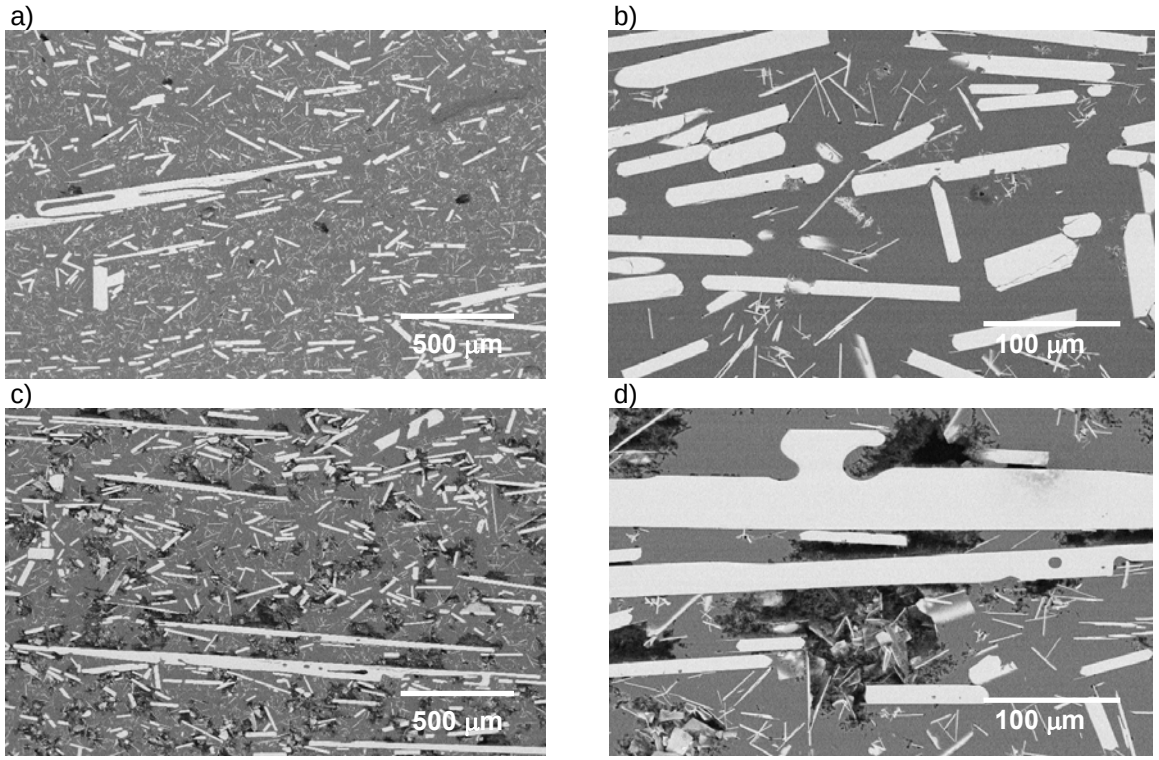

Figure 3.5 – SEM micrographs obtained on Al/Al_3Zr FGMs 120 *G*. Before polarization test: a) and b). After polarisation tests: c) and d).

As indicated by the open circuit potential and potentiodynamic polarisation results, Al/Al_3Zr FGMs samples obtained with 60 *G* and 120 *G* revealed a worst behaviour when compared with the Al/Al_3Zr obtained with 30 *G*. This phenomenon can be explained by the lower area fraction of platelets found in the sample obtained with 30 *G* (see figure 3.6).

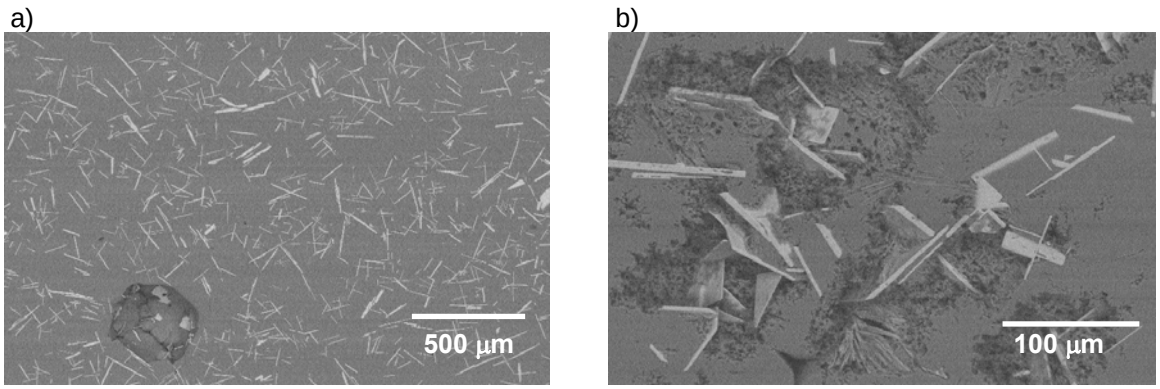

Figure 3.6 – SEM micrographs obtained on Al/Al_3Zr FGMs 30 *G*. Before polarization test: a). After polarisation tests: b).

In fact, as before mentioned, at high applied centrifugal forces, Al_3Zr particles have a higher segregation rate. Therefore we can presume that the degradation of FGMs material intensifies as the concentration of reinforcement platelets increase. In a previous work, Sequeira et al. [15] evaluated the area fraction of these intermetallic compounds and verified that higher applied centrifugal force increases both Al_3Ti and Al_3Zr intermetallic particles area fraction in the outer regions of the FGMs. Moreover, the increase of applied centrifugal force from 60 *G* to 120 *G* does not affect significantly the area fraction for the outermost region of the FGMs but does increase it for the adjacent regions (see Figure 3.7).

Based in these results, the area fraction occupied by particles on the region of the corrosion test was calculated and is present in Table 3.2. In fact, the area fraction of Al_3Ti at the surface of the samples is almost independent on the centrifugal force used for producing them. However, in the Al/Al_3Zr FGMs group, a clear increase in the area fraction with the raise in centrifugal force is observed.

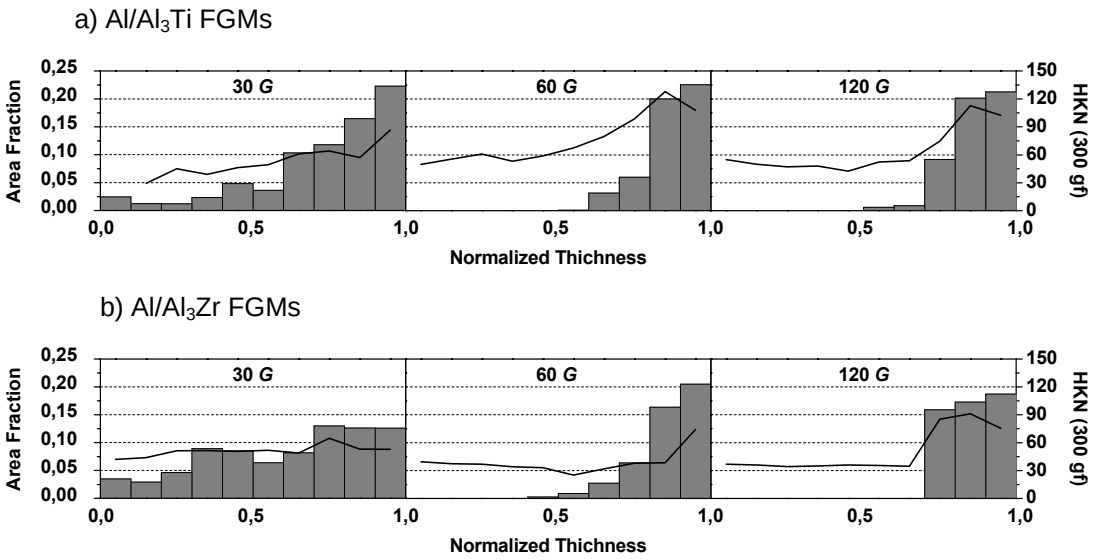

Figure 3.7 – Intermetalic particles area fraction (columns) and Knoop hardness distribution (lines). The outer of the ring is represented as the position 1,0 of the normalized thickness and the inner region by the position 0,0 [15].

Table 3.2 – Area fraction occupied by particles on the region of corrosion test.

Samples	Al/Al_3Ti FGMs			Al/Al_3Zr FGMs		
	30 *G*	60 *G*	120 *G*	30 *G*	60 *G*	120 *G*
Area fraction	0,17	0,17	0,18	0,13	0,15	0,17

Birbilis et al [2] refer that the corrosion resistance of Al alloys is influenced by the presence of intermetallic particles exhibiting different electrochemical characteristics from those of the matrix. When the intermetallic particles are cathodic relatively to the matrix, as it happens with Al_3Ti and Al_3Zr, the circumferential pits appear as a ring of attack around a more or less intact particle. This type of morphology has been ascribed to localized galvanic attack of the more active matrix by the nobler particle.

According to Pardo et al [17], pitting attack is reported to be the major form of corrosion in Al-MMCs. Preferentially, the attack occurs at the reinforcement/matrix interface. Furthermore, pores, matrix second phases and interfacial reaction products can all influence corrosion behaviour in a significant way. The addition of a reinforcing phase could lead to further discontinuities in the film, increasing the number of sites where corrosion can be initiated and rendering the composite liable to severe attack. On

the other hand, more pits are formed on Al matrix composites than on unreinforced alloys.

In fact, for the systems under study in this work, the intermetallic platelets are strongly cathodic when compared with the Al matrix and might act as cathodic regions, facilitating the dissolution of the protective passive film and conducing to a preferential attack in the regions of the matrix near to the reinforcements. Thus, the higher degradation observed in the outer region of Al/Al_3Zr FGMs samples (obtained with 60 *G* and 120 *G*) is explained by the higher concentration of particles (highest cathodic area e.i, lowest anodic area) in this region of the sample when compared with the Al/Al_3Zr FGMs obtained with 30 *G*.

3.3.2 – Electrochemical Impedance Spectroscopy and Spectra Modelling

Experimental EIS results from Al/Al_3Ti and Al/Al_3Zr FGMs after 1, 3, 6 and 10 days exposure to the 0.6 M NaCl solution are presented in the Bode plots in Figures 3.8 and 3.9, respectively. Analysing the graphs corresponding to each material, Al/Al_3Ti FGMs and Al/Al_3Zr FGMs, it is possible to observe some instability at low frequencies. Based on the analysis of the impedance spectra, the equivalent circuit depicted in Figure 3.10 was proposed to describe the corrosion behaviour of this kind of materials. The components of these equivalent circuits are: R_Ω (ohmic resistance of the electrolyte), R_{pf} (resistance of the passive film); C_{pf} (capacitance of the passive film); C_{dl} (double-layer capacitance); R_{ct} (charge-transfer resistance) [18].

The value of polarization resistance, R_p, was calculated by the sum of R_{pf} and R_{ct} [19].

The evolution of R_p, R_{pf} and C_{pf} with the immersion time is presented in Figure 3.11. As it can be seen in Figure 3.11 a), the Al/Al_3Ti 60 *G* sample presents the highest R_p values (from 1 to 10 immersion days) when compared with the other Al/Al_3Ti FGMs samples. The Al/Al_3Ti 30 *G* and 60 *G* samples, present an increase in the R_p values from 1 to 3 immersion days, after this time and until 10 immersion days a slightly decrease in Al/Al_3Ti 60 *G* sample is observed and the Al/Al_3Ti 30 *G* sample reaches the same value than that present in the Al/Al_3Ti 120 *G* sample. Besides, this last sample

presents an increase in the R_p values from 1 to 6 immersion days. The Al/Al3Ti 60 *G* sample, presents highest R_{pf} values, which stay practically constants during all immersion time. The Al/Al_3Ti 30 *G* and 120 *G* samples, starting from 3 days of immersion present the same R_{pf} values. The Al/Al_3Ti 60 *G* sample reveals the lowest C_{pf} values, revealing its better protective character when compared with the other samples. The Al/Al_3Ti 120 *G* sample presents the same tendency with the immersion time, but with higher C_{pf} values. The Al/Al_3Ti 30 *G* sample presents a considerable increase of C_{pf} values from 3 to 10 immersion days revealing a higher decrease in the protective character of the passive film formed when compared with the other two samples. These results are in accordance with the open circuit potential and the potentiodynamic polarization results, which showed a little better corrosion behaviour for Al/Al_3Ti 60 *G* sample (see Figures. 3.2 a) and 3.3 a). This sample shows highest R_p and R_{pf} values and lowest C_{pf} values when compared with the other Al/Al_3Ti FGMs samples.

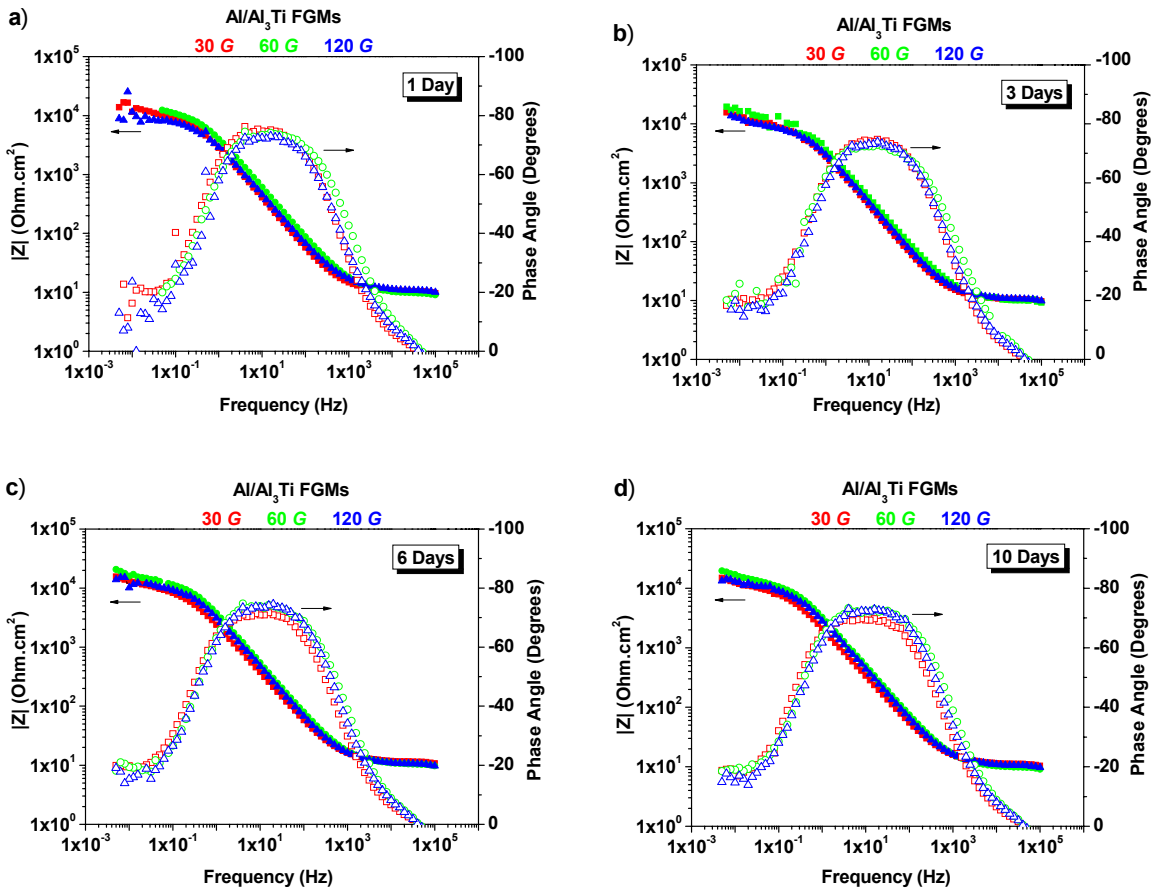

Figure 3.8 – Bode plots of EIS spectra of Al/Al_3Ti exposed to 0.6 M NaCl solution: a) 1day; b) 3 days; c) 6 days and d) 10 days.

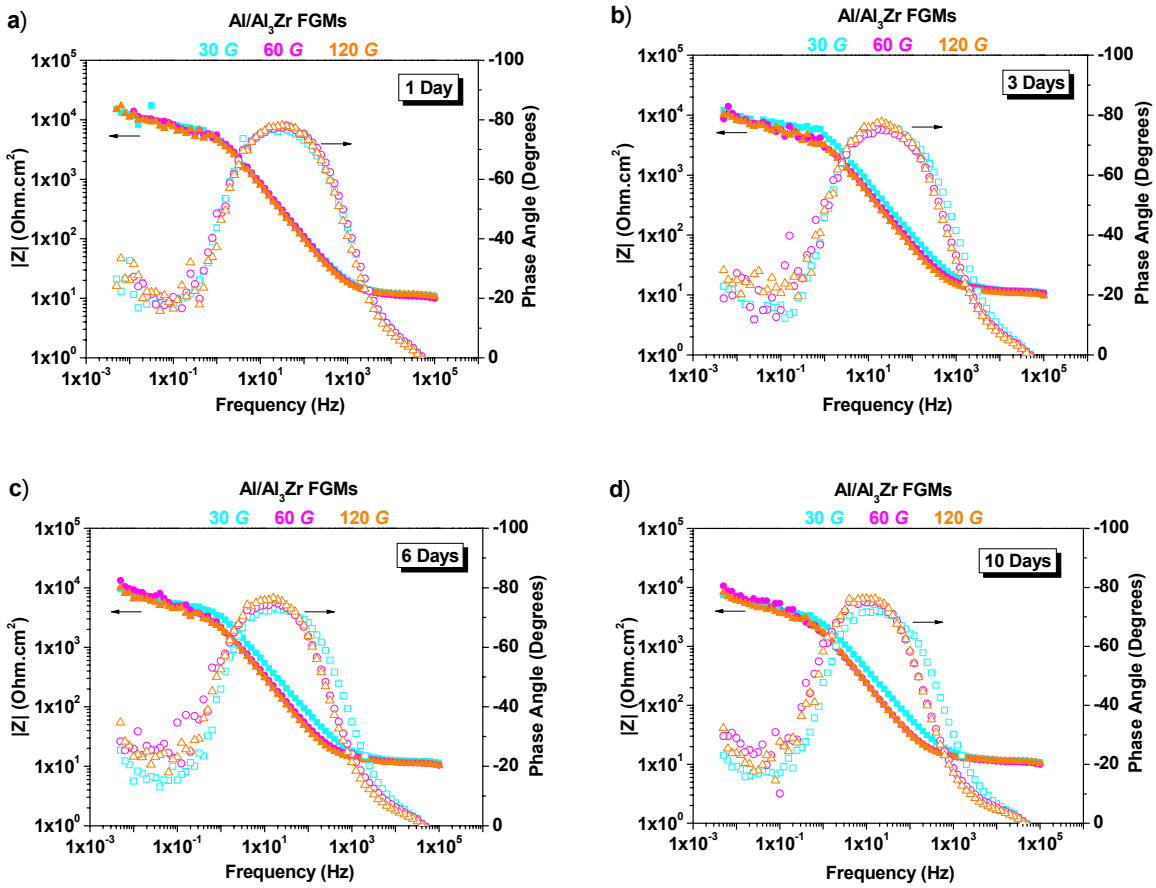

Figure 3.9 – Bode plots of EIS spectra of Al/Al$_3$Zr exposed to 0.6 M NaCl solution: a) 1day; b) 3 days; c) 6 days and d) 10 days.

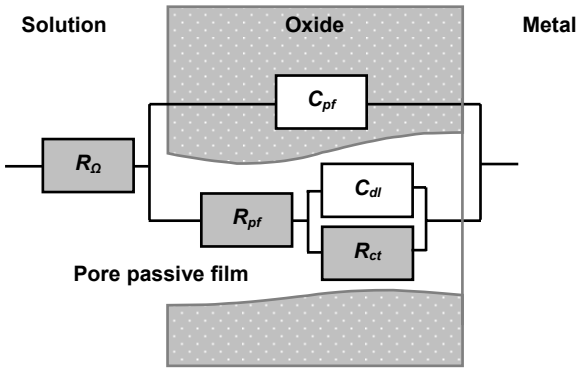

Figure 3.10 – Equivalent circuit used for fitting the experimental data and its possible corresponding physical structure used for the Al/Al$_3$Ti FGMs and Al/Al$_3$Zr FGMs. Equivalent circuit: (R_{pf}) resistance of the passive film; (R_{Ω}) ohmic resistance of the electrolyte; (C_{pf}) capacitance of the passive film; (C_{dl}) double-layer capacitance; (R_{ct}) charge-transfer resistance.

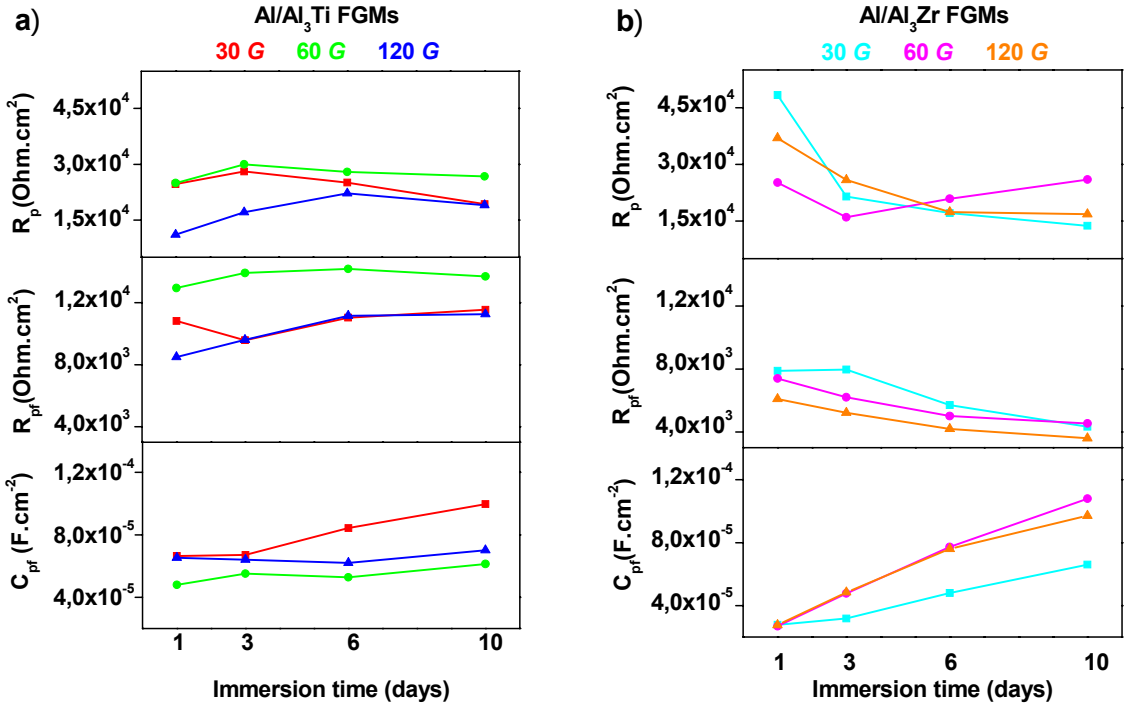

Figure 3.11 – Influence of the immersion time on the polarization resistance (R_p), film polarization resistance (R_{pf}) and capacitance of the film (C_{pf}): a) Al/Al_3Ti FGMs samples; b) Al/Al_3Zr FGMs samples.

On the other hand, the group of Al/Al_3Zr FGMs samples presents an abrupt decrease in the R_p values from 1 to 3 immersion days. Also, from 3 up to 10 days of immersion the samples showed a soft decrease of R_p. An exception occurs with the sample obtained with 60 *G*, which reveals an increase in the R_p from 3 to 10 days of immersion time. This can be attributed to the formation of corrosion products inside of the degraded areas. In this group of samples the R_{pf} diminish along of the 10 days of immersion for all samples, indicating the degradation of passive film. This phenomenon is corroborated by the evolution of the C_{pf} in all Al/Al_3Zr FGMs samples, which increase monotonically with the immersion time. The lowest C_{pf} values found in 30 *G* sample is a indication of the better corrosion behaviour of this sample, as indicated in the open circuit potential and potentiodynamic polarisation test.

3.4 – Conclusions

In the present study, the corrosion behaviour of Al/Al_3Ti and Al/Al_3Zr FGMs, when immersed in 0.6 M NaCl solution, at different immersion times (1, 3, 6 and 10 days) was investigated:

1) The electrochemical behaviour of FGMs samples showed that galvanic effects between the intermetallic particles and the metal matrix affect the overall corrosion resistance of FGMs;

2) In case of Al/Al_3Ti FGMs group, the samples obtained with 60 *G* present the better corrosion resistance. In case of Al/Al_3Zr FGMs group, sample obtained with 30 *G* revealed better behaviour when compared with the obtained with 60 *G* and 120 *G*;

3) In general terms this behaviour can be associated to the particles segregation level, i. e., when a low segregation of particles is found in the material, associated to low applied centrifugal forces, the corrosion resistance of FGM appear to increase.

Acknowledgements

The authors gratefully acknowledge the financial support provided by 21st COE Research of the Ministry of Education Culture, Sports Science and Technology of Japan. Acknowledgments also to "FCT", Portugal, through the project SFRH/BPD/5518/2001.

3.5 – References

[1] C. Gouveia-Caridade, M.I.S. Pereira, C.M. A. Brett, Electrochemical Acta 49 (2004) 785.

[2] N. Birbilis, R.G. Buchheit, Journal of The Electrochemical Society 152 (2005) 140.

[3] M.V. Karpets, Yu.V. Milman, O.M. Barabash, N.P. Korzhova, O.N. Senkov, D.B. Miracle, T.N. Legkaya, I.V. Voskoboynik, Intermetallics 11 (2003) 241.

[4] K.I. Moon, S.C. Kim, K.S. Lee, Intermetallics 10 (2002) 185.

[5] A. Aballe, M. Bethencourt, F.J. Botana, M.J. Cano, M. Marcos, Corrosion Science 45 (2003) 161.

[6] A. Barbucci, G. Bruzzone, M. Delucchi, M. Panizza, G. Cerisola, Intermetallics 8 (2000) 305.

[7] Y. Fukui, JSME International Journal 34 (1991)144.

[8] Y. Watanabe, Y. Yamanaka, Y. Fukui, Zeitschrift für Metallkde 88 (1997) 717.

[9] Y. Watanabe, N. Yamanaka, Y. Fukui, Metallurgical and Materials Transactions A (1999) 3253.

[10] Y. Watanabe, Y. Fukui, Recent Res. Devel. Metallurg. & Materials Sci. 4 (2000) 51.

[11] Y. Watanabe, Y. Fukui, Aluminium Transactions 2 (2000)195.

[12] Y. Watanabe, T. Nakamura, Intermetallics 9 (2001) 33.

[13] Y. Watanabe, H. Eryu, K. Matsuura, Acta Materialia 49 (2001) 775.

[14] Y. Watanabe, A. Kawamoto, K. Matsuura, Compositesa Science and Technology 62 (2002) 881.

[15] P.D. Sequeira, Y. Watanabe, L.A. Rocha, Proceedings of the 8th International Symposium on Multifunctional and Functionally Graded Materials, Trans Tech Publication, Leuven, 2004, p. 609.

[16] P.D. Sequeira, Y. Watanabe, L.A. Rocha, 2nd International Conference on Texture and Anisotropy of Polycrystals, Metz, 2004.

[17] A. Pardo, M.C. Merino, S. Merino, F. Viejo, M. Carboneras, R. Arrabal, Corrosion Science 47 (2005) 1750.

[18] J.E.G. González, J.G. Mirza-Rosca, Journal of Electroanalytical Chemistry 471 (1999) 109.

[19] C. Liu, A. Leyland, Q. Bi and A. Mattehews, Surface and Coating Technology 141 (2001) 164.

CHAPTER 4

Microstructural Characterization and Tribocorrosion Behaviour of Al/Al_3Ti and Al/Al_3Zr FGMs

P.D. Sequeira [a,b], S.C. Ferreira [a], Y. Watanabe [b], L.A. Rocha [a,c], E. Ariza [a], J. R. Gomes [a,c]

[a]Research Centre on Interfaces and Surface Performance, University of Minho, Campus de Azurém, 4800-058 Guimarães, Portugal

[b]Department of Engineering Physics, Electronics and Mechanics, Graduate School of Engineering, Nagoya Institute of Technology, Gokiso-Chu, Showa-Ku, 466-8555 Nagoya, Japan

[c]Department of Mechanical Engineering, University of Minho, Campus de Azurém, 4800-058 Guimarães, Portugal

Abstract

Al/Al_3Ti and Al/Al_3Zr functionally graded materials (FGMs) are manufactured through a centrifugal method from Al-5 mass % Ti and Al-5 mass % Zr, respectively. Applied centrifugal forces were 30, 60 and 120 *G* (units of gravity). Microstructural characterization was performed to evaluate intermetallic particles volume fraction and orientation distributions. The influence of the reinforcing phase on the tribocorrosion behaviour of the FGMs was investigated. An increase in both the intermetallic particles volume fraction as well as their orientation in the outer regions of the FGMs was found as the applied centrifugal force increased. Al_3Ti particles were found to have a higher segregation rate with lower applied centrifugal forces than the Al_3Zr particles; a

situation that was reversed for higher applied centrifugal forces. Better tribocorrosion behaviour was found in the samples containing the highest concentration of reinforcing particles.

Keywords: Trialuminide Intermetallics; Functionally Graded Materials (FGMs); Tribocorrosion.

4.1 – Introduction

Dispersion of hard intermetallic compounds in Al alloys has been studied as a means to improve the alloys' mechanical properties [1-4].

When the reinforcing phase has a higher density than the matrix, the centrifugal method is attractive due to the fact that there is a selective reinforcement of the surface of the component while gradually increasing the relative amount of ductile phases towards the inner region. This results in a higher wear resistance in the surface as well as maintaining high bulk toughness [5-8]. In fact, the presence of the reinforcing phase, in this case Al_3Ti or Al_3Zr platelets, has a strong influence on the local mechanical properties. The shape, size and spatial orientation of the reinforcing phase will also play an essential role on the wear performance of the material [9-13].

As stated above, particle segregation during casting with the centrifugal method occurs due to the difference in density between the particles and molten alloy [14], therefore, the study of two Al/intermetallic compounds systems where the intermetallic compounds have different density values, Al_3Ti and Al_3Zr have densities of 3.4 and 4.1 $g.cm^{-3}$, respectively, is of interest.

There are some published works dealing, independently, on the wear or corrosion behaviour of composites reinforced with intermetallic particles, however, no studies were published on the tribocorrosion behaviour of this kind of materials when they are in contact with aggressive environments. The tribocorrosion behaviour of the Al/Al_3Ti and Al/Al_3Zr FGMs is important to evaluate, once that, the particulate reinforced aluminum matrix composites (AlMCp) have received increasing demands for aerospace and automotive applications [15]. Compared to ceramic reinforcements, the employement of intermetallics as mechanical resistant reinforcement has advantages. In

addition to their high level of hardness, elastic modulus, melting temperature and thermal stability, the thermal expansion coefficients of intermetallics is much closer to those of Al alloys. The smaller discrepancy in thermal expansion coefficients will decrese the residual stress at reinforcement/matrix interfaces when the composite is exposed to thermal cycles, hence guarantying a lower degree of failure originated at the interface [16].

The material exposed to a tribocorrosion environment, i. e. where interactions between mechanical and corrosion degradation processes occur, suffers an irreversible transformation leading to decrease of the performance of that material [17]. The total metal removal rate is usually not simply the sum of the corrosion rate and the wear rate measured in separate experiments. In many cases corrosion is accelerated by wear and similarly, wear may be accelerated by corrosion [18]. The mutual dependence of mechanical and chemical metal removal rates in a tribocorrosion system can be due to phenomena as: local abrasion of the passive film can lead to wear accelerated corrosion due to rapid dissolution of the locally depassivated metal surface, followed by repassivation; the abrasive action of hard oxide particles formed by corrosion can accelerate the mechanical metal removal by wear; the plastic deformation of the surface layer of a rubbing metal can lead to transfer of material to the opposite body resulting in a reduction of the corrosive, and others [17-19].

In the present study microstructural characterization was performed on Al/Al_3Zr and Al/Al_3Ti FGMs processed with different applied centrifugal forces. Also tribocorrosion behaviour of Al/Al_3Ti and Al/Al_3Zr FGMs has been studied in the outer region of the FGMs. Results indicate that an increase in the applied centrifugal forces increases both the particles' volume fraction as well as their orientation in the outer regions of the fabricated FGM rings. Also for lower applied centrifugal forces the Al_3Ti particles migrate faster than the Al_3Zr particles, a situation that is reversed for higher applied centrifugal forces. Higher tribocorrosion resistance was found for the samples produced with higher centrifugal force.

4.2 – Experimental Methods

Al/Al_3Ti and Al/Al_3Zr FGMs were produced by the centrifugal method, from Al-5 mass % Ti and Al-5 mass % Zr commercial alloys, respectively. The crystal structures and densities of the intermetallic compounds and of aluminium are presented in Table 4.1. Since the relative atomic masses of Al, Ti and Zr are 26.98, 47.88 and 91.22, respectively, the theoretical volume fraction of Al_3Ti in the master alloy was calculated to be approximately 11 vol % and that of Al_3Zr as approximately 7 vol %.

Table 4.1 – Crystal structure and density

Element or compound	Crystal structure	Density (g.cm^{-3})
Al	*Fcc*	2.7
Al_3Ti	$D0_{22}$	3.4
Al_3Zr	$D0_{23}$	4.1

In the centrifugal method the alloy is heated up to a temperature located between its *solidus* and *liquidus* temperatures, were most of the intermetallic platelets remain solid in a liquid Al-based matrix. It is then poured into a rotating mould in order to obtain ring-shaped samples which have an outer diameter of 90 mm, 25 mm in height and a length of 20-25 mm. The temperature of the melting furnace was 1173 K and the applied centrifugal casting forces were 30, 60 and 120 *G* (units of gravity). A detailed description of the centrifugal method is available elsewhere [5-9].

Samples were cut, polished and divided into ten regions of equal width along the centrifugal force direction. The outer surface of the ring is therefore represented as the position 1.0 of the normalized distance and the inner surface by the position 0.0.

Optical micrographs were taken and from those intermetallic particles distribution, size, shape and orientation were measured along two planes, perpendicular to the rotating axis (referred as OP1 in the subsequent text) and perpendicular to the rotating direction (OP2), as seen in Figure 4.1 a). Knoop hardness tests were performed, with the indenter's long diameter normal to the centrifugal force direction.

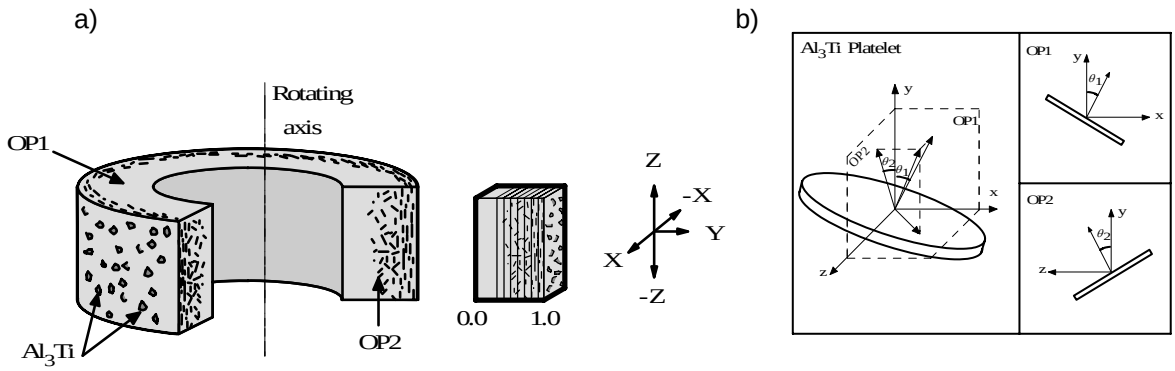

Figure 4.1 – a) Schematic representation of the FGM ring. b) Definition of orientation angle, θ. Two-dimensional orientation of the particles can be described by the angle, θ, between the direction perpendicular to the disc plane and the reference axis, y, which is the direction of applied centrifugal force.

Potentiodynamic polarisation curves of both Al/Al$_3$Ti and Al/Al$_3$Zr FGMs samples were obtained a 0.6 M NaCl solution by scanning the potential from -1400 up to 200 mV at a scan rate of 2 mV.s^{-1} using a PGP201 Potentiostat/Galvanostat (Radiometer Denmark), controlled by the VoltaMaster-1 software. The area of the working electrode was set in 0.385 cm^2, the counter electrode was a platinum sheet with an area of 1 cm^2 and a saturated calomel electrode (SCE) was used as reference.

The tribocorrosion tests were performed using a reciprocating tribometer (Plint TE67/R). An alumina pin (truncated cone geometry and with a tip of 1 mm in diameter) was used as counterbody and mounted vertically on the samples immersed in the electrolyte (exposed area = 0.95 cm^2). The samples were used as plates positioned horizontally and mounted in an acrylic electrochemical cell (20 ml of a 0.6 M NaCl solution was used as electrolyte), as seen in Figure 4.2. All potentials were measured and expressed with reference to a standard calomel electrode (SCE), and a platinum wire with an area of 1 cm^2 served as counter electrode. A Voltalab PGZ100 Potentiostat (Radiometer Analytical, Denmark), controlled by Voltamaster-4 software was used in the electrochemical measurements. Samples were previously cathodically polarised at -1400 mV vs. SCE, during 3 min, in order to clean the surface. Subsequently, a potential of -825 mV vs. SCE was applied to stabilise the samples by a period of 10 min. Then, the mechanical contact between the alumina pin and the sample plate was established. The last applied potential was selected from the potentiodynamic polarization curves

and was used during and after the sliding time. The reciprocating wear test was performed with a normal load of 3 N, displacement amplitude of 2 mm and a frequency of 1 Hz. The sliding time was 900 s. When sliding was stopped, the pin and the sample were removed from the solution and ultrasonically cleaned in ethanol. For each sample the tests were repeated twice. The total wear volume, caused by the contribution of wear and corrosion, was determined by a profilometer method, using a Perthometer S5P roughness meter, by calculating the average of the cross-sectional area multiplied by the stroke length. The chemical wear volume (V_{chem}) was determined from measured current, using Faraday's law:

$$V_{chem} = \frac{Q \cdot M}{n \cdot F \cdot \rho} \qquad (4.1)$$

where, Q is the electric charge, which is obtained by integrating of the current density curve with the time, along of the sliding time ($Q = \int I\,dt$), M is the atomic mass of aluminium (27 g.mol^{-1}), n the valence of dissolution of the aluminium (+3), F the Faraday's constant (9.649·10^{-4} C.mol^{-1}) and ρ is the density of the aluminium (2.7·10^{-3} g.mm^{-3}). The mechanical wear volume, which is the volume of material removed mechanically, was obtained by subtraction of the calculated chemical wear volume to the total wear volume.

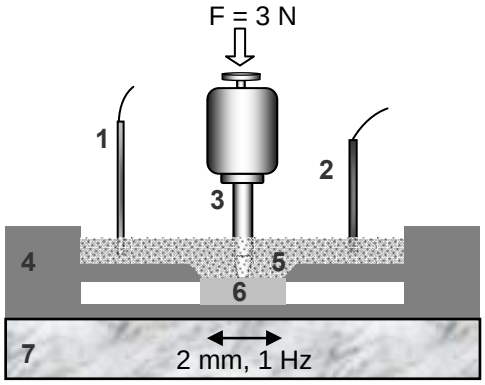

Figure 4.2 – Schematic view of the electrochemical cell used in the tribocorrosion tests: (1) Reference electrode, (2) Auxiliary electrode, (3) Alumina pin, (4) Acrylic recipient, (5) Electrolyte, (6) Working electrode (sample), (7) Tribometer.

The topographical features of the worn surfaces were investigated using scanning electron microscopy (SEM) in an attempt to study the tribocorrosion mechanisms.

4.3 – Results and Discussion

4.3.1 – Intermetallic Compounds Volume Fraction and Knoop Hardness Distributions

Figure 4.3 shows optical micrographs of the typical microstructure found in the produced FGMs. As seen in Figures 4.4 and 4.5 in all samples the volume fraction occupied by Al_3Ti or Al_3Zr particles decreases from the outer (1.0 position in the abscissa of the figures) to the inner regions (position 0.0) of the FGM rings. In fact, with samples cast under 60 and 120 *G* there is an absence of particles from around the middle to the inner region of the rings in both the Al/Al_3Ti and Al/Al_3Zr FGMs.

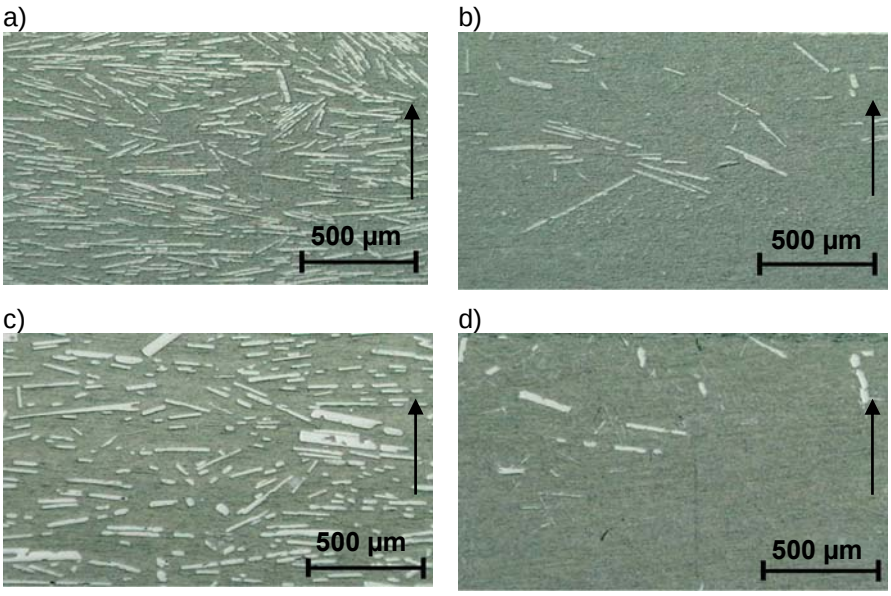

Figure 4.3 – Optical micrographs, brighter areas are the intermetallic particles. a) and b) are from the Al/Al_3Ti FGM cast at 60 *G* at the outer and interior regions, respectively. c) and d) are from the Al/Al_3Zr FGM cast at 60 *G* at the outer and interior regions, respectively. The arrows indicate the direction of applied centrifugal force.

From Figure 4.4, an increase in the applied centrifugal force does not appear to significantly increase the intermetallic particle fraction at the outermost region of the Al/Al_3Ti FGMs rings, which remain around 20-25 vol %, but does increase the volume fraction in the adjacent regions. All the Al/Al_3Zr FGMs present lower volume fractions than the Al/Al_3Ti FGMs, as expected due to the initial lower theoretical volume fraction (Figure 4.5).

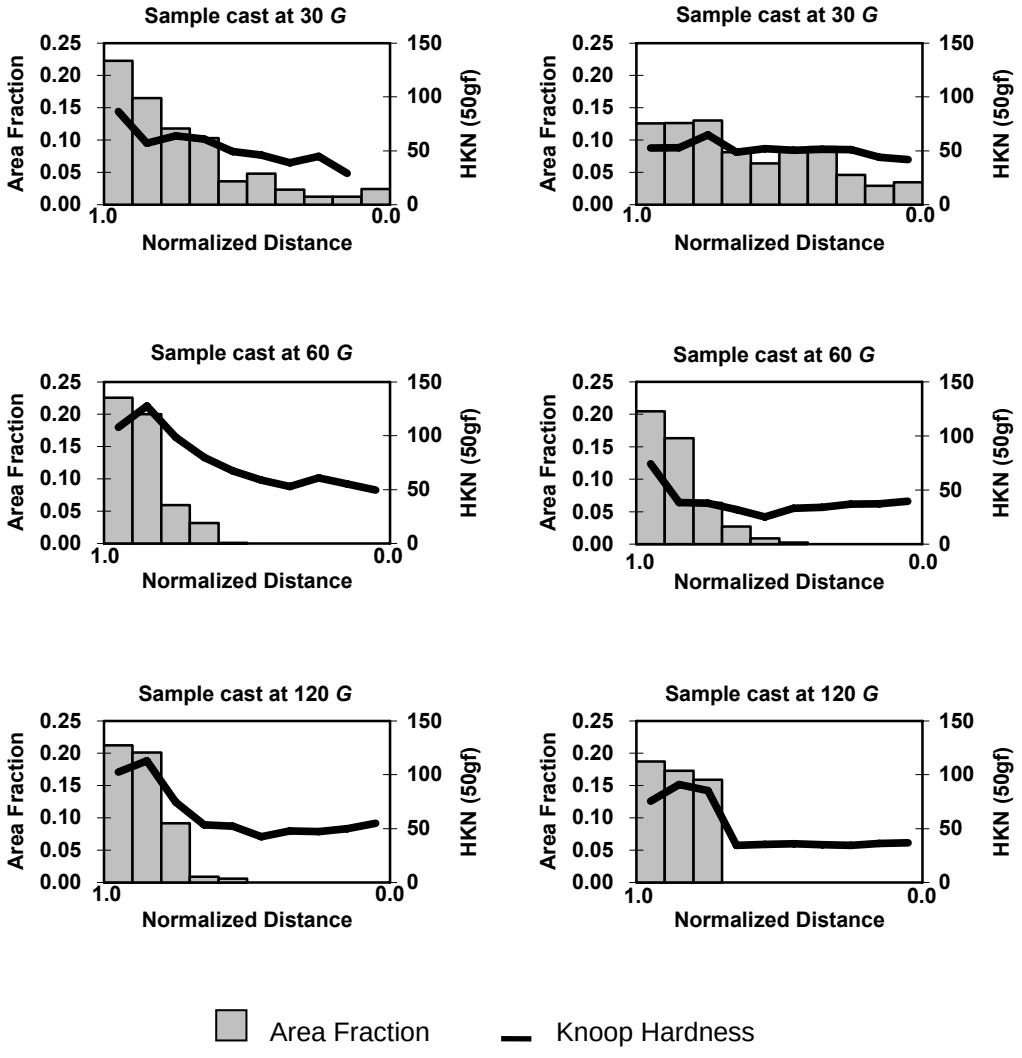

Figure 4.4 – Intermetallic particles area fraction and Knoop hardness distribution for the Al/Al_3Ti FGMs.

Figure 4.5 – Intermetallic particles area fraction and Knoop hardness distribution for the Al/Al_3Zr FGMs.

At applied centrifugal force of 30 *G* the Al/Al_3Zr FGM exhibits a very low gradient when compared to the Al/Al_3Ti sample. The samples from both systems cast at 60 *G* display a very similar trend while, for the samples subjected to a centrifugal force of 120 *G*, a higher relative clustering of particles on the outermost regions is found for the Al/Al_3Zr FGM.

Al_3Ti particles have a higher segregation rate with lower applied centrifugal forces than the Al_3Zr particles; a situation that is reversed for higher applied centrifugal forces.

It has been accepted, in general, that the viscosity of a suspension rises with to the increase in number of particles in the suspension. Since the motion of spherical particles in a viscous liquid under a centrifugal force can be determined by the simple Stokes' law, the volume fraction gradient within the spherical particle reinforced FGM becomes steeper by decreasing the mean volume fraction of particles [7]. Easier migration of the particles in sparser suspensions, compared with denser suspensions, could not explain the lower gradient obtained in the Al/Al_3Zr FGMs at low applied centrifugal force when compared to the Al/Al_3Ti FGMs. In this way, the present results, relating to the effect of mean volume fraction, contradicts the previous results for spherical particles [7]. On the other hand the same effect has been found to occur in Al/Al_3Ti FGMs with different volume fraction of particles, that is, an increase in volume fraction leads to steeper gradients [6]. Therefore it is apparent that the simple Stokes' law is not applicable to the Al/Al_3Ti and Al/Al_3Zr systems.

Knoop hardness measurements for the Al/Al_3Ti FGMs (Figure 4.4) in general follow the same trend as the area fraction for each sample, with values around 50 HKN in the regions without particles and over 100 in areas with the higher intermetallic content. A similar trend is also observed in the Al/Al_3Zr FGMs (Figure 4.5).

4.3.2 – Orientation Distribution of Al_3Zr and Al_3Ti Platelets

As mentioned above, it was found that in the outer region of the ring, most of platelets are oriented with their planes nearly perpendicular to the radial direction. In order to describe the degree of orientation let us define the reference axes, *x*, *y* and *z*, as shown in Figure 4.1. Planes OP1, OP2 and OP3 correspond to *x*-*y* plane, *y*-*z* plane and

z-x plane, respectively. Figure 4.1 b) shows the definition of the orientation angles θ_1 and θ_2 on the Planes OP1 and OP2, respectively. Two-dimensional (2-D) orientation of the platelet can be described by the angle, θ, between the direction perpendicular to the disc plane and the reference axis, *y*, (the centrifugal force direction, *i.e.* radial direction of the ring as shown in Figure 4.1a). The 2-D platelet orientation distributions are obtained from micrographs. Furthermore, in order to describe this orientation tendency quantitatively, the following Hermans orientation parameter, *fp* [20,21] was calculated.

$$fp = [\, 2 \langle \cos^2\theta \rangle - 1] \qquad (4.2)$$

Where the trigonometric average is,

$$\langle \cos^2\theta \rangle = \int_{-\pi/2}^{\pi/2} \cos^2\theta \, n(\theta) \, d\theta \qquad (4.3)$$

The term $n(\theta)$ is the orientation distribution function which specifies the fraction of platelets within the angular element $d\theta$. The parameter *fp* becomes 0 for a random distribution of platelets, and it becomes 1 for perfect alignments of the platelets with their planes perpendicular to the direction of the applied centrifugal force. Intermediate values of this parameter correspond to partial states of orientation. Negative value of *fp* indicates the alignment with their planes parallel to the direction of the applied centrifugal force.

As seen in Figures 4.6 and 4.7 the platelets tend to be oriented normal to the centrifugal force direction. The trend is similar along both observation planes (OP1 and OP2), with exception of the Al/Al_3Zr sample cast under 30 *G*. Also the orientation of platelets in the outer regions is increased with the increase in applied centrifugal force, although, as with the volume fraction values, the increase of applied centrifugal force from 60 to 120 *G* does not affect significantly the orientation parameter for the outermost region but does increase it for the adjacent regions, a similar effect is observed for the Al/Al_3Zr FGMs. Also higher orientation parameter values are obtained for the Al/Al_3Ti FGMs. The higher volume fraction of Al_3Ti platelets leads to the necessity of a closer packing between them, which is facilitated by their shape and size (see Figure 4.3). As for the behaviour of the Al_3Zr platelets, a very low orientation parameter is found in the outer regions of the sample cast under 30 *G* and an essentially random orientation in the interior regions. The low particle orientation in this sample is

furthermore corroborated by the lack of correlation between the observed values in OP1 and OP2. At applied centrifugal forces of 60 and 120 *G*, the Al/Al_3Zr FGMs follow the same trend as the Al/Al_3Ti FGMs although with a lower overall value, in this case the lower volume fraction allows for a greater freedom of movement of the Al_3Zr platelets, leading to lower orientation parameter values.

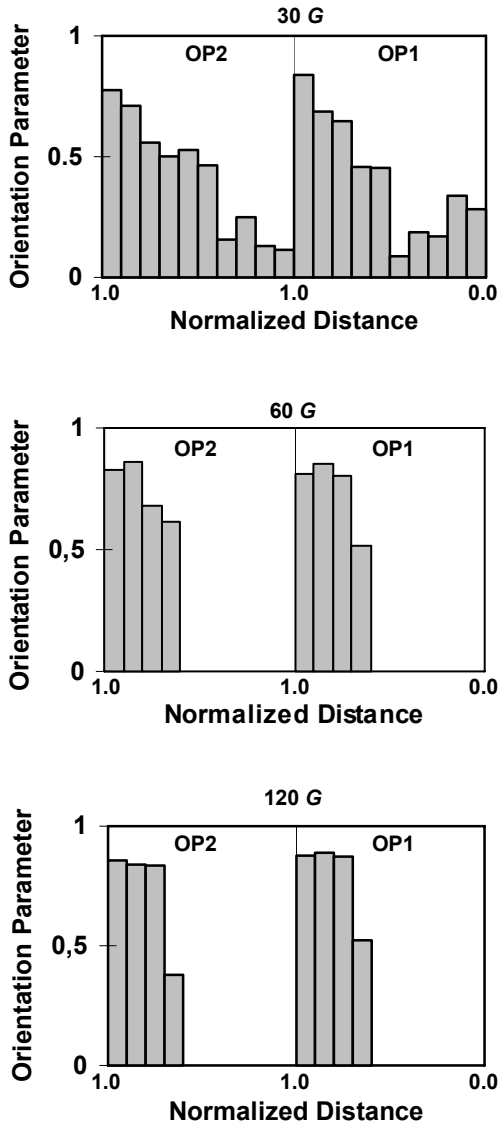

Figure 4.6 – Al_3Ti platelets Hermans orientation parameter distribution.

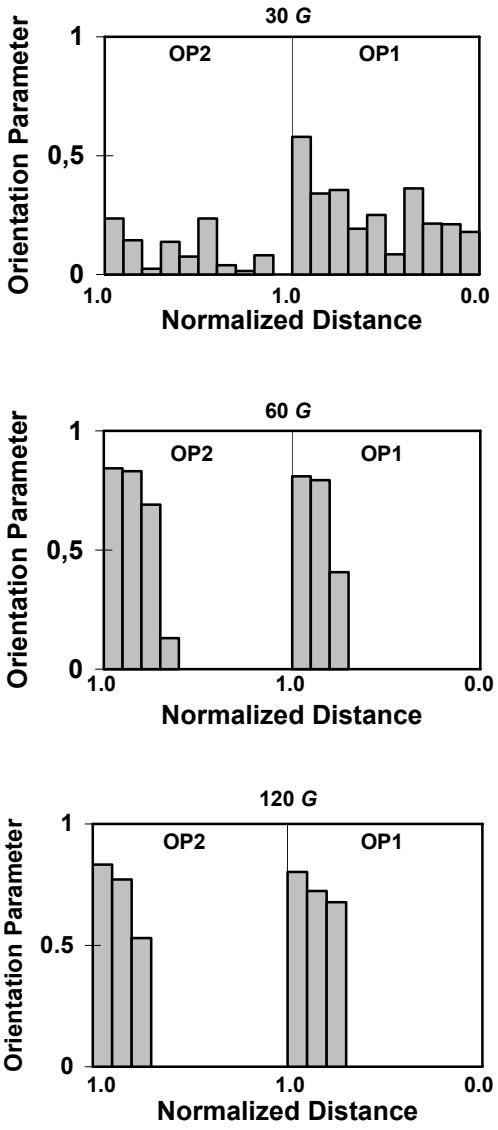

Figure 4.7 – Al_3Zr platelets Hermans orientation parameter distribution

4.3.3 – Tribocorrosion Behaviour

Polarisation curves obtained in all samples are show in Figure 4.8. As it can be observed in Figure 4.8 a), the corrosion potential ($E_{i=0}$) values of Al/Al_3Ti 30, 60 and 120 *G* samples are very similar, -830, -800 and -840 mV, respectively. However, the sample obtained with 60 *G* reveals a little better behaviour, but also, more noise. In the case of Al/Al_3Zr FGMs (Figure 4.8 b), the samples present a more dispersed behaviour. The sample of 30 *G* reveals a corrosion potential ($E_{i=0}$) of -825 mV clearly higher than the 60 *G* and 120 *G* samples, -900 mV and -945, respectively. As it can be seen, the determination of the corrosion current density (i_{corr}) for all samples presents some difficulties because of the noise and instability of the samples immersed in the electrolyte.

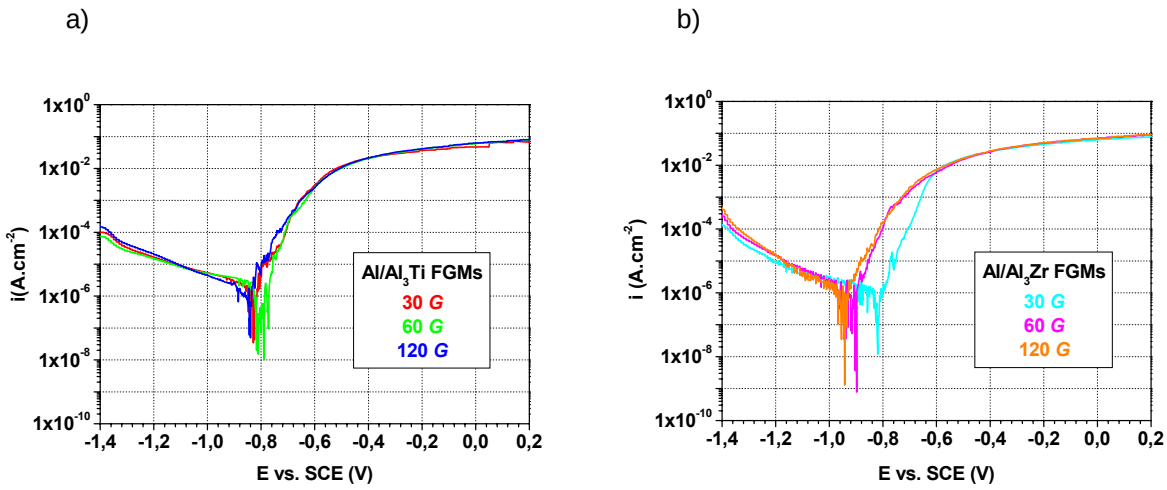

Figure 4.8 – Potentiodynamic polarisation curves obtained in the FGMs samples when immersed in a 0.6 M NaCl solution: a) Al/Al_3Ti FGMs; b) Al/Al_3Zr FGMs.

Results of tribocorrosion tests obtained in Al/Al_3Ti FGMs samples are presented in Figure 4.9. As it can be seen in Figure 4.9 a), all samples show a similar evolution of the current with the time. The drastic increase in the current at 180 seconds is due to the change of the applied potential from -1400mV (to clean the sample) to -825mV to stabilize the same. Figures 4.9 b), c) and d) show the evolution of the current density and of the friction coefficient, μ, with the time during the sliding period, obtained in all Al/Al_3Ti FGMs samples. All samples show an increase in the current at the beginning

of sliding, corresponding to the initial contact between the counter body and the surface of the sample. After this, the current density decreases until reaching the stable state. The 30 *G* sample achieves a stable state after 40 seconds, while the 60 *G* sample takes much more time to reach a stable state and the 120 *G* sample after 60 seconds. It is possible to observe that at the end of sliding the 30 and 60 *G* samples have similar current density values (~20 $\mu A.cm^{-2}$). An exception occurs with the 120 *G* sample, which presents the lowest current (~10 $\mu A.cm^{-2}$). In terms of friction coefficient all samples show similar behaviour. The friction coefficient (μ) was calculated as an average of values, eliminating the initial sliding values, i.e., eliminating the running-in period. As observed, the μ varies between 0.4 and 0.5, the lowest value corresponding to the 120 *G* sample. Thus, although all samples show similar behaviour, this last sample (120 *G*) presents a relatively better tribocorrosion behaviour when compared with the other samples, *i.e.*, shows the lowest friction coefficient and the lowest current density. Figure 4.10 a) presents the overall topography of Al/Al_3Ti FGM 120 *G*. The evidence of abrasive scratches and cracking of the intermetallic platelets is clearly visible on the deformed wear zone (Figure 4.10 b) and c). In a general way, in all Al/Al_3Ti FGMs samples the wear scar shows signs of severe wear.

Figure 4.11 presents the results of tribocorrosion tests obtained for the Al/Al_3Zr FGMs samples. Figure 4.11 a) shows the evolution of the corrosion current density with the time. As it can be seen, the current density has a evolution similar to that found in the Al/Al_3Ti FGMs samples (see Figure 4.9 a). In Figures 4.11 b), c) and d) the evolution of the current density and of the friction coefficient (μ) with the time in the sliding period is presented. As it can be observed, the 30 and 60 *G* samples show similar current density values along of sliding (~60 $\mu A.cm^{-2}$), which is very high when compared with the 120 *G* sample (~20 $\mu A.cm^{-2}$). In the case of friction coefficient for all samples, it varies between 0.4 and 0.6. The sample with the more stable μ along of sliding time is the 30 *G* sample, with a μ approximately of 0.5. The sample with the lowest μ (~0.4 at the end of sliding) is the 60 *G* sample; in this sample the μ decreases abruptly until 1200 s and then stabilizes. In the case of the 120 *G* sample, the friction coefficient is very unstable during the sliding time and is the highest (~0.54) when compared with the other samples. Figure 4.12 a) shows the overall topography of Al/Al_3Zr FGM 120 *G*. The evidence of plastic deformation is clearly visible on the

deformed wear zone (Figure 4.12 b). Also, in all Al/Al_3Zr FGMs samples the wear scar shows signs of severe wear.

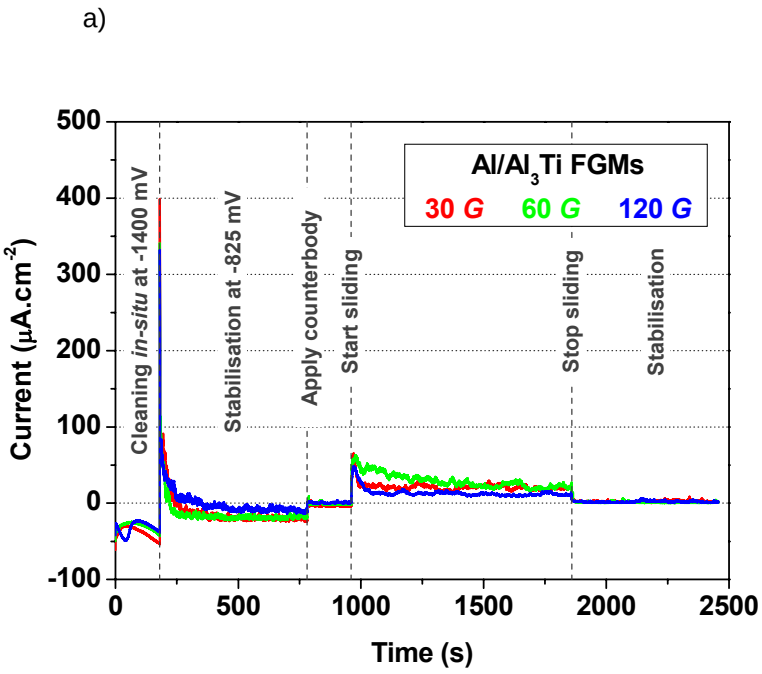

Figure 4.9 – Evolution of the current density and the friction coefficient with time in the tribocorrosion tests a); evolution of the current density and the friction coefficient during the sliding period: b) Al/Al_3Ti FGM 30*G*; c) Al/Al_3Ti FGM 60*G*; d) Al/Al_3Ti FGM 120*G*.

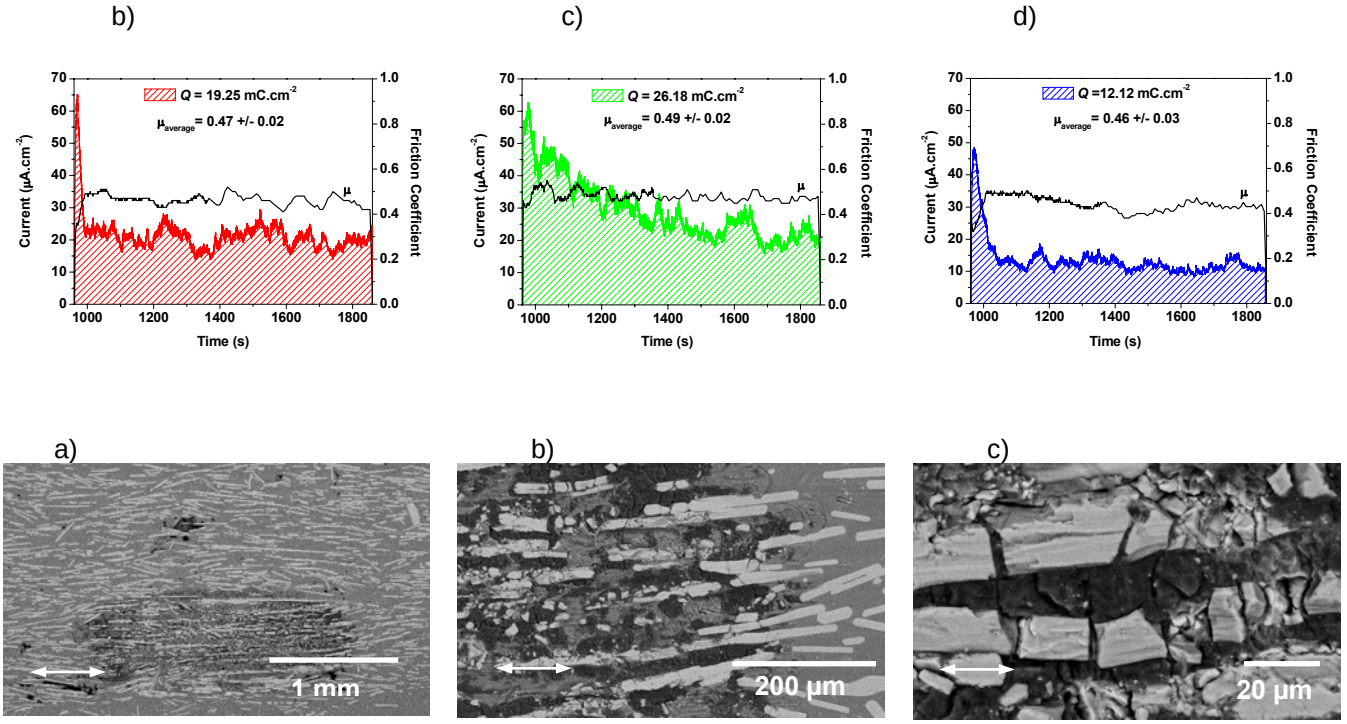

Figure 4.10 – SEM micrograph revealing the detailed topographical features from surface of Al/Al_3Ti FGM 120 *G* after sliding against an alumina pin in 0.6 M NaCl. A double pointed arrow indicates the sliding direction: a) wear scars, b) Detail of the inside and out of the wear cracks, c) Detail of the Al_3Ti platelets break of the wear.

In general terms it can be concludes that Al/Al$_3$Zr FGMs samples have a worse tribocorrosion behavior when compared with the Al/Al$_3$Ti FGMs samples. This assumption is made on the basis of high friction coefficient and low current densities found in these last samples.

a)

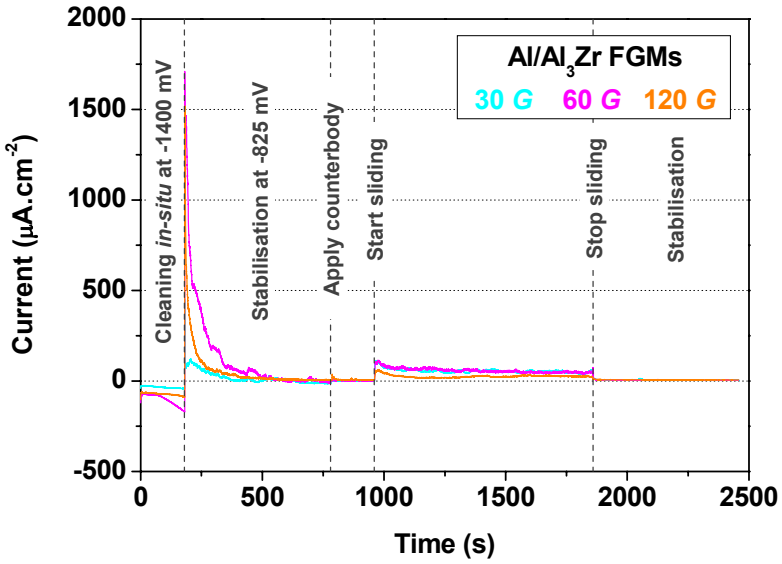

Figure 4.11 – Evolution of the current density and the friction coefficient with time in the tribocorrosion tests(a); evolution of the current density and the friction coefficient during the sliding period: b) Al/Al$_3$ZrFGM 30*G*; c) Al/Al$_3$Zr FGM 60*G*; d) Al/Al$_3$Zr FGM 120*G*.

b)

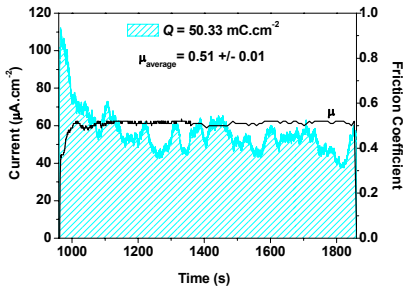

c)

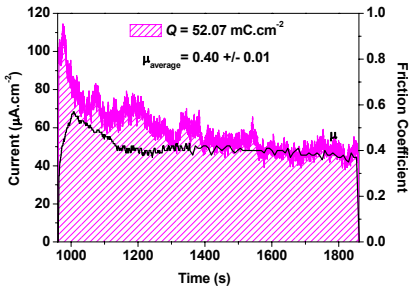

d)

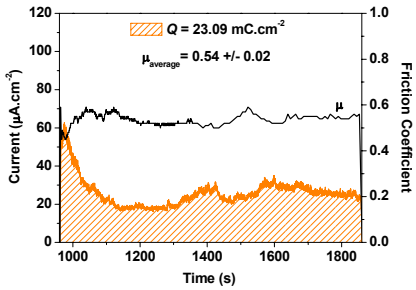

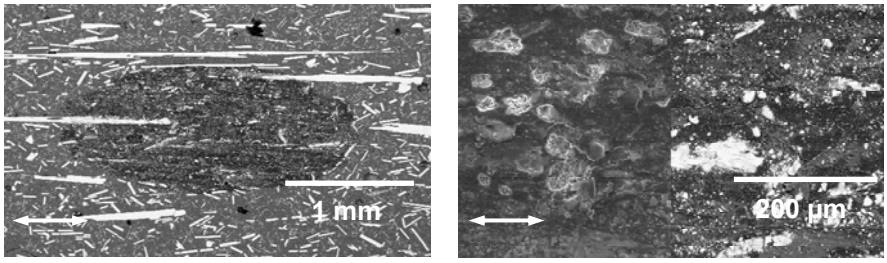

Figure 4.12 – SEM micrograph revealing the detailed topographical features from surface of Al/Al_3Zr FGM 120 *G* after sliding against an alumina pin in 0.6 M NaCl. A double pointed arrow indicates the sliding direction: a) wear scars, b) Detail of the inside of the wear cracks.

Regarding to the synergism between the wear and corrosion phenomena, Figure 4.13 shows a relation between the removed volumes by the mechanical (V_{mech}) and electrochemical (V_{chem}) processes. All the samples show negligible V_{chem} when compared to V_{mech}. This should be a good indication that the tribocorrosion process is mainly governed by the mechanical wear. It is also observed that the samples having a large V_{mech} show a larger V_{chem}, indicating probably that there exists an increase in the corrosion rate due to wear. Other important characteristic is that the samples with a less total wear volume are the 120 *G* ones. This phenomenon can be explained by the higher volume fraction of particles obtained from a higher applied centrifugal, such as occurs in all 120 *G* samples. On the other hand, the samples of 30 *G* and 60 *G* of the Al/Al_3Ti FGMs present a smaller total wear volume than the respective 30 *G* and 60 *G* of the Al/Al_3Zr FGMs, probably due to the higher segregation rate and higher orientation of intermetallic particles obtained in Al/Al_3Ti samples.

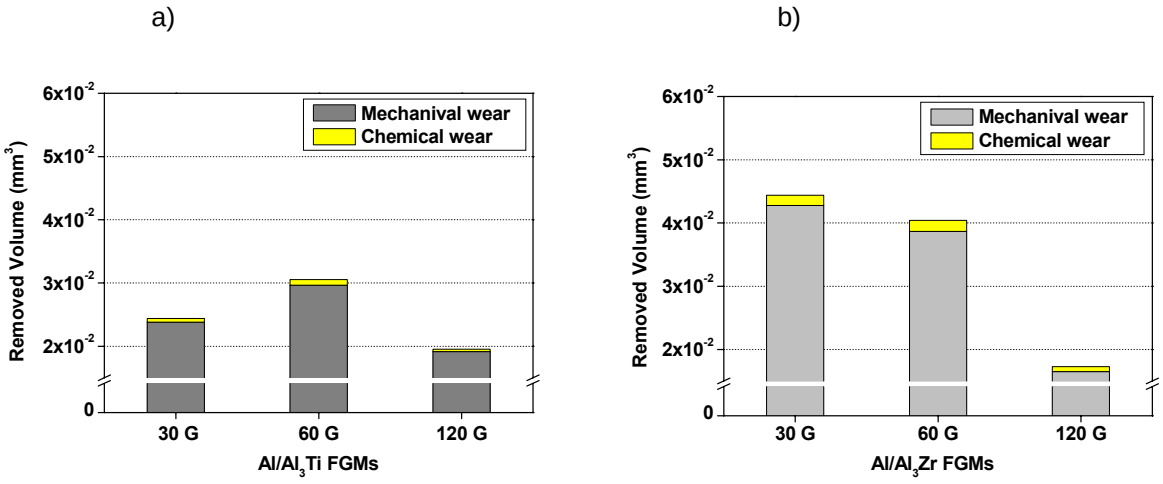

Figure 4.13 – Remove volumes by mechanical and electrochemical processes, in the tribocorrosion tests. a) Al/Al$_3$Ti FGMs samples, b) Al/Al$_3$Zr FGMs samples.

4.4 – Conclusions

In the present work Al/Al$_3$Ti and Al/Al$_3$Zr functionally graded materials (FGMs), fabricated by the centrifugal method, were microstructuraly characterized and studied in terms of its tribocorrosion behaviour:

1) Higher applied centrifugal force increases both the intermetallic particles volume fraction as well as their orientation in the outer regions of the FGMs;

2) The increase of applied centrifugal force from 60 to 120*G* does not affect significantly the volume fraction or the orientation parameter distribution for the outermost region of the FGMs but does increase it for the adjacent regions;

3) Al$_3$Ti particles have a higher segregation rate with lower applied centrifugal forces than the Al$_3$Zr particles; a situation that is reversed for higher applied centrifugal forces;

4) Higher orientation values for the intermetallic platelets are found in the Al-Al$_3$Ti FGMs;

5) Better tribocorrosion behaviour was found in the samples containing the highest concentration of reinforcing particles;

6) The tribocorrosion processes of Al-Al_3Ti and Al-Al_3Zr FGMs samples are mainly governed by mechanical wear. It was verified that exits a synergism between the wear and the corrosion process in which this last increases with wear acts.

Acknowledgements

The authors gratefully acknowledge the financial support provided by 21st COE Research of the Ministry of Education Culture, Sports Science and Technology of Japan. Acknowledgments also to "FCT", Portugal, through the project SFRH/BPD/5518/2001.

4.5 – References

[1] M. Yamaguchi, Y. Umakoski, Intermetallic Compounds, Tokyo, Japan: Nikkan Kogyou Shinbunsya, (1984).

[2] S.H. Wang, P.W. Kao, Acta Mater 46 (1998) 2675.

[3] S.H. Wang, P.W. Kao, C.P. Chang, Scripta Mater 40 (1999) 289.

[4] Z. Sun, H. Hashimoto, Q. Wang, Y. Park, T. Abe, Mater Trans 41 (2000) 597.

[5] Y. Fukui, JSME Inst J Series III 34 (1991) 144.

[6] Y. Fukui, Y. Watanabe, Metal Mater Trans A 27A (1996) 4145.

[7] Y. Watanabe, N. Yamanaka, Y. Fukui, Composites Part A 29A (1998) 595.

[8] Y. Watanabe, Y. Fukui, Aluminum Trans 2 (2000) 195.

[9] Y. Watanabe, N. Yamanaka, Y. Fukui, Metal Mater Trans A 30A (1999) 3253.

[10] Y. Watanabe, H. Eryu, Y. Fukui, Ceramic Trans 114 (2001) 675.

[11] H. Asanuma, M. Hirohashi, K. Miyoshi, Y. Sakamoto, K. Hayashi, Proc 3rd Int SAMPE Met Conf (1992) M581.

[12] R.B. Pipes, R.L. McCullough, D.G. Taggart, Polymer Compo 3 (1982) 34.

[13] R.C. Wetherhold, P.D. Scott, Compo Sci Tech 62 (2002) 393.

[14] L. Lajoye, M. Suery, Proc Int Symp on Advances in Cast Reinforced Metal Composites, ASM International (1988) 15.

[15] D. Roy, B. Basu, A.B. Mallick, Intermetallics 13 (2005) 733.

[16] J.M. Wu , Z.Z. Li, Wear 244 (2000) 147.

[17] D. Landolt, S. Mischler, M. Stemp, Electrochimica Acta 46 (2001) 3913.

[18] P. Jemmely, S. Mischler, D. Landolt, Tribology International 32 (1999) 295.

[19] P. Jemmely, S. Mischler, D. Landolt, Wear 237 (2000) 63.

[20] S.H. McGee, R.L. McCullough, J. Appl. Phys. 55 (1984) 1394.

[21] L.M. Gonzalez, F.L. Cumbrera, F. Sanchez-Bajo, A. Pajares, Acta Metall. Mater. 42 (1994) 689.

CHAPTER 5

Influence of the Reinforcing Particles Distribution on the Study of Tribocorrosion of Al/Al_3Zr FGMs Produced by Centrifugal Casting

Sónia C. Ferreira [1], Edith Ariza [2], Luís A. Rocha [3], Paulo D. Sequeira [4], Yoshimi Watanabe [5]

[1] Researcher, Materials Engineering – CIICS, Centro de Investigação em Interfaces e Comportamento de Superfícies, Universidade do Minho, Campus de Azurém, 4800-058 Guimarães, Portugal.

[2] Postdoctoral Researcher, Metallurgical Engineering – CIICS, Centro de Investigação em Interfaces e Comportamento de Superfícies, Universidade do Minho, Campus de Azurém, 4800-058 Guimarães, Portugal.

[3] Associate Professor - CIICS, Centro de Investigação em Interfaces e Comportamento de Superfícies, Universidade do Minho, Campus de Azurém, 4800-058 Guimarães, Portugal.

[4] Researcher, Materials Engineering – Department of Engineering Physics, Electronics and Mechanics, Graduate School of Engineering, Nagoya Institute of Technology, Gokiso-cho, Showa-ku, Nagoya 466-8555, Japan. CIICS – Centro de Investigação em Interfaces e Comportamento de Superfícies, Universidade do Minho, Campus de Azurém, 4800-058 Guimarães, Portugal.

[5] Associate Professor, Department of Engineering Physics, Electronics and Mechanics, Graduate School of Engineering, Nagoya Institute of Technology, Gokiso-cho, Showa-ku, Nagoya 466-8555, Japan

Abstract

Zirconium trialuminide (Al_3Zr) possess low density, high hardness, good oxidation resistance, thermal stability and high melting temperature. However, their application is limited because they are brittle at low temperatures. However, these intermetallics have shown sufficient promising characteristics to reinforce aluminium alloys for advanced applications. Some works have been carried out on Al/Al_3Zr FGMs concerning their microstructural characteristics and wear behaviour. Nevertheless, tribocorrosion studies had still not been carried out. In this work, the corrosion-wear of Al/Al_3Zr immersed in 0.6 M NaCl solution and sliding against an alumina pin is analyzed. These materials were produced by centrifugal casting from an Al-5 mass % Zr alloy with centrifugal forces applied to the mould of 30, 60 and 120 *G* (units of gravity). Before tribocorrosion tests, the corrosion behaviour was evaluated by potentiodynamic polarization. The tribocorrosion tests were performed in the pin-on-plate configuration. The tests were made in the perpendicular direction to the centrifugal force in two areas with different gradient of distribution of Al_3Zr. After the tests, the samples were analyzed by SEM to identify the phenomena of corrosion and wear in the surfaces.

Keywords: Corrosion, Tribocorrosion, Al/Al_3Zr FGMs

5.1 – Introduction

Aluminium-intermetallic compounds fabricated by centrifugal casting have been extensively studied due to the promising properties of the material, simple fabrication technology, easiness to control technology parameters and small investment [1,2]. The Al/Al_3Zr functional graded material (FGM) fabricated by centrifugal casting, present a gradient distribution of intermetallic compounds [3] that may result in better properties than homogenous materials. This method, which was proposed by Fukui et al. [4], consists on the application of a centrifugal force to a suspension of dispersed material, such as ceramics or intermetallic particles, in the molten metal. Acting on the centrifugal casting parameters the formation of the desired gradation is obtained. In fact,

the composition gradient is achieved primarily by the difference in density between the molten metal and particles.

Tribocorrosion is an irreversible transformation of a material resulting from simultaneous physico-chemical and mechanical surface interactions occurring in a tribological contact. In general, tribocorrosion leads to the degradation of the materials and conduces to the weakening of the performance of a contact [7-11].

The study of the tribocorrosion behaviour of Al/Al_3Zr FGMs is important because these composites are intended to be used for aircraft and automotive applications [5-6]. In practice, most of these components will be under corrosion-wear interaction, which might cause material to be removed from sliding surfaces exposed to corrosion environments, such as organics fluids or aqueous lubricants [7]. In a tribocorrosion system, the chemical and mechanical degradation mechanisms are not independent of each other and synergistic effects can result in accelerated material removal [8]. In this paper, corrosion and tribocorrosion behaviour of Al/Al_3Zr FGMs were studied in two regions with different gradients of intermetallic compounds.

5.2 – Experimental Methods

The Al/Al_3Zr FGMs were produced by the centrifugal method, from Al-5 mass % Zr commercial alloy, as described by Sequeira et al. [3]. In the centrifugal method the master-alloy ingot is heated up to a temperature located between its *solidus* and *liquidus* temperatures, where most of the intermetallic platelets remain solid in the liquid matrix. It is then poured into a rotating mould in order to obtain ring-shaped samples which have an outer diameter of 90 mm, 25 mm in height and a length of 20-25 mm (see Figure 5.1). The temperature of the melting furnace was 1173 K and the applied centrifugal casting forces were 30, 60 and 120 *G* (units of gravity).

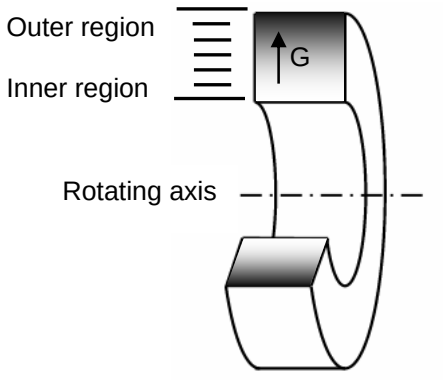

Figure 5.1 – Schematic of the FGM ring showing the studied plane, perpendicular to the rotation direction.

Samples surfaces were polished using SiC papers and diamond paste up to 1 μm. Before corrosion and tribocorrosion tests, the samples were ultrasonically cleaned in ethanol for 15 minutes and then in distilled water for 10 minutes and finally dried.

The corrosion behaviour was evaluated by potentiodynamic polarization tests at room temperature in a 0.6 M NaCl solution. The electrochemical cell consisted in a standard three electrode arrangement. The auxiliary electrode was a platinum sheet with an area of 1 cm^2 and a saturated calomel electrode (SCE) was used as reference. The area of the working electrode was set in 0.2 cm^2. A PGP201 Potentiostat/Galvanostat (Radiometer Denmark), controlled by the VoltaMaster-1 software, was used to carry out the polarization measurements. Prior to polarization tests, the open circuit potential (OCP) was monitored during 3600 s, after which the samples were anodically polarized from -1500 to 200 mV at a scan rate of 2 mV s^{-1}.

The tribocorrosion tests were performed using a reciprocating tribometer (Plint TE67/R). An alumina pin (truncated cone geometry and with a tip of 0.8 mm in diameter) was used as counterbody and mounted vertically on the samples immersed in the electrolyte (exposed area = 0.95 cm^2). The samples were used as plates positioned horizontally and mounted in an acrylic electrochemical cell (20 ml of 0.6 M NaCl solution was used as electrolyte) (see Figure 5.2). All potentials were measured and expressed with reference to a standard calomel electrode (SCE), and a platinum wire with an area of 1 cm^2 served as auxiliary electrode. A Voltalab PGZ100 Potentiostat

(Radiometer Analytical, Denmark), controlled by Voltamaster-4 Software was used in for potentiostatic control.

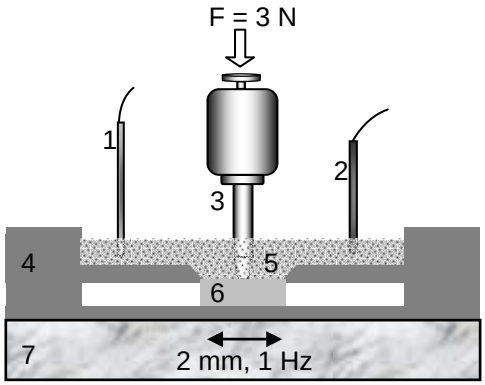

Figure 5.2 – Schematic view of the electrochemical cell used in the tribocorrosion tests: (1) Reference electrode, (2) Auxiliary electrode, (3) Alumina pin, (4) Acrylic recipient, (5) Electrolyte, (6) Working electrode, (7) Tribometer.

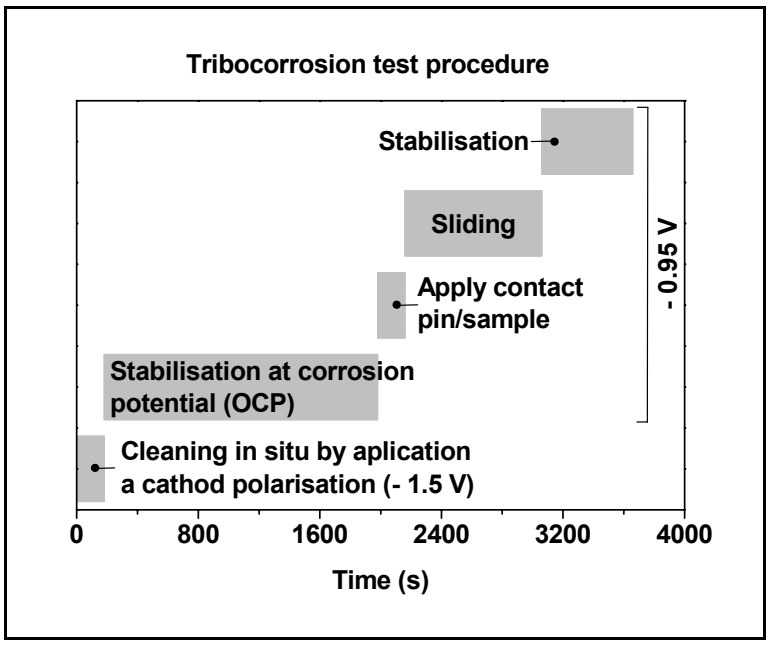

Figure 5.3 – Histogram of the tribocorrosion test.

Samples were previously cathodically polarised at -1500 mV vs. SCE, during 180 sec. Subsequently, a potential of -950 mV vs. SCE was applied to stabilise the samples by a period of 1800 sec. Then, the mechanical contact between the alumina pin

and the sample plate was applied and after 180 sec the sliding began. The reciprocating wear test was performed with a normal load of 3 N, displacement amplitude of 2 mm and a frequency of 1 Hz. The sliding time was 900 s. A histogram of tribocorrosion test is present in figure 5.3. When sliding was stopped, the pin and the sample were removed from the solution and cleaned ultrasonically in ethanol. The total wear volume ($V_{tot} = V_{mech} + V_{chem}$) [7,11], caused by the contribution of wear and corrosion, was determined by a profilometer method, using a Perthometer S5P roughness meter, by calculating the average of the cross-sectional area multiplied by the stroke length. The chemical wear volume (V_{chem}) was determined from the measured current, using Faraday's law, $V_{chem} = (Q \cdot M) / (n \cdot F \cdot \rho)$; where, Q is the electric charge, which is obtained by integrating the current density curve with the time, along of the sliding time, M is the atomic mass of the aluminium (27 $g.mol^{-1}$), n the valence of dissolution of the aluminium (+3), F the Faraday's constant ($9.649 \cdot 10^{-4}$ C mol^{-1}) and ρ is the density of the aluminium($2.7 \cdot 10^{-3}$ $g.mm^{-3}$). The mechanical wear volume, V_{mech} which is the volume of material mechanically removed was obtained by subtracting $V_{tot} - V_{chem}$ [7,8,11].

5.3 – Results and Discussion

5.3.1 – Corrosion Behaviour

After being immersed in the 0.6 M NaCl solution, the corrosion potential (E_{corr}) of the samples was monitored during 60 min. The obtained curves, smoothed because of its high fluctuation, are presented in Figure 5.4 a.1), b.1) and c.1). As it can be observed, all samples, except the 120 *G* inner, reveal an increase in the corrosion potential with the time, indicating the formation of a passive film.

The Al/Al_3Zr FGMs 30 *G* and 60 *G* samples show a similar behaviour, in terms of thermodynamic stability (E_{corr} between -1100 and -800 mV). The sample obtained with 30 *G* reveals a little better behaviour. Conversely, the Al/Al_3Zr FGMs 120 *G* inner sample presents a different behaviour. The more active corrosion potential exhibited by this last sample reflects less thermodynamic stability and therefore its higher corrosion tendency.

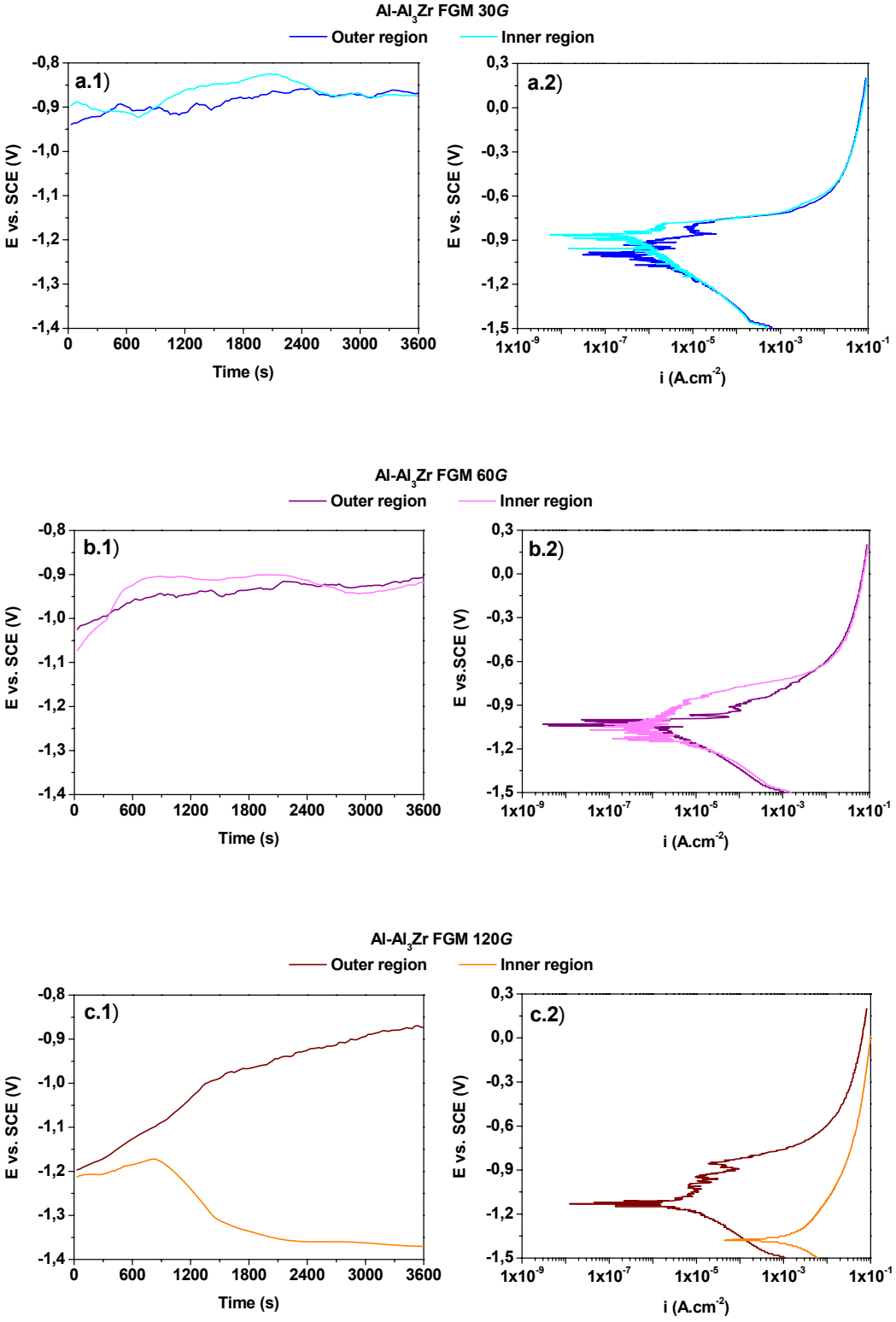

Figure 5.4 – Evolution of corrosion potential with time and anodic polarisation curves obtained for Al/Al$_3$Zr FGMs immersed in 0.6 M NaCl solution.

Figure 5.4 a.2), b.2) and c.2) presents the anodic polarisation curves obtained for all samples. As it can be observed the corrosion behaviour of Al/Al_3Zr FGMs samples is similar, except for the sample 120 *G* inner. In this case, in according to the open circuit potential results, reveals the worst corrosion behaviour. As it can be seen, the determination of the corrosion current density (i_{corr}) for all samples presents some difficulties because of the lot of noise and instability of the samples immersed in the electrolyte.

5.3.2 – Tribocorrosion Behaviour

Results of tribocorrosion tests obtained in Al/Al_3Zr FGMs samples are presented in Figure 5.5. As it can be seen all samples show a similar evolution of the current with the time. The drastic increase in the current at 180 seconds is due to the change of the applied potential from -1500 mV (to clean the sample) to -950mV to stabilize the same. The evolution of the current density and the friction coefficient (μ) with the time in the sliding period is also presented. As it can be seen, all samples show an increase in the current density at the beginning of sliding, corresponding to the initial contact between the counterbody and the surface of the sample. After this, the current density of all samples decreases attempting to reach a steady state. An exception occurs with 60 *G* and 120 *G* outer samples. In these last samples besides the little decrease of current density after the initial contact with the counterbody, the current values are higher when compared with the other samples. It is also possible to note that at the end of sliding period, the current density of all samples decrease reaching values similar to those observed before sliding. This behaviour shows a clear negative influence of the sliding processes on the deterioration of surface samples. In terms of friction coefficient (μ) all samples show a similar behaviour, i. e. increases until achieving a steady state. Once again and similarly as the current density evolution, an exception occurs with the 60 *G* outer and 120 *G* outer samples. The μ of these last samples monotonically increase with the sliding time.

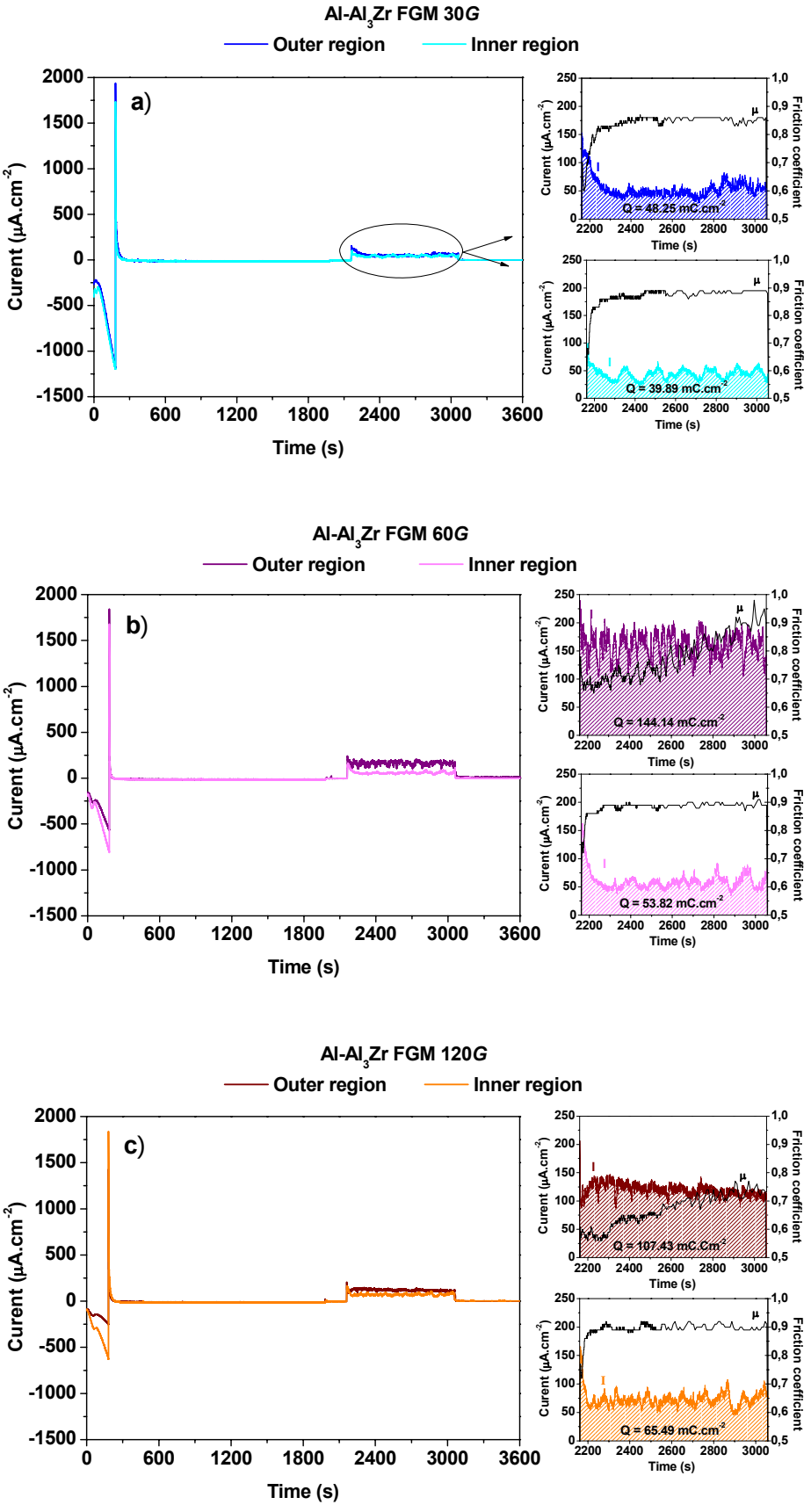

Figure 5.5 – Evolution of the current density during the tribocorrosion test.

The friction coefficient was calculated as an average of the values obtained during sliding period, eliminating the initial sliding values, i.e, excluding the running-in period (2160-2400 s). As it can be observed in Figure 5.6, the values of the μ for 30 *G* outer, 30 G inner, 60 *G* inner and 120*G* inner are near to 0.9. In the 60 *G* outer and 120 *G* outer samples, the μ increases along the sliding time, not reaching a steady state, being for this reason impossible to calculate μ average.

Regarding the synergism between the wear and corrosion phenomena, Figure 5.6 shows a relation between the removed volumes by the mechanical (V_{mech}) and electrochemical (V_{chem}) processes. As it can be seen, all the samples show negligible V_{chem} in front to large V_{mech}. This should be a good indication that the tribocorrosion process is mainly governed by the mechanical wear. Other important observation is that samples exhibiting highest electrochemical removed volume are the 60 G outer and 120 G outer. Additionally, the sample with the highest mechanically removed volume is the 60 G outer.

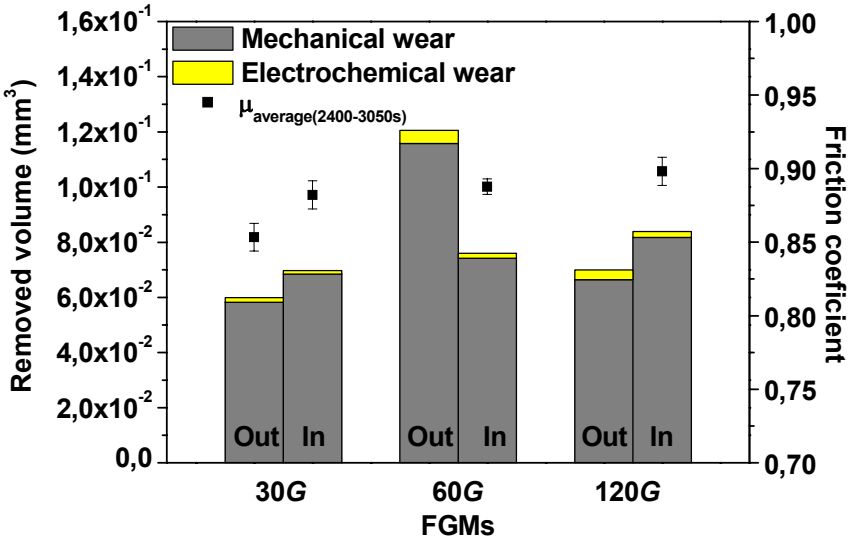

Figure 5.6 – Removed volume by mechanical and electrochemical processes and average friction coefficient in tribocorrosion test.

Figure 5.7 shows the morphology of wear tracks of all Al-Al_3Zr FGMs samples. As it can be observed, the shape and size of the wear tracks are quite similar. In addition, it seems that third body particles and/or some wear debris accumulate at the ends of the wear scar after tribocorrosion tests. It is important to refer that the 60G outer and 120G outer samples, which shown the highest electrochemical removed volume (see Figure 5.6), are the samples with the highest amount of reinforcing particles. This is an indication that the presence of the reinforcing intermatallics promotes a superior electrochemical degradation of the samples, probably due to the galvanic couple effects between the intermetallic compounds and the metallic matrix, as discussed in a previous work [12].

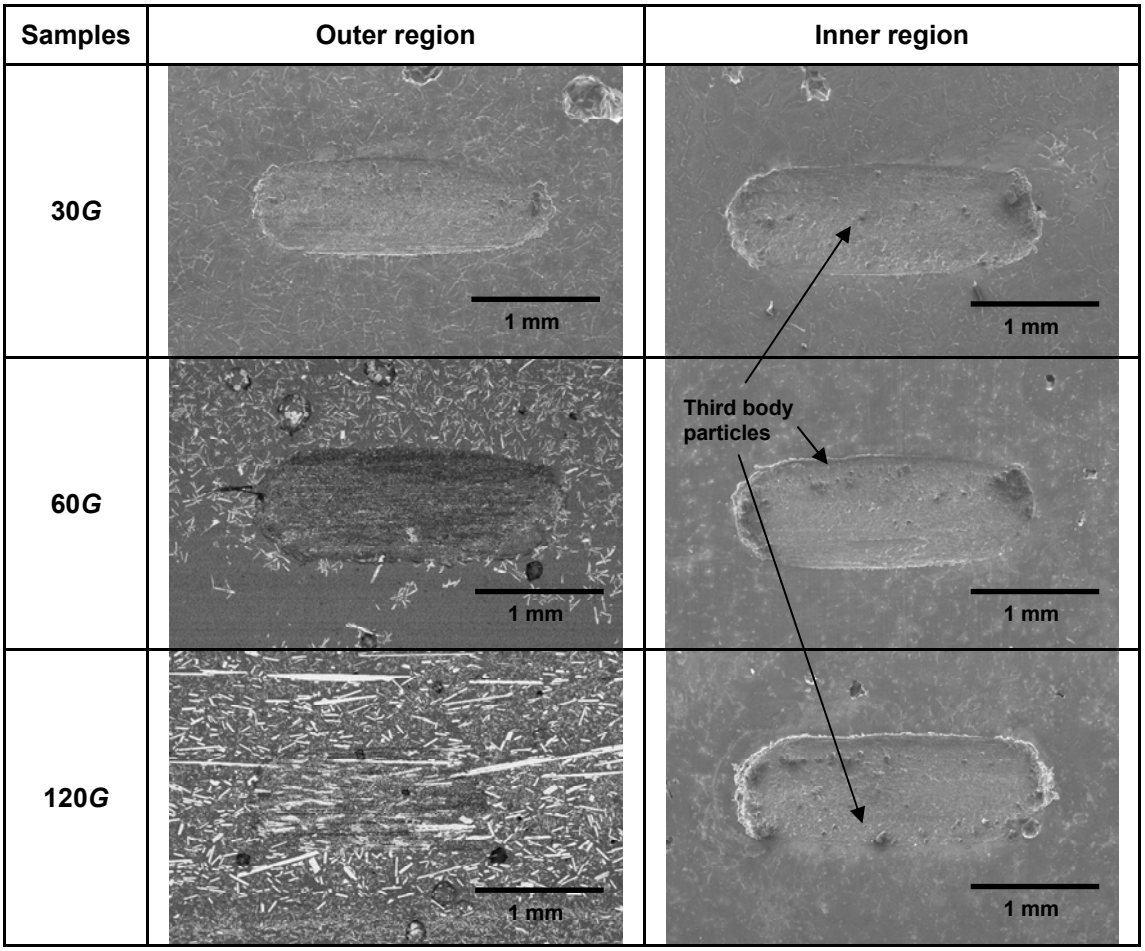

Figure 5.7 – SEM images of the Al/Al_3Zr FGMs after sliding in 0.6 M NaCl.

Other important remark is the different wear behaviour of the 60 *G* outer and 120 *G* outer samples. These samples having the highest particles content (see Figure 5.7), and the highest electrochemical removed volume, show a very dissimilar mechanically removed volume. The lower removed volume by mechanical action and the lower μ shown by the 120 *G* sample, when compared with the 60 *G* outer sample, can be explained by the higher volume fraction of particles obtained from a higher applied centrifugal, such as occurs in the 120 *G* sample.

Figure 5.8 shows the centre of the wear track on Al/Al_3ZrFGMs. In this figure one observes a disrupted surface characterized by plastic deformation and cracks. In the 60 *G* outer and 120 *G* outer was verified that the Al_3Zr platelets are squeezed and/or left by the sliding. In the 60 *G* inner and 120 *G* inner no platelets are observed.

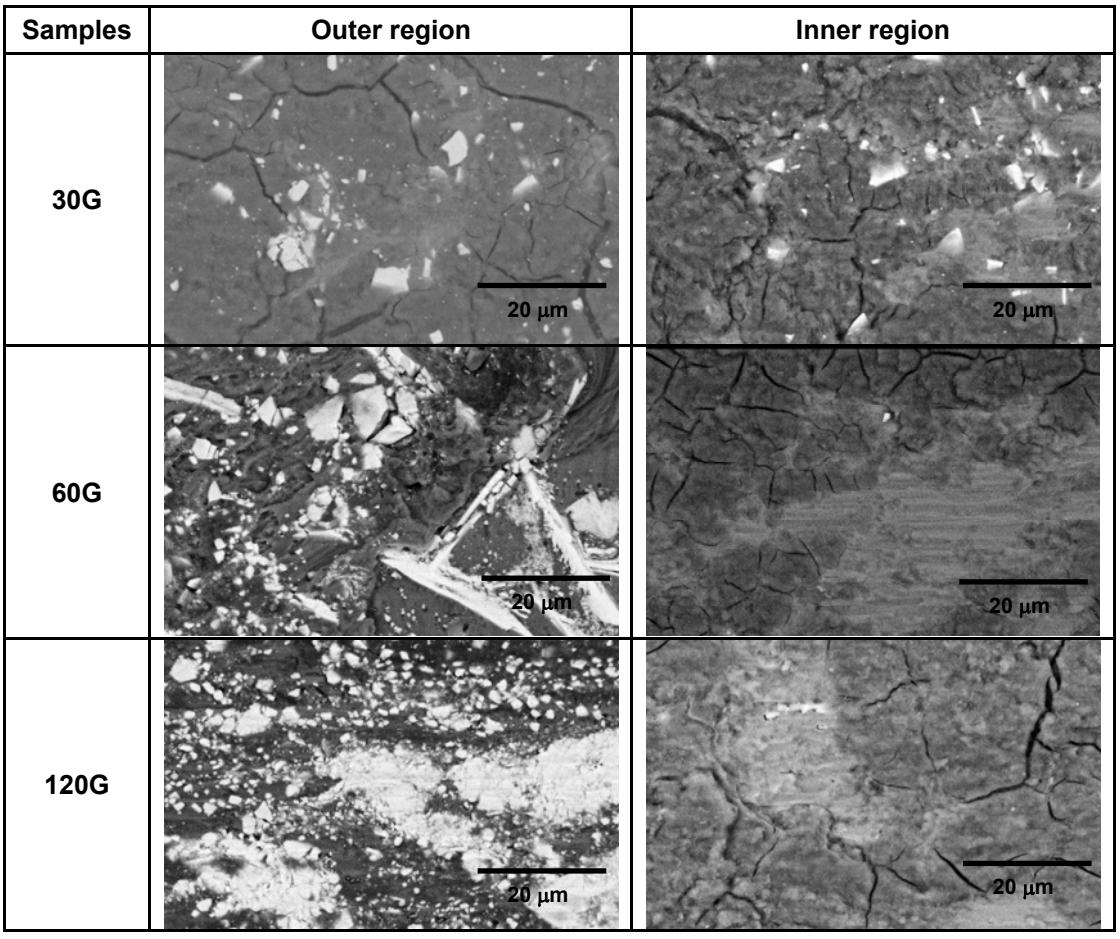

Figure 5.8 – SEM images of the wear track center of the Al/Al_3Zr FGMs.

5.4 – Conclusions

In the present study, the tribocorrosion behaviour of Al/Al_3Zr FGMs, was investigated in a 0.6 M NaCl solution:

1) The electrochemical behaviour of samples showed that some galvanic effects between the intermetallic particles and the metal matrix might affect the overall corrosion process.

2) The tribocorrosion degradation of Al/Al_3Zr FGMs is mainly governed by the mechanical wear.

3) The better tribocorrosion behaviour, i.e., the lowest removal volumes by both mechanical and chemical action, was observed in the samples containing the smaller concentration of reinforcing particles.

Acknowledgements

The authors gratefully acknowledge the financial support provided by 21st COE Research of the Ministry of Education Culture, Sports Science and Technology of Japan. Acknowledgments are also presented to "FCT", Portugal, through project SFRH/BPD/5518/2001.

5.5 – References

[1] Y. Watanabe, Y. Fukui, Rec. Res. Devel. Metall. Mater. Sci. 4 (2000) 51.

[2] Y. Watanabe, Y. Fukui, Aluminum Trans. 2 (2000) 195.

[3] P.D. Sequeira, Y. Watanabe, L.A. Rocha, Mater. Sci. Forum 492 (2005) 609.

[4] Y. Fukui, JSME Int. J. Series III 34 (1991) 144.

[5] D. Roy, B. Basu, A.B. Mallick, Intermetallics 13 (2005) 733.

[6] J.R. Gomes, A.S. Miranda, L.A. Rocha, S.J. Crnkovic, V. Silva, R.F. Silva, Int. J. Appl. Mech. Eng. 7 (2002) 791.

[7] S. Mischler, A. Spiegel, M. Stemp, D. Landolt, Wear 251 (2001) 1295.

[8] S. Mischler, A. Spiegel, D. Landolt, Wear 225-229 (1999) 1078.

[9] P. Jemmely, S. Mischler, D. Landolt, Tribology International 32 (1999) 295.

[10] P. Jemmely, S. Mischler, D. Landolt, Wear 237(2000) 63.

[11] D. Landolt, S. Mischler, M. Stemp, Electrochim. Acta 46 (2001) 3913.

[12] S.C. Ferreira, L.A. Rocha, E. Ariza, J.R. Gomes, P.D. Sequeira, Y. Watanabe, *Tribocorrosion Behaviour of Al-Al_3Ti and Al-Al_3Zr FGMs*, European Corrosion Conference (EUROCORR 2005), Lisbon, Portugal, September, 2005.

CHAPTER 6

Microstructural Characterization and Wear Behaviour of Two-Phase Al-5 mass % Ti Alloy Deformed By Equal-Channel Angular Pressing

P.D. Sequeira [a], S.C. Ferreira [a], Y. Watanabe [b], L.A. Rocha [a,c],J.R. Gomes [a,c]

[a] Research Centre on Interfaces and Surface Performance, University of Minho, Campus de Azurém, 4800-058 Guimarães, Portugal

[b] Department of Engineering Physics, Electronics and Mechanics, Graduate School of Engineering, Nagoya Institute of Technology, Gokiso-Chu, Showa-Ku, 466-8555 Nagoya, Japan

[c] Department of Mechanical Engineering, University of Minho, Campus de Azurém, 4800-058 Guimarães, Portugal

Abstract

Equal-channel angular pressing (ECAP) was used to induce large plastic strains in an Al/Al_3Ti composite (Al-5 mass % Ti alloy). Microstructural changes and mechanical properties were studied for the as-cast alloy and for samples pressed from 1 up to 6 passes through the die. Due to the high strain imposed in the ECAP process Al_3Ti particles break-up occurs and they become aligned in bands in the deformation direction. Hardness increases with an increase in the number of passes through the die. The wear resistance is lower in the deformed samples than in the as-cast composite. Al_3Ti particle alignment in bands along the deformation direction leads to anisotropy in

the wear behaviour, with higher wear resistance found in the direction parallel to the deformation direction.

Keywords: Equal-Channel Angular Pressing (ECAP); Titanium Aluminides; Wear

6.1 – Introduction

Al-rich intermetallic compounds as reinforcing dispersoids in Al alloys are of significant interest as they affect mechanical properties, corrosion resistance, surface finish and electrical resistivity of Al alloys. Moreover, intermetallic compounds such as Al_3Ti are thermally stable making Al alloys reinforced by Al_3Ti dispersoids attractive for elevated temperature applications [1].

A high interest exists in using ECAP for processing of ultrafine-grained (UFG) microstructures. With this method, by multiple passes through a die, very high strains can be achieved without any change in the billet dimensions. The resulting UFG metallic materials exhibit high strength while maintaining toughness and ductility [2-5].

Most of the previous studies have been performed mainly in single-phase alloys, although research into processing of two-phase Al alloys by ECAP has recently been gaining more attention. Shin et al. [6-8] have reported on the strengthening effect of ECAP on low-carbon steels. Microstructure of two-phase Al-1.7 at % Cu alloy deformed by ECAP was studied by Murayama et al. [9]. Stolyarov et al. [10] study on the processing of Al-5 wt % Fe alloy by ECAP revealed enhanced Fe solubility in the Al alloy and also improvement in strength, ductility and microhardness. Also Al metal matrix composites reinforced by silicon carbide (SiC) whiskers [11] or by aluminium oxide (Al_2O_3) particles [12] have been the object of recent research.

Due to potential tribological application in the automotive and aerospace industries, wear behaviour of Al alloys reinforced by Al_3Ti dispersoids has been studied previously. Cold deformation of Al-10 wt % Ti alloy was shown to decrease the wear resistance at the adhesive wear regime but to improve it, to a certain degree, at the oxidation stage [13]. In another study it was indicated that the dry sliding wear resistance of the Al alloys reinforced by Al_3Ti dispersoids increases with increasing

particle volume fraction and decreasing particle size [14]. Furthermore, Watanabe et al. reported on anisotropic wear conditions of Al/Al_3Ti composites due to particle orientation [15].

In this study microstructural and mechanical properties characterization of an Al-5 mass % Ti alloy before and after processing by ECAP from 1 up to 6 passes was performed. Wear experiments were carried out in two directions, parallel and perpendicular to the deformation direction.

6.2 – Experimental Procedure

Rod-shaped samples of an Al-5 mass % Ti alloy, 10 mm diameter and 50 mm in length, were used. The samples were subjected to ECAP at room temperature using MoS_2 as a lubricant. The schematic of the die used during pressing is shown in Figure 6.1. The die contains two channels equal in cross-section. Those channels intersect at an internal angle of ϕ and the outer arc of curvature is defined as ψ. As reported by Iwahashi et al. [16] the sheer strain, ε_N, introduced during ECAP is given by:

$$\varepsilon_N = \frac{N}{\sqrt{3}}\left[2\cot\left(\frac{\phi}{2}+\frac{\psi}{2}\right)+\psi\,\mathrm{cosec}\left(\frac{\phi}{2}+\frac{\psi}{2}\right)\right] \qquad (6.1)$$

where N is the number of passes through the die. The die used during this study had ϕ = 90° and ψ = 45° and subjected to the ECAP procedure from 1 up to 6 passes. Nakashima et al. [17] calculated that regardless of the values of ψ, a single passage through a die with ϕ = 90° will result in a strain close to 1.

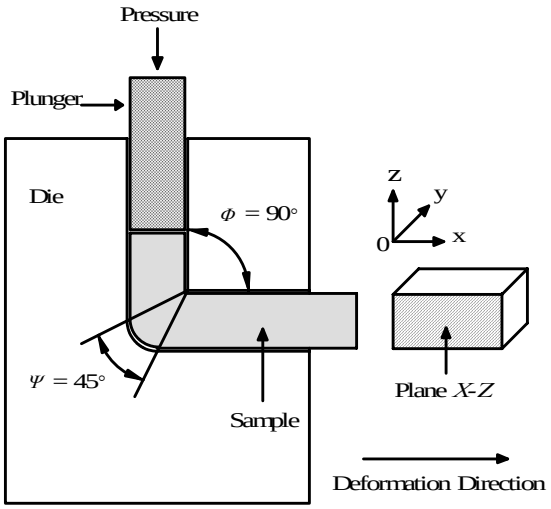

Figure 6.1 – Schematic representation of the ECAP die.

6.2.1 – Microstructural Analysis

Samples were cut along the longitudinal plane (plane *x-z* in Figure 6.1) and characterized by optical microscopy (OM) and scanning electron microscopy (SEM). Computer analysis was performed and size and volume fraction of Al_3Ti particles measured.

6.2.2 – Mechanical Properties

The wear tests were carried out in a Plint TE67 tribometer in the ball-on-plate test geometry with reciprocating motion of the plate. The ECAP samples were used as plate and AISI 52100 steel as ball, with 0.4 mm diameter. Sliding was performed in the absence of lubrication at ambient temperature, under controlled conditions of humidity in the surrounding atmosphere, with relative humidity of 50 % ± 5 % and with the absence of lubrication. The normal applied load was fixed at 3 N. The total sliding distance was 10 m, displacement was 6 mm and the frequency of the oscillation motion was 1 Hz. The wear coefficient, *K*, was quantified by equation:

$$K = \frac{V}{W \cdot x} \qquad (6.2)$$

with V being the volume of wear in mm^3, W the normal load in N and x the distance of sliding in m.

The wear experiments were carried out in x-z plane (see Figure 6.1) and two sliding directions were used, parallel and perpendicular to the deformation direction.

6.3 – Results and Discussion

6.3.1 – Microstructural Analysis

In Figure 6.2 are presented typical microstructures obtained by either OM (6.2 a) and b) or SEM (6.2 c) and d), for the as-cast and samples processed by ECAP for 1, 3 and 6 passes. In the as-cast sample the Al_3Ti particles are large and randomly distributed. After 1 pass through the die, due to the high shear strain introduced by the ECAP process, break-up is clearly visible. Further passes through the die continue to break-up the particles and they begin to align in bands along the deformation direction.

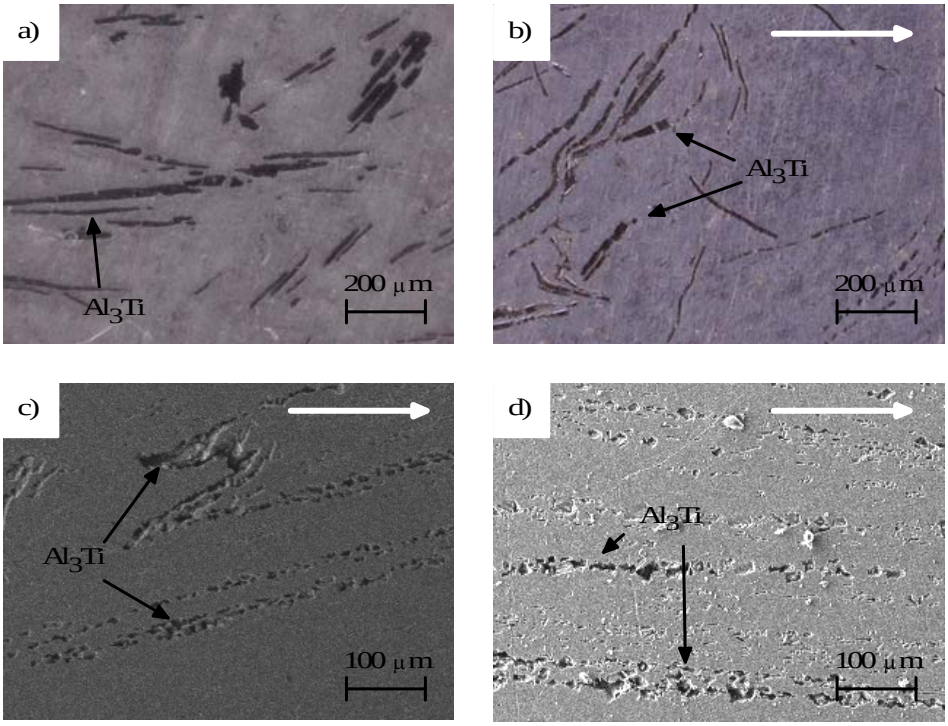

Figure 6.2 – Typical microstructures in the samples before (a) and after one (b), three (c) and six (d) passes through the die. Deformation direction is indicated by the white arrow in the upper right corner of the micrographs of the extruded samples.

In Figure 6.3, the mean volume fraction of Al_3Ti particles as a function of the number of passes of ECAP is shown. Volume fraction of Al_3Ti particles in the Al-5 mass % Ti alloy is 11 %. As can be seen in Figure 6.3 there is a significant decline in Al_3Ti particle volume fraction up to 3 passes and a smaller decline after that. This decline might be attributed to two phenomena. Particles are refined into very fine dispersoids not measurable in the graphic analysis technique used in the present study and also by dissolution of Ti in the Al matrix. In fact, *Stolyarov et al.* [10] describe an increase of Fe solubility in an Al matrix after processing of an Al-5 mass % Fe alloy by ECAP.

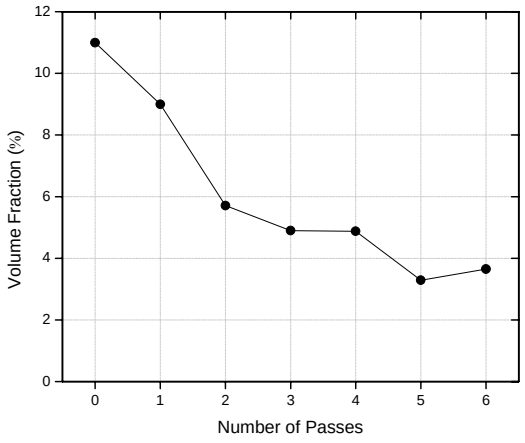

Figure 6.3 – Volume fraction of Al_3Ti particles as a function of the number of passes through the die.

The mean equivalent area particle diameter as a function of ECAP passes is presented in Figure 6.4. The computer analysis technique used has a lower particle diameter resolution limit of 10 μm. Still it is clear that successive passes through the die lead to a considerable decrease in the particle size.

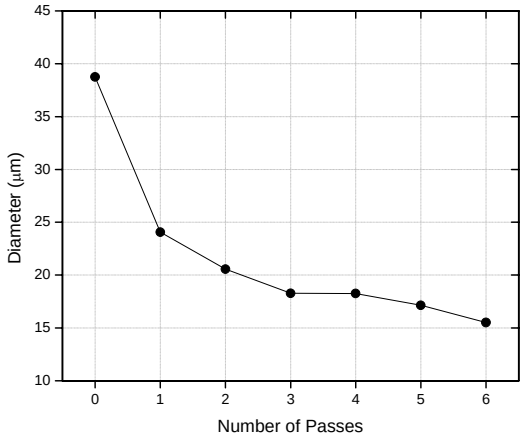

Figure 6.4 – Mean equal area diameter of Al_3Ti particles as a function of the number of passes through the die.

6.3.2 – Mechanical Properties

Figure 6.5 shows the effect of the number of ECAP passes on the hardness of the Al-5 mass % Ti alloy. An increase of the hardness from the as-cast sample up to 6 ECAP passes occurs. Refining of both the Al matrix grains and the intermetallic phase leads to this increase in the materials hardness. However, this increase is more pronounced during the first extrusion pass becoming then almost linear from 1 to 6 passes. This trend was also observed in other studies [7,10,18].

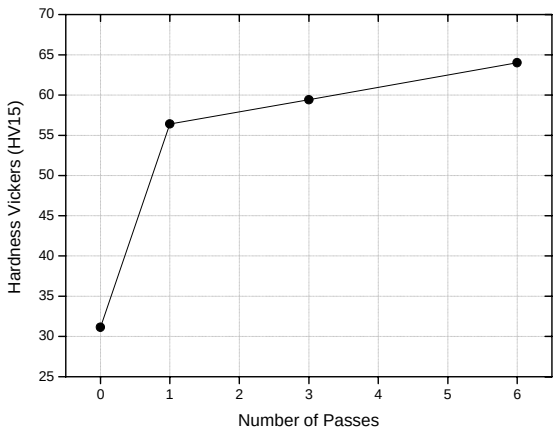

Figure 6.5 – Vickers Hardness as a function of the number of passes through the die.

The influence of the number of passes of the Al-5 mass % Ti alloy on the wear behaviour against AISI 52100 steel is shown in Figure 6.6.

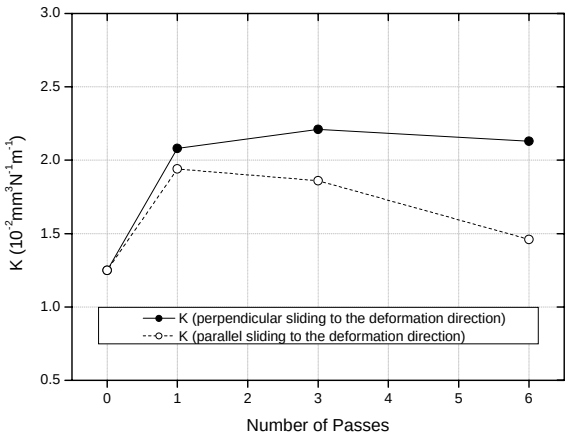

Figure 6.6 – Influence of the number of ECAP passes on the wear behaviour of an Al-5 mass % Ti against AISI 52100 steel.

A notable increase of the wear rate from the as-cast sample to the sample deformed after 1 pass is evident in both the sliding perpendicular and parallel to the ECAP deformation direction. Considering the wear coefficient values in the sliding direction perpendicular to the direction of deformation one can see that they are higher than those referring to the wear coefficients in the parallel sliding direction. The wear coefficient values in the sliding direction perpendicular to the direction of deformation show a small variation ($2x10^{-2}$ to $2.2x10^{-2}$), while, the values in the parallel sliding direction tend to decrease from 1 to 6 passes.

The morphological wear features corresponding to zero and six passes of the ECAP are presented in Figure 6.7. In these pictures, the sliding direction is parallel (6.7 b) and perpendicular (6.7 c) to the deformation direction of the ECAP. Micrographs of one and three passes are not show because the wear pattern of this material is similar to that of six passes sample.

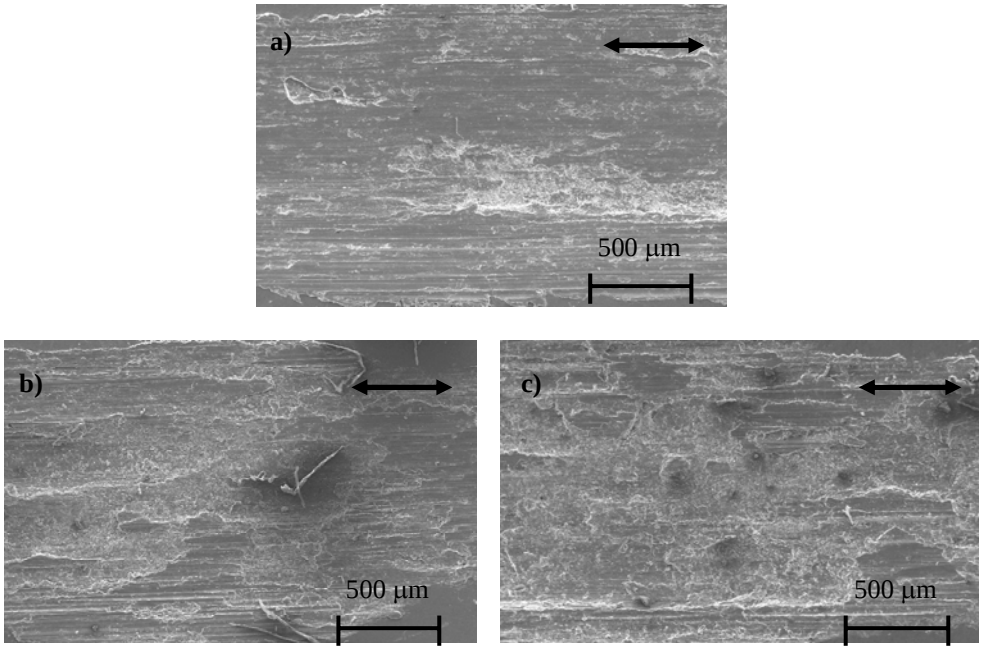

Figure 6.7 – SEM images of the samples after wear experiment: a) zero passes sample, b) parallel sliding to the deformation direction with six passes and c) perpendicular sliding to the deformation direction with six passes. Sliding direction is indicated by the black arrow.

Upon further deformation, with a continued particle size reduction and their alignment in bands along the deformation direction, a decrease in wear is observed in the direction parallel to the deformation direction. At this stage it is believed that the reduction in size of Al_3Ti particles will lead first to a loss of load bearing capabilities and an increase in wear rate. The high strain imposed by the ECAP procedure might also weaken the particle-matrix interface. However, as the particles are refined they will then have a strengthening effect on the matrix reducing the wear coefficient in the direction parallel to the deformation direction. Wu et al. [14] found that decreasing Al_3Ti particle size in an Al-Ti alloy lead to an increase in wear resistance, attributed to the predominance in oxidative and adhesion wear mechanisms. The same effect does not occur in the direction perpendicular to the deformation direction where the wear rate remains almost constant. It is believed that this can be attributed to the observed banded microstructure. Contact between plate and ball will occur in successive bands of reinforced and non reinforced regions facilitating particle pull-out.

6.4 – Conclusions

An Al-5 mass % Ti alloy was processed by ECAP from 1 up to 6 passes. Microstructural and mechanical properties characterization was performed.

1) Al_3Ti particle break-up and alignment in the deformation direction was observed.

2) The increase of passes in the ECAP process for the Al- 5 mass% Ti alloy increases the hardness of the alloy.

3) Reduction of wear resistance in the deformed alloys compared to the non deformed alloy was found.

4) Anisotropic wear resistance was observed perpendicular and parallel to the deformation direction by ECAP. With a recovery of wear resistance in the sliding direction parallel to the deformation direction.

Acknowledgments

This study was partially supported by the Grant-in-Aid for 21st Century COE Program *"Advanced Fiber Science and Textile Technology"* by the Ministry of Education, Culture, Sports, Science and Technology of Japan.

6.5 – References

[1] S.K. Das, Al-Rich Intermetallics in Aluminum Alloys, in Intermetallic Compounds, ed J.H Westbrook and R.L. Fleischer; Volume 3, Wiley, 2000, p.179.

[2] V.M. Segal, V.I. Reznikov, A.E. Drobyshevskiy V.I. Kopylov, Russian Mettalurgy, (Engl. Transl.) 1 (1981) 99.

[3] V.M. Segal, Mater. Sci. Eng. A 197 (1995) 157.

[4] M. Furukawa, Z. Horito, M. Nemoto and T.G. Landon, J. Mater. Sci. 36 (2001) 2835.

[5] M. Murayama, Z. Horita and K. Hono, Acta Mater. 49 (2001) 21.

[6] D.H. Shin, W.J. Kim, W.Y. Choo, Scripta Mater 41 (1999) 259.

[7] D.H. Shin, C.W. Seo, J. Kim, K.T. Park, W.Y. Choo, Scripta Mater 42 (2000) 695.

[8] D.H. Shin, B.C. Kim, K.T. Park, W.Y. Choo, Acta Mater 48 (2000) 3245.

[9] M. Murayama, Z. Horita, K. Hono, Acta Mater 49 (2001) 21.

[10] V.V. Stolyarov, R. Lapovok, I.G. Brodova, P.F. Thomson, Mater Sci Eng A357 (2003)159.

[11] D.Ma, J. Wang, K. Xu. Mater Letters 56 (2002) 999.

[12] I. Sabirov, O. Kolednik, R.Z. Valiev, R. Pippan, Acta Mater. (2005).

[13] J.M. Wu, S.L. Zheng, Z.Z. Li, Y. W. Zeng, Wear 232 (1999) 25.

[14] J.M. Wu, Z.Z. Li , Wear 244 (2000) 147.

[15] Y. Watanabe, N. Yamanaka, Y. Fukui, Metall. Mater. Trans. A 30A (1999) 3253.

[16] Y. Iwahashi, M. Furukawa, Z. Horita, M. Nemoto, T.G. Langdon, Metall. Mater. Trans. A 29A (1998) 2245.

[17] K. Nakashima, Z. Horita, M. Nemoto, T.G. Langdon, Acta Mater. 46 (1998) 1589.

[18] Z. Zhang, Y. Watanabe, I. Kim, Mater. Sci. Tec. 21 (2005) 1.

CHAPTER 7

General Discussion and Comparison of the Experimental Results

In this chapter, the experimental results presented in each previous chapter of three to six on the subject of corrosion and tribocorrosion behaviour of the Al/Al_3Ti and Al/Al_3Zr FGMs and wear behaviour of Al-5 mass % Ti alloy deformed by ECAP are compared and discussed, in order to understand the relationships between them.

The corrosion behaviour of Al/Al_3Ti and Al/Al_3Zr FGMs was evaluated through OCP, potentiodynamic polarization and EIS in a 0.6 M NaCl solution at room temperature (Figures 3.2 and 3.3). The analysed region on the ring FGM obtained by centrifugal casting was the outer region of the perpendicular plane to rotation axis (OP1). In OP1, the volume fraction occupied by Al_3Ti or Al_3Zr particles increases from the inner to the outer regions of the FGM rings. Moreover, the samples 60 and 120 *G* have absence of particles from around the middle to the inner region of the rings in both the Al/Al_3Ti and Al/Al_3Zr FGMs. The concentration of particles is larger in the outer region (Figure 3.7). It should be referred that, the outer zones of the Al/Al_3Ti FGMs group are similar in terms of area fraction of particles, in opposing of the Al/Al_3Zr FGM group, where the 30 *G* sample presents smaller concentration of particles in the outer region than the 60 and 120 *G* samples.

By monitoring the corrosion potential (E_{corr}) for the period of 60 minutes, all samples revealed an increase in the corrosion potential with the time, indicating the formation of a passive film (Figure 3.2). The Al/Al_3Ti FGMs group shows a similar behaviour, in terms of thermodynamic stability. In this group, the sample obtained with centrifugal force of 60 *G* reveals a little better behaviour. On the contrary, the Al/Al_3Zr FGMs group presents a more dispersed behaviour. Here, 30 *G* sample reveals a E_{corr}

clearly higher than the 60 *G* and 120 *G* samples. The more active corrosion potential exhibited by these last samples reflects its less thermodynamic stability and therefore its higher corrosion tendency.

The anodic polarisation curves revealed accord with the OCP results (Figure 3.3). Al/Al_3Ti FGMs group is also very similar. In case of Al/Al_3Zr FGMs group, the samples obtained with 60 *G* and 120 *G* revealed the worst corrosion behaviour. This phenomenon can be explained by the low segregation of particles found in the sample obtained with 30 *G*. This group shows that the degradation of samples intensifies with the increase of the concentration particles.

It is well known that corrosion attack is a function of matrix composition and increases with reinforcement volume concentration [1]. Moreover, in aluminium matrix composites both, ceramic particles/matrix and intermetallic compounds/matrix interfaces are preferential sites of localized attack with pits of larger size. The pits nucleation preferentially begins at the matrix/ceramic particles and matrix/intermetallic compounds interfaces [1-3].

As reported in [4], the aluminium alloys containing intermetallic phases can be characterized as undergoing localized attacks basically in the zones surrounding particular types of intermetallic compounds. This type of attack leads to the formation of large numbers of pits, which extend to a large proportion of the exposed surface area. This process is associated with the cathodic character of the precipitates of Al_3Ti and Al_3Zr [5], in nearness to which this type of attack is produced. The cavities formed are a consequence of the loss of contact between reinforcements and the matrix.

Thus, the higher degradation of the outer region of Al/Al_3Zr FGMs samples obtained with 60 *G* and 120 *G* is explained by the higher concentration of particles. The cathodic area is highest in this region compared with anodic area.

The effect of corrosion of the matrix in the zone surrounding the precipitates of Al_3Ti and Al_3Zr was clearly observed in the scanning electron microscopy (SEM) image. The morphology of the FGMs samples revealed a large degradation, in the adjacent regions to the reinforced particles, but the particles are not attacked (figures 3.4 and 3.5). In case of Al/Al_3Zr FGMs group, the concentration of small particles appears to be higher than that found in Al/Al_3Ti sample. In a similar manner, both FGMs groups after polarisation test suffered a high degradation in the adjacent regions to the particles.

The corrosion current density (i_{corr}) was not possible to estimate by extrapolating linear portions of the anodic and cathode branches, known as Tafel plots, due to the high noise level present in the anodic polarisation curves.

Experimental EIS results from Al/Al_3Ti and Al/Al_3Zr FGMs after 1, 3, 6 and 10 days were analysed with base in an equivalent circuit described in Chapter 3 (Figure 3.11). Evaluating the Al/Al_3Ti FGMs group, the 60*G* sample presents the highest polarization resistance (R_p) and resistance of the passive film (R_{pf}), indicating its relatively better corrosion behaviour. So that, this sample reveals the lowest capacitance of the passive film (C_{pf}), revealing its better protective character. These results are in total accordance with the OCP and the potentiodynamic polarization results, which showed a little better corrosion behaviour for this sample. With relationship to the group of Al/Al_3Zr FGMs, this presented an abrupt decrease in the R_p values from 1 to 3 immersion days. Also, from 3 up to 10 days of immersion the samples showed a slight decrease of R_p. An exception occurs with the sample obtained with 60 *G*, which reveals an increase in the R_p from 3 to 10 days of immersion time. The R_{pf} decrease along of the 10 days of immersion for all samples, indicate the degradation of the passive film. This phenomenon is confirmed by the evolution of the C_{pf} in all Al/Al_3Zr FGMs samples, which increase with the immersion time. As suggested by the OCP and potentiodynamic polarisation tests, 30 *G* sample show the highest R_{pf} and the lowest C_{pf} values indicating the better corrosion behaviour of this group.

In terms of the corrosion behaviour, the Al/Al_3Ti FGMs 60 *G* and Al/Al_3Zr FGMs 30 *G* samples present the better corrosion resistance, inside of the corresponding group.

Following, the investigation of the synergic effect of corrosion-wear in the same samples and same regions was performed (Chapter 4). Results of tribocorrosion tests obtained in FGMs samples show a similar evolution of the current with the time (Figures 4.9 and 4.11). All samples show an increase in the current at the beginning of sliding, corresponding to the initial contact between the counter body and the surface of the sample. After this, the current density decreases until reaching the stable state. In the Al/Al_3Ti FGMs group, the 30 *G* sample achieves a stationary state more early. The sample 120 *G* follows a similar behaviour, while the sample 60 *G* takes much more time

to reach a stable state. At the end of sliding, the 60 *G* samples have current density values similar to 30 *G* and higher than 120 *G* sample which presents the lowest current.

In terms of friction coefficient all samples show similar behaviour, μ varies between 0.4 and 0.5, the lowest value corresponding to the 120 *G* sample. This sample presents the lowest average friction coefficient and the lowest current density.

The results of tribocorrosion tests obtained for the Al/Al_3Zr FGMs group (Figure 4.11), the 30 *G* and 60 *G* samples show similar current density values during the sliding, which is twice when compared with the 120 *G* sample. In this group, the μ varies between 0.4 and 0.6. The sample with the more stable μ during the sliding time is the 30 *G* sample. The sample with the lowest μ is the 60 *G* sample. μ decreases abruptly in the first 3 minutes of wear and then stabilizes. In the case of the 120 *G* sample, the μ is very unstable during the sliding time and is the highest when compared with the other samples.

The morphologies of SEM of the FGM samples indicated abrasive scratches and cracking of the intermetallic platelets on the deformed wear zone. Plastic deformation was clearly visible on the deformed wear zone i.e, the wear scar shows signs of severe wear (Figures 4.10 and 4.11).

Al/Al_3Ti FGMs samples present slightly lower friction coefficient and lower current densities when compared with Al/Al_3Zr FGMs samples.

Regarding to the synergism between the wear and corrosion phenomena, all the samples show insignificant removed volumes by electrochemical process (V_{chem}) when compared to the amount of material removed by the mechanical process (V_{mech}). This indicates that the tribocorrosion process in these materials is mainly governed by the mechanical wear (Figure 4.13). It is also observed that the samples having a large V_{mech} show a larger V_{chem}, indicating probably that there is an increase in the corrosion rate due to wear. Other important characteristic is that the samples with a less total wear volume are the 120 *G* ones. This phenomenon can be explained by the higher volume fraction of particles obtained from a higher applied centrifugal, such as occurs in all 120 *G* samples. In general terms, better tribocorrosion behaviour was found in the samples containing the highest concentration of reinforcing particles.

It is important to refer that the Al/Al_3Ti FGMs 60 *G* and Al/Al_3Zr FGMs 30 *G* samples that show better corrosion behaviour, are those showing a worst behaviour in terms of tribocorrosion.

In the tribocorrosion tests, the action of the mechanical loading is much more aggressive than the corrosion effect. Also, the presence of hard particles has a positive effect in terms of resistance to mechanical wear, as shown by several authors in studies of Al-based MMCs in dry sliding [6,7]. The addition of hard particles, until a convenient percentage and size improved the wear rate of the Al alloy. This behaviour is due to the capacity of support of load of the reinforcement particles. However if the amount of particles is too high they will fracture, decreasing the wear resistance of the material [6-9]. In Al-based FGMs, the reinforcing particles with higher bulk density than liquid aluminium segregate towards the outer regions as a result of the forces created during the centrifugal casting process. Additionally, hardness values, wear test results, and wear track analysis were consistent with the microstructural gradient observed in composites. In effect, the higher volume density of reinforcing particles in the outer regions of the centrifugally cast samples translates into a higher hardness and higher overall wear resistance on those regions [10-13].

The tribocorrosion processes of Al/intermetallics compounds FGMs are mainly governed by mechanical wear. It was verified that exits a synergism between the wear and the corrosion process; corrosion will increase together with wear rate.

The study of the corrosion and tribocorrosion behaviour was just performed in Al/Al_3Zr FGMs group in the plan perpendicular to the rotating direction (OP2) in two regions, outer and inner of the ring (Chapter 5).

In this case, all samples, except the 120 *G* inner, reveal an increase in the corrosion potential with the immersed time, indicating the formation of a passive film (Figure 5.4). The Al/Al_3Zr FGMs 30 *G* and 60 *G* samples show a similar behaviour, in terms of thermodynamic stability. The sample obtained with 30 *G* reveals a little better behaviour, (as seen in OP1) and 120 *G* inner reveals the worst corrosion behaviour. The anodic polarisation curves obtained for all Al/Al_3Zr FGMs samples are similar, except for the sample 120 *G* inner. Thus, these results appear to be in accordance with OCP results.

Results of tribocorrosion tests obtained in Al/Al_3Zr FGMs samples show a similar evolution of the current with the time (Figure 5.5). All samples show an increase in the current density at the beginning of sliding, corresponding to the initial contact between the counterbody and the surface of the sample. After this, the current density of all samples decreases attempting to reach a steady state. An exception occurs with 60 *G* and 120 *G* outer samples. It is also possible to note that at the end of sliding period, the current density of all samples decrease reaching values similar to those observed before sliding. This behaviour shows a clear negative influence of the sliding processes on the deterioration of surface samples. In comparison with the plane OP1, the plane OP2 has larger values of *Q*, in other words, higher electrochemical degradation. Additionaly, the 60 *G* sample show a larger *Q*. The observation of the larger *Q* of 120 outer sample in OP2, is in opposition with smaller *Q* in OP1.

In terms of μ, all samples show a similar behaviour, i.e. increases until achieving a steady state. Once again and similarly as the current density evolution, an exception occurs with the 60 *G* outer and 120 *G* outer samples. The μ of these last samples monotonically increase with the sliding time.

Regarding the tribocorrosion phenomena, all the samples show negligible V_{chem} in front to large V_{mech} (Figure 5.6), as in OP1 (Figure 4.13 b). This indicates that the tribocorrosion process is mainly governed by the mechanical wear. Other important observation is that samples exhibiting highest electrochemical degradation are the 60 *G* outer and 120 *G* outer. Additionally, the sample with the highest mechanically removed volume is the 60 *G* outer. This is in contrast with the result found in the plane OP1. It was expected that 60 *G* outer had lesser removed volume total that the 30 *G* samples and 60 *G* inner. So, in this sample, the tribocorrosion test might have been performed in a region of porosity which is able of increasing the degradation by chemical action and beyond of the action of third body in the tribological contact. In 30 G and 120 G samples, as expected, the inner regions were fairly depleted of reinforcement particles and, thus, were subject to higher wear rates.

The values of the μ and removed volume total for OP1 are lower than found in OP2 for Al/Al_3Zr FGMs.

The morphology of wear tracks of all Al/Al_3Zr FGMs samples show some third body particles and/or wear debris accumulate at the wear scar after tribocorrosion tests (Figure 5.7).

In Chapter 6 was described a study of wear resistance of Al-5 % mass Ti alloy deformed by ECAP for 1, 3 and 6 passes.

An increase of the hardness since 0 up to 6 passes occurs. However, this increase is more pronounced between 0 to 1 passes becoming then almost linear from 1 to 6 passes (Figure 6.5).

The first remark to be done relates to the fact that the alloys possess a very low wear resistance (Figure 6.6). A significant increase of the wear occurs from 0 to 1 passes can also be evidenced in the perpendicular sliding but also in the parallel to the direction of deformation by ECAP. Considering the values of the wear coefficient values in the sliding direction perpendicular to the direction of deformation, $K_{\perp}$, one can see that they are higher than those referring to the wear values in parallel sliding direction, $K_{||}$. The values of $K_{\perp}$ show a variation of the next values between themselves, while, the values of $K_{||}$ tend to decrease from 1 to 6 passes.

The increase of the number of passes causes high degree of deformation and a microstructure that increases the material hardness. However, as shown by the obtained results, it does not confer an increase of the wear resistance.

In fact, it was expected that an increase of the number of passes, despite increasing the hardness, would also increase the wear resistance, which was not the case in this work.

7.1 – References

[1] A. Pardo, M.C. Merino,S. Merino, F. Viejo, M. Carboneras,R. Arrabal, Corros. Sci. 47 (2005) 1750.

[2] A. Pardo, M.C. Merino, R. Arrabal, F. Viejo, M. Carboneras, J.A. Muñoz, Corrosion Science (2005), in press.

[3] A. Pardo, M.C. Merino, R. Arrabal, S. Feliú Jr., F. Viejo, M. Carboneras, Electrochim Acta (2006), in press.

[4] A. Aballe, M. Bethencourt, F.J. Botana, M.J. Cano, M. Marcos, Corros. Sci. 45 (2003) 161.

[5] N. Birbilis, R. G. Buchheit, J. Electrochem. Soc. 152 (2005) B140.

[6] D.P. Mondal, S. Das, R.N. Rao, M. Singh, Mater. Sci. Eng. A 402 (2005) 307

[7] H. Sevik, S.C. Kurnaz, Mater. Des. 27(2006) 676.

[8] M. Kök, Composites: Parte A 37 (2006) 457.

[9] Y. Sahin, Mater. Des. (2006) in press.

[10] J.R. Gomes, A.S. Miranda, D.F. Soares, A.E. Dias, L.A. Rocha, S.J. Crnkovic, R.F. Silva, Ceramics Trans. 114 (2000) 579.

[11] J.R. Gomes, A.S. Miranda, L.A. Rocha, S.J. Crnkovic, V. Silva, R.F. Silva, Int. J. Appl. Mech. Eng. 7 (2002) 791.

[12] J.R. Gomes, L.A. Rocha, S.J. Crnkovic, R.F. Silva, A.S. Miranda, Mater. Sci. Forum 423 (2003) 91.

[13] Z.H. Melgarejo, O. M. Suárez, K. Sridharan, Scripta Mater (2006) in press.

CHAPTER 8

Conclusions

A study on corrosion, tribocorrosion and wear in Al/intermetallic composites was presented in this work. The main conclusions of this work were presented throughout this these and the most important writing here.

The corrosion resistance of Al/intermetallic FGMs is influenced by galvanic effects between the intermetallic particles and the metal matrix that present divergent electrochemical characteristics. In general terms, the corrosion resistance of FGM appears to increase when a low segregation of particles is found in the material, associated to low applied centrifugal forces, i.e., the higher degradation of the outer region of Al FGMs samples obtained with larger centrifugal forces is explained by the higher concentration of particles. The cathodic area is highest in this region compared with anodic area. This is an indication that the presence of the reinforcing intermatallics promotes a superior electrochemical degradation of the samples, due to the galvanic couple effects between the intermetallic compounds and the metallic matrix.

The tribocorrosion processes of Al/Al_3Ti and Al/Al_3Zr FGMs are mainly governed by mechanical wear. Better tribocorrosion behaviour was found in the samples containing the highest concentration of reinforcing particles. And it was verified that exits a synergism between the wear and the corrosion process in which this last is increasing with the wear acts.

The increase of passes in the ECAP process for the Al-5 mass % Ti alloy increases the hardness of the alloy. However, in comparison with the not deformed alloy, the wear resistance diminishes in the deformed alloys both in the perpendicular and in the parallel way of the deformation direction by ECAP.

CHAPTER 9

Perspectives of Future Work

During this research, phenomena not fully reported in this thesis occurred. Thus, an extensive study for provide complementary information would be required. For better comprehension of the concept the Al-based composites containing Al-rich intermetallic compounds, it would be interesting to do the following:

- Development of a theoretical model (3D) to predict the redistribution of the intermetallic platelets in the molten aluminium matrix for different rotations speeds. The same procedure should be followed to predict, the orientation of platelets on Al-Ti alloy deformed by ECAP;
- Study the effect of the presence of other alloying elements on the Al-Ti and Al-Zr alloys;
- Study the effect of the variation of the Ti and Zr content on the respectively alloys (Al-Ti and Al-Zr) to analyze its influence on the volume fraction distribution of platelets in the composite;
- Production of the FGMs with appropriate dimensions for mechanical tests and characterization of mechanical properties;
- General corrosion and tribocorrosion behaviour of the Al-Ti deformed by ECAP.